nature aging

Supplementary information

https://doi.org/10.1038/s43587-024-00662-8

The genetic architecture of biological age in nine human organ systems

In the format provided by the authors and unedited

Table of contents

Supplementary Note 1: The definition of genomic loci, independent significant SNP, lead SNP, candidate SNP

FUMA defined the significant independent SNPs, lead SNPs, candidate SNPs, and genomic risk loci as follows (https://fuma.ctglab.nl/tutorial#snp2gene):

Independent significant SNPs
They are defined as SNPs with $P \leq 5 \times 10^{-8}$ that are independent of each other at the user-defined r^2 (set to 0.6 in the current study). FUMA further describes *candidate SNPs* as those in linkage disequilibrium (LD) with independent significant SNPs. FUMA then queries each candidate SNP in the GWAS Catalog to check whether any clinical traits have been reported to be associated with previous GWAS studies. As mentioned in the main manuscript, this situation could result in redundant associations due to high correlations among these candidate SNPs with the top lead SNP or independent significant SNPs. We addressed this issue, as described in **Methods** in the main manuscript, to ensure that only one SNP was taken into account for each genomic locus shown in **Fig. 2a**.

Lead SNPs
Lead SNPs are defined as independent significant SNPs that are also independent of each other at $r^2 < 0.1$. If multiple independent significant SNPs are correlated at $r^2 \geq 0.1$, then the one with the lowest individual *P*-value becomes the lead SNP. If r^2 threshold is set to 0.1 for the independent significant SNPs, then they would constitute the identical set as the lead SNPs by definition. FUMA thus advises setting r^2 to be 0.6 or higher. The current study used the threshold as 0.6 for r^2.

Genomic risk loci
FUMA defines genomic risk loci to include all independent signals physically close or overlapping in a single locus. First, independent significant SNPs dependent on each other at $r^2 \geq 0.1$ are assigned to the same genomic risk locus. Then, independent significant SNPs with less than the user-defined distance (250 kb by default) away from one another are merged into the same genomic risk locus - the distance between two LD blocks of two independent significant SNPs is the distance between the closest points from each LD block. Each locus is represented by the SNP within the locus with the lowest *P*-value – the top lead SNP.

In FUMA, the users can adapt these parameters, but our current study used the default values suggested by FUMA. FUMA employes a similar approach to other studies in the field when considering linkage disequilibrium to annotate independent genetic signals. We will list two studies for illustration purposes:

- In the very first large-scale UKBB brain imaging GWAS by Elliot and colleagues[1], the authors used the following procedure to annotate independent genomic loci: "For each GWAS we first identified all variants with –log10(P) > 7.5. We applied an iterative process that starts by identifying the most strongly associated variant, storing it as a lead variant, and then removing it, and all variants within 0.25 cM from the list of variants (equivalent to approximately 250 kb in physical distance). The process was then repeated until the list of variants was empty. We applied this process to each GWAS using two filters on MAF: (a) MAF > 0.1%, and (b) MAF > 1%. We grouped associated lead SNPs across phenotypes into clusters. This process first grouped SNPs within 0.25 cM of each other, and this mostly

produced sensible clusters, but some hand curation was used to merge or split clusters based on visual inspection of cluster plots and levels of linkage disequilibrium between SNPs. For some clusters in Extended Data Table 1, we report coding SNPs that were found to be in high linkage disequilibrium with the lead SNPs." In their approach, they defined the gnomic loci as clusters, and using the coding SNPs in high LD with the lead SNPs to represent the loci.

- An additional example is from the study by Kurki et al. 2023[2] using the FinnGen data. The authors employed Bayesian-based fine-mapping methodologies (e.g., SuSiE) to enhance the definition of independent genetic signals, which they termed "independent hits" in their publication. Specifically, they stated: "To define independent signals within a locus, we utilized fine-mapping results. For each locus, we report the credible set as an independent hit if it represents a primary strongest signal with lead $P < 5 \times 10-8$. For secondary hits, we required genome-wide significance and log Bayes factor (BF) > 2. The BF filtering was necessary because SuSiE sometimes reports multiple credible sets for a single strong signal but this is indicated in SuSiE as a low BF (the model does not improve by adding another signal in the region that is not an independent signal)."

In general, we consider these approaches to be equally effective in managing linkage disequilibrium, provided that the methodology is clearly outlined in a transparent manner.

Supplementary Note 2: Sensitivity check analyses for the main GWAS of the nine BAGs using European ancestry

We fully considered linkage disequilibrium and only included the independent significant SNPs in this sensitivity check analysis. We exemplified this analysis in the split-sample GWAS. We first used the Plink *clump* command *(--clump-p1 0.00000005 --clump-p2 0.05 --clump-r2 0.60 --clump-kb 250*) to define the independent significant SNPs for the split1 and split2 GWAS. We then included all the unique independent significant SNPs in either of the two split GWASs. We then calculated three statistics to scrutinize the concordance of the two split GWASs:

- *r-β*: Pearson's *r* between the two sets of *β* coefficients from the two splits;
- *C-β*: concordance rate of the sign of the *β* coefficients from the two splits – if the same SNP exerts the same protective/risk effect between the two splits;
- *P-β*: the difference between the two sets of *β* coefficients from the two splits – if the two sets of *β* coefficients (mean) statistically differ.

The three metrics were calculated for sex-stratified, fastGWA, and non-Euroepan GWAS sensitivity check analyses.

Split-sample GWAS

P-values:

In the split1 GWAS, we found 6, 28, 20, 117, 62, 160, 37, 40, and 127 independent significant SNPs for the brain, cardiovascular, eye, hepatic, immune, metabolic, musculoskeletal, pulmonary, and renal BAGs, and 5, 30, 21, 110, 55, 164, 45, 43, and139 independent significant SNPs in split2 GWAS.

For the brain BAG, we obtained an *r-β* of -0.06 (P-value=0.84; *N*=11), but the two sets of coefficients did not statistically differ (*P-β*=0.70). All the 11 independent significant SNPs showed the same direction of effect (*C-β*=1). The low *r-β* was likely due to small sample sizes in the brain BAG. For all the other 8 BAGs, we obtained significantly h70h *r-β* estimates ($0.90<r\text{-}\beta<0.99$; P-value$<1\times10^{-19}$). The two sets of coefficients did not statistically differ (*P-β*>0.48). All independent significant SNPs showed the same direction of effect (*C-β*=1). Detailed results of these SNPs are presented in **Supplementary Source Data 2** for split-sample GWAS. The scatter plot of the independent SNPs' *β* coefficients is shown below.

Sex-stratified GWAS

In the female GWAS, we found 7, 24, 23, 286, 116, 142, 153, 30, and 131 independent significant SNPs for the brain, cardiovascular, eye, hepatic, immune, metabolic, musculoskeletal, pulmonary, and renal BAGs, and 7, 38, 22, 126, 275, 286, 42, 71, and 167 independent significant SNPs in the male GWAS.

For the brain BAG, we obtained an *r-β* of -0.869 (P-value=5.29×10^{-5}, *N*=14), but the two sets of coefficients did not statistically differ (*P-β*=0.66). 13 out of the 14 independent significant SNPs showed the same direction of effect (*C-β*=0.93). The one independent significant SNP (rs1634777) that had the opposite *β* sign in males compared to females was because the *β* coefficient was close to 0 (*β*=-0.000417162) and was not statistically significant (P-value=0.99). For all the other 8 BAGs, we obtained significantly high *r-β* estimates ($0.30<r\text{-}\beta<0.96$; P-value$<2.57\times10^{-7}$). The two sets of coefficients did not statistically differ (*P-β*>0.40), except for the immune BAG (*P-β*=0.013). Most independent significant SNPs showed the same direction of effect (*C-β*>0.89), except for the immune (0.54) and musculoskeletal BAGs (0.70). Detailed

results of these SNPs are presented in **Supplementary Source Data 3** for sex-stratified GWAS. The scatter plot of the independent SNPs' β coefficients is shown below.

fastGWA vs PLINK GWAS

In the PLINK GWAS, we found 27, 124, 69, 289, 217, 422, 147, 272, and 331 independent significant SNPs for the brain, cardiovascular, eye, hepatic, immune, metabolic, musculoskeletal, pulmonary, and renal BAGs, and 27, 124, 69, 292, 218, 422, 148, 269, and 333 independent significant SNPs in fastGWA GWAS.

For all the nine BAGs, we found almost perfect concordance between the PLINK and fastGWA GWASs using the three proposed metrics (r-β=1; C-β=1; P-β=1). Detailed results of these SNPs are presented in **Supplementary Source Data 4** for method-specific GWAS. The scatter plot of the independent SNPs' β coefficients is shown below.

European vs. non-European GWAS

In the European GWAS, we found 27, 124, 69, 289, 217, 422, 147, 272, and 331 independent significant SNPs for the brain, cardiovascular, eye, hepatic, immune, metabolic, musculoskeletal, pulmonary, and renal BAGs, and 0, 2, 1, 16, 2, 23, 1, 1, and 35 independent significant SNPs in non-European GWAS (with much smaller sample sizes).

For all the nine BAGs, we found a high concordance between the European and non-Euroropean GWASs using the three proposed metrics ($0.85<r$-$\beta<0.95$; $0.89<C$-$\beta<1$). The two sets of β coefficients did not significantly differ (P-$\beta>0.12$). Detailed results of these SNPs are presented in **Supplementary Source Data 5** for ancestry-specific GWAS. The scatter plot of the independent SNPs' β coefficients is shown below.

Supplementary Note 3: The characteristics of genomic loci linked to the nine BAG.
Certain genomic loci exhibited unique associations with individual organs, whereas others displayed connections to multiple organ BAGs in close genomic proximity based on their cytogenetic position. For instance, the locus on chromosome 6 associated with the hepatic (rs62401887, position: 24416482 at 6p22.3), immune (rs80215559, position: 25918225 at 6p22.3), metabolic (rs79220007, position: 26098474 at 6p22.2), musculoskeletal (rs2744575, position: 24494975 at 6p22.3), pulmonary (rs411535, position: 22061040 at 6p22.3), and renal BAGs (rs55925606, position: 25878848 at 6p22.2) was close with each other on the human genome. Bayesian colocalization[3] analyses supported two distinct causal SNP within this locus with the liver and musculoskeletal BAGs. Our results showed a posterior possibility (PP) of two distinct causal variants (PP.H3.ABF=0.744) or one shared causal variant (PP.H4.ABF=0.256) associated with both traits in the *GPLD1* gene, although the PP.H4.ABF hypothesis did not achieve the suggested threshold (>0.8)[3]. Detailed results are presented in **Supplementary Figure 10**. However, note that these loci on chromosome 6 are near the major histocompatibility complex (MHC) region; further dedicated analyses are needed to understand the underlying genetics across different BAGs (e.g., pleiotropy).

Many of these loci were mapped to protein-encoding genes and provided functional insights. For example, the top lead SNP (rs62401887 at 6p22.3) within the locus of the hepatic BAG was mapped to the *MRS2* gene by position (with a deleterious score of 14.89) and expression quantitative trait loci (eQTL, P-value=1.09×10^{-10}), which enables magnesium ion transmembrane transporter activity. We illustrate the regional Manhattan plot for the genomic locus with the highest significance for each organ BAG in **Supplementary Figure 11**. For instance, the brain BAG exhibited a highly significant locus (top lead SNP: rs371185851 at 17q21.31) with multiple protein-encoding genes, including the widely recognized *MAPT* gene encoding tau protein associated with neurodegenerative diseases, such as Alzheimer's disease (AD)[4]. Moreover, the SNPs within this locus included enhancers and transcription start sites specific to brain tissue chromatin states, highlighting their functional relevance in brain-related processes (**Supplementary Figure 11a**).

Supplementary Note 4: Phenome-wide association query using the GWAS Atlas platform

To comprehensively encompass the genetic landscape reported in previous literature, we comparatively conducted a phenome-wide association query using the GWAS Atlas platform (https://atlas.ctglab.nl/PheWAS). We applied the same P-value threshold search criteria as those used in the EMBL-EBI GWAS Catalog (P-value<$1x10^{-5}$). These findings are presented as a supplementary search to complement the results shown in **Fig. 2a**. The details of this comparative search are presented in **Supplementary Source Data 7**.

It's important to note that the two platforms may exhibit variations in their curated GWAS datasets, the genome build versions utilized, and the specific P-value thresholds set for their search analyses by default. We tried our best to harmonize the query criteria. Hence, this comparative search was not exhaustive, and the results may differ. Rather, we intend to offer a broad overview of the two platforms commonly employed for phenome-wide association studies (PheWAS). Given the rapid updates in GWAS summary statistics in the field, it's worth mentioning that this comparative search was originally conducted on October 23, 2023, and revised on January 13, 2024, based on the reviewer's comments. The results from the GWAS Atlas are shown in the figure below.

In the GWAS Atlas platform, we identified 8,576 significant associations between the identified loci in our GWAS and clinical traits. The genomic loci associated with the brain BAG exhibited the highest proportion of associations (109 out of 308) with traits related to the brain. The brain BAG loci were also largely linked to many other traits related to other organ systems, evidencing inter-organ connections, including metabolic (*N*=78/308), lifestyle factor (*N*=13/308), neurodegenerative traits (*N*=5/308), and immune (*N*=35/308). For the eye BAG loci, most associations were found in the musculoskeletal (*N*=139/279), eye (*N*=14/279), and mental traits (*N*=19/279), among many others.

For the seven body organ systems, among the loci associated with the cardiovascular BAG, most associations were observed with musculoskeletal traits (*N*=249/611) and cardiovascular traits (166/611). 29 out of 1009 associations were related to hepatic traits (e.g., blood protein, cirrhosis, and bilirubin) for the hepatic BAG loci. Among the loci associated with the immune BAG, abundant associations were found enriched in immune (*N*=467/1062) traits. For the metabolic BAG loci, most associations were observed in metabolic traits (*N*=993/1990). We found a significant intertwining of musculoskeletal systems with other organ systems in the GWAS Atlas platform. Details of the phenome-wide associations are presented in **Supplementary Source Data 7**.

Supplementary Note 5: Additional analyses to elucidate the genetic signals across the nine BAGs

It is widely recognized that the effect size of common genetic variants tends to increase as the allele frequency decreases. This "inverse relationship" was evidenced by our data using independent significant SNPs from the 9 BAGs (**Extended Data Figure 3**). We then hypothesized that the smaller sample sizes of the brain and eye BAGs enabled us to detect significant variants with a relatively higher allele frequency but could not identify the SNPs with a relatively lower allele frequency associated with the body organ BAGs. This relationship persisted by subsampling the population of other BAGs to that of the brain BAGs, which is presented in **Extended Data Figure 2c**. As expected, the β coefficients derived from the whole samples (N>10k for body organ BAGs) were not significantly different from the results using the brain-BAG comparable down-sampled samples (N=30,108) (**Supplementary Table 2**).

Another hypothesis is that the features used to compute the brain and eye BAGs – *in vivo* imaging features – are more heritable than those of the body-organ systems. We compared the genetic structure of the nine BAGs and the individual features used to compute the BAGs. This comparison is crucial for gaining insights into how the choice of predictors impacts the results of BAG GWAS, which, in turn, is fundamental for subsequent analyses related to pleiotropy and trait associations. We first estimated the SNP-based heritability for four pulmonary features and compared these with a set of multimodal brain imaging-derived phenotypes from our previous studies[5–9] using the same GCTA software. We hypothesized that the brain imaging features would exhibit a higher degree of heritability than the 4 pulmonary features of the pulmonary BAG (i.e., forced vital capacity, forced expiratory volume, peak expiratory flow, and the ratio of forced expiratory volume to forced vital capacity), supported by the results in **Supplementary Table 1c**. We then performed GWAS for the four pulmonary features within the European ancestry populations. The Manhattan and QQ plots are presented in **Supplementary Figure 13**. The pulmonary BAG showed high genetic correlations using LDSC with the four pulmonary features ($-0.79<g_c<0.83$, **Supplementary Table 3**). Using Bayesian colocalization analysis, we identified 99 potential causal variants (PP.H4.ABF>0.80) between the pulmonary BAG and the four underlying features (**Supplementary Source Data 8**). We showcased one causal variant evidenced at one locus (4q24) between the pulmonary BAG and the FEV/FCV feature (**Extended Data Figure 4**). The PP.H4.ABF (0.99) denotes the posterior probability of hypothesis H4, which suggests that both traits share the same causal SNP (rs7664805, mapped gene: *NPNT*). SNPs in linkage disequilibrium with the causal SNP were previously linked to chronic obstructive pulmonary disease in the GWAS Catalog. To elucidate the genetic overlap at the individual SNP level, we showed the β coefficient of the 48 potential causal variants that passed the genome-wide significance for the pulmonary BAG and at least one pulmonary feature in **Supplementary Figure 14**.

Supplementary Note 6: Sensitivity check analyses for the causality between the nine BAGs

A) Sensitivity analyses on body weight for the bi-directional causality between the hepatic and musculoskeletal BAGs

We conducted a revised Mendelian randomization analysis by introducing body weight as a covariate in the split-sample GWASs for hepatic and musculoskeletal BAGs. In this approach, we employed hepatic BAG as the exposure variable in split1 GWAS and musculoskeletal BAG as the outcome variable in split2 GWAS. Likewise, we reversed the roles, using musculoskeletal BAG as the exposure variable in split1 GWAS and hepatic BAG as the outcome variable in split2 GWAS, thus assessing the inverse causal relationship. This methodology ensured the absence of overlapping populations while effectively controlling for the influence of body weight. Compared to the original results, this bi-directional causality persisted while adjusting the body weight as a covariate, shown in **Supplementary Table 6A** and **B**.

B) Sensitivity analysis for the hepatic BAG on musculoskeletal BAG excluding the *APOE* gene

We conducted a revised Mendelian randomization analysis by excluding SNPs within the *APOE* gene for the causal relationship from the hepatic BAG to the musculoskeletal BAGs; all other significant causality did not involve the two common *APOE* gene SNPs (rs429358 and rs7412). In this approach, we employed hepatic BAG as the exposure variable in split1 GWAS and musculoskeletal BAG as the outcome variable in split2 GWAS. Compared to the original results, this causality persisted while excluding the SNP (rs429358) as an IV, shown in **Supplementary Table 6C**.

C) Sensitivity analyses for metabolic BAG on body weight

We showcased sensitivity analyses to investigate potential violations of the three IV assumptions. To illustrate this, we showcased the sensitivity analysis results for the causal effect of the metabolic BAG on body weight (**Supplementary Figure 31**). In a leave-one-out analysis, no single SNP overwhelmingly drove the overall effect. There was evidence for minor heterogeneity[10] of the causal effect amongst SNPs (Cochran's Q value=57.33, P-value<$1x10^{-5}$). Some SNPs exerted opposite causal effects compared to the model using all SNPs. The scatter plot indicated two obvious SNP outliers (rs117233107 and rs33959228), and the funnel plot showed slight asymmetry. Finally, the MR Egger estimator allows for pleiotropic effects independent of the effect on the exposure of interest (i.e., the InSIDE assumption[11]). Our results from the Egger estimator showed a small but not significant positive intercept ($3.62x10^{-4}\pm1.67x10^{-3}$, P-value=0.83), which may indicate that the IVW estimate is not likely biased[11]. We re-analyzed the IVW MR analyses by excluding the two outliers identified in **Supplementary Figure 31** (rs117233107 and rs33959228), which led to a similar OR [0.94 (0.91, 0.97) vs. 0.95 (0.92, 0.98)] and a less significant P-value [$6.9x10^{-4}$ vs. $1.2x10^{-3}$].

Supplementary Note 7: Additional details on the machine learning models used for computing the BAG and comparison with the literature

In each of the 20-fold cross-validation iterations, a linear support vector machine was employed to predict chronological age. The training set consisted of 19 folds of individuals, and the fitted regression coefficients (feature weights) were then applied iteratively to the remaining held-out set (test set) to predict the chronological age of each healthy individual. This approach ensured that the prediction model was not trained using the same individuals for which it made predictions, minimizing the risk of overfitting. Before each iteration of model training, all measures (excluding categorical variables) were standardized using the weighted column mean and standard deviation computed within the training set. The SVM box constraint and kernel scale were set to unity, while the half-width of the epsilon-insensitive band was set to a tenth of the standard deviation of the interquartile range of the predicted variable (chronological age). The SVM was solved using sequential minimal optimization with a gap tolerance of 0.001. The mathematical principles of support vector machines are well-established in the field and have been widely recognized[12]. Further details on this topic can be found in our previous study[13].

The concept of biological age gap derived from artificial intelligence has been widely investigated, especially the brain age[14,15]. The calculation of the nine BAGs were established in our previous works[5,13]. We previously showed that the prediction accuracy of biological age was not influenced by the number of phenotypes, despite variations across different organ systems. While some prior studies[16] used deep learning for brain BAG and obtained a lower mean absolute error, we have previously demonstrated that lower mean absolute error might compromise sensitivity to disease-related information[17]. In our previous GWAS[5], which separately examined three multimodal brain BAGs derived from T1-weighted, diffusion, and resting-state fMRI data, we extensively investigated the influence of various brain imaging feature types and study designs on the genetic signals. Our results unveiled both the consistency and distinctions in the genetic foundations across these diverse contexts. Finally, we recognize that ascertainment bias may be present in our GWAS due to variations in sequencing techniques, differences between populations (e.g., disease populations vs. healthy controls), and socioeconomic factors that have not been explicitly modeled in our study.

Supplementary Figure 1: GWAS Manhattan plots for the brain BAG

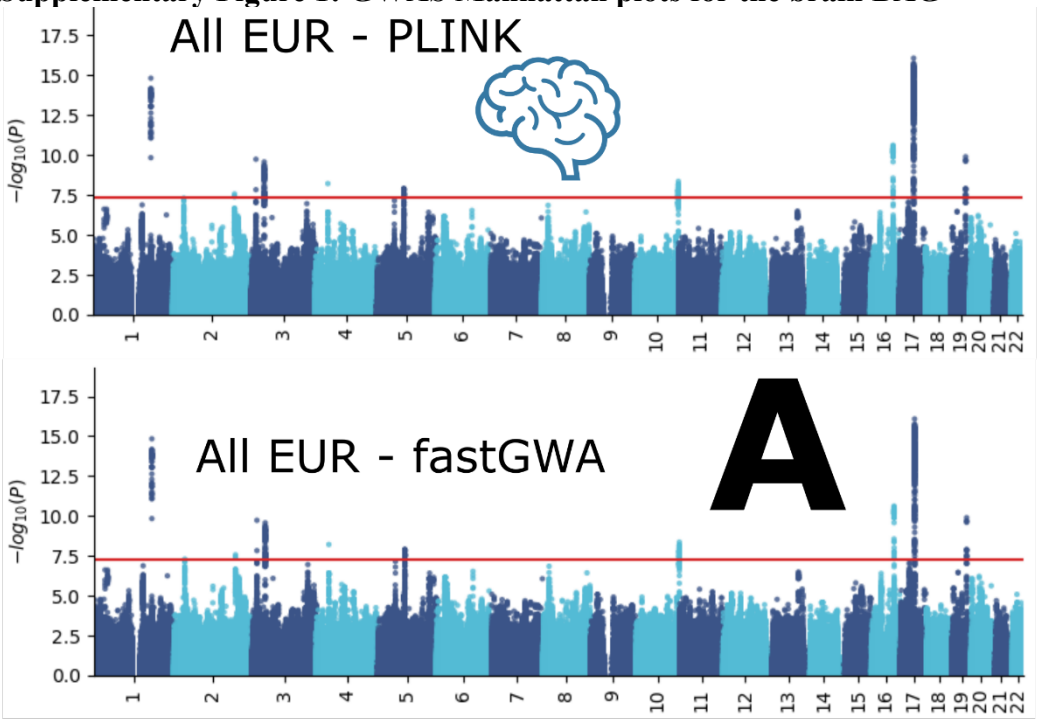

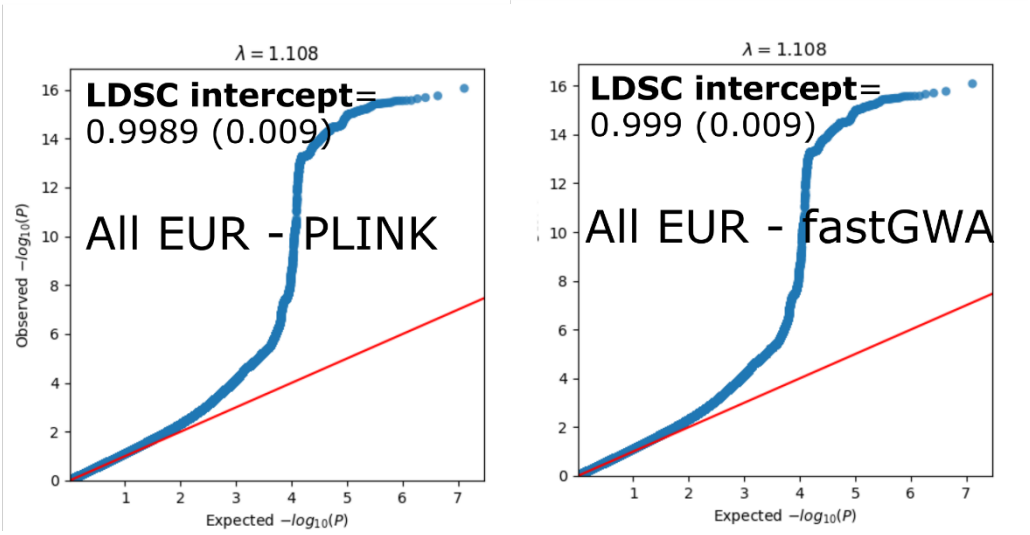

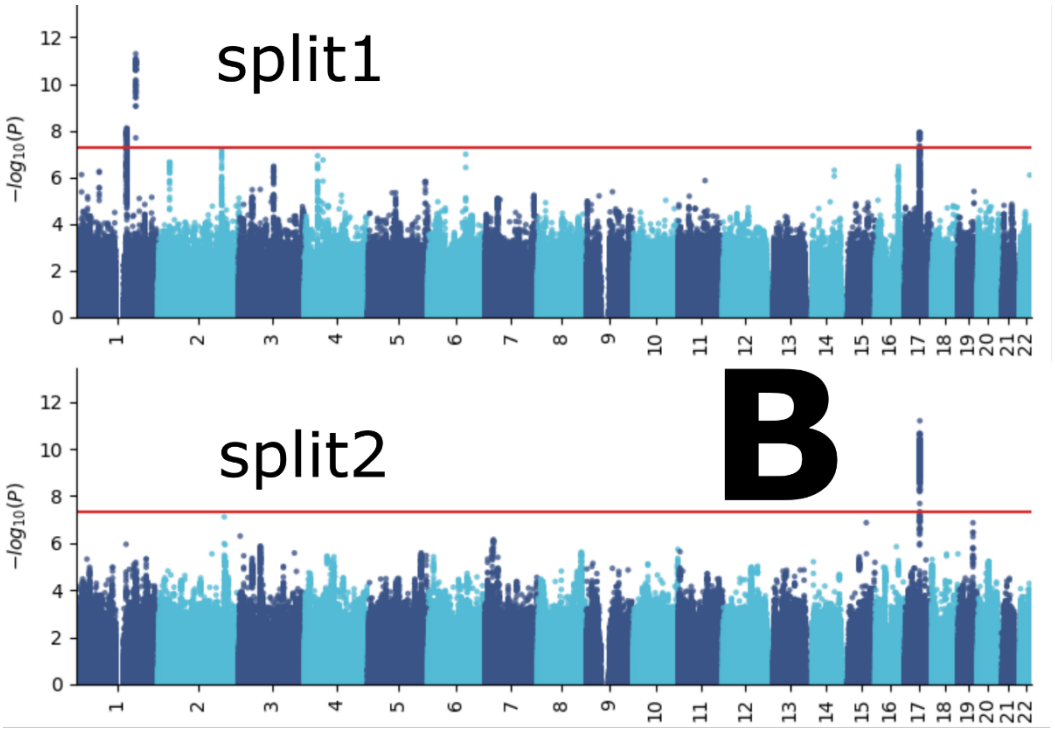
split1
split2
B
$-log_{10}(P)$

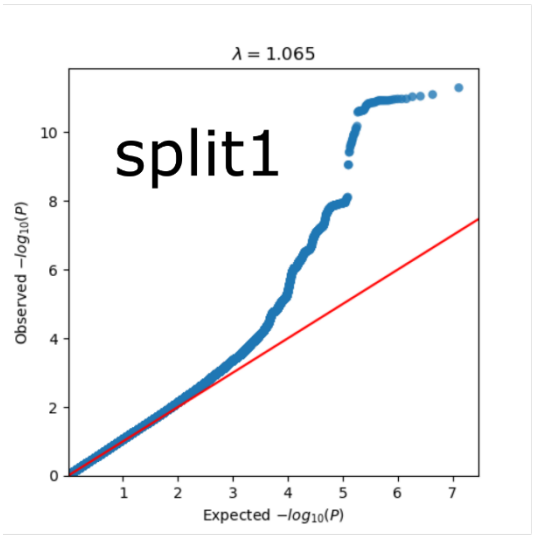
$\lambda = 1.065$
split1
Observed $-log_{10}(P)$
Expected $-log_{10}(P)$

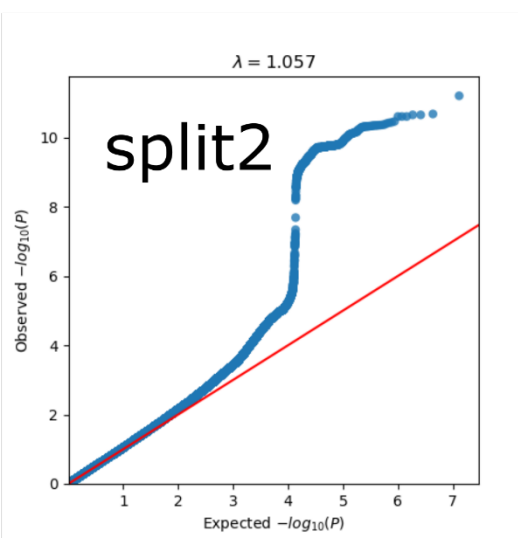
$\lambda = 1.057$
split2
Observed $-log_{10}(P)$
Expected $-log_{10}(P)$

381

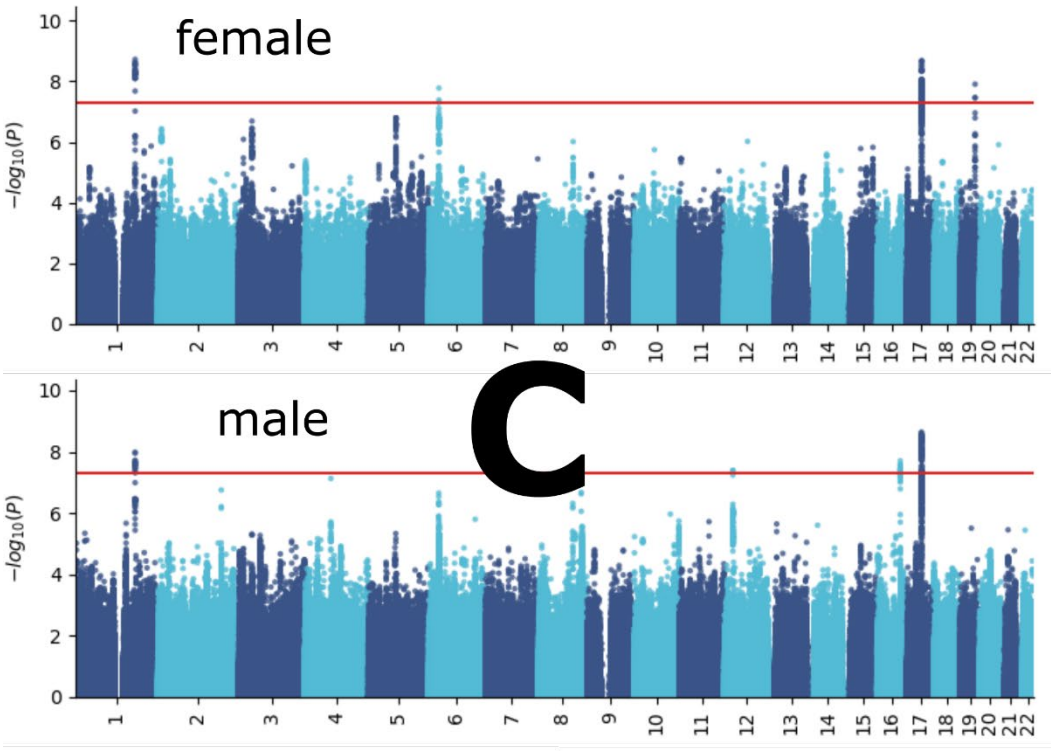
female
male
C
$-log_{10}(P)$
1 2 3 4 5 6 7 8 9 10 11 12 13 14 15 16 17 18 19 20 21 22

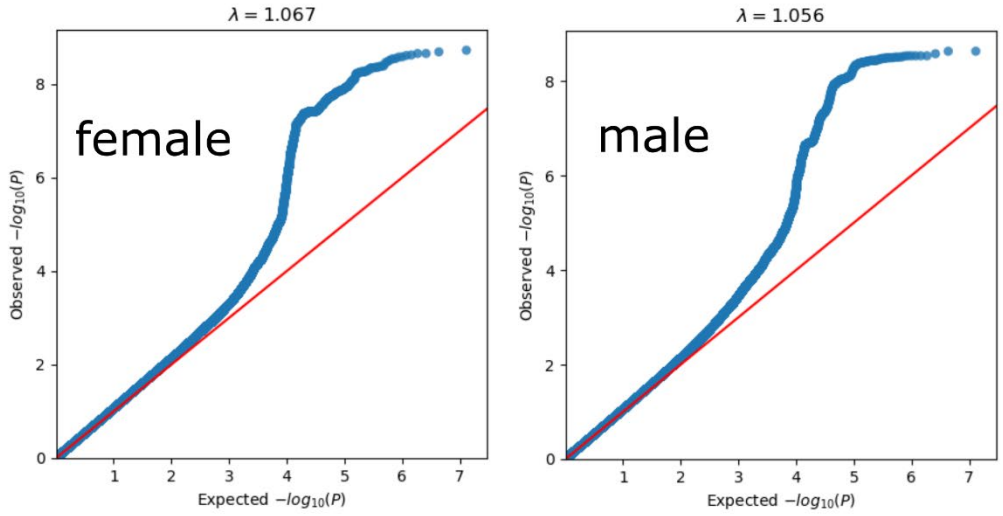
λ = 1.067
λ = 1.056
female
male
Observed $-log_{10}(P)$
Expected $-log_{10}(P)$

382

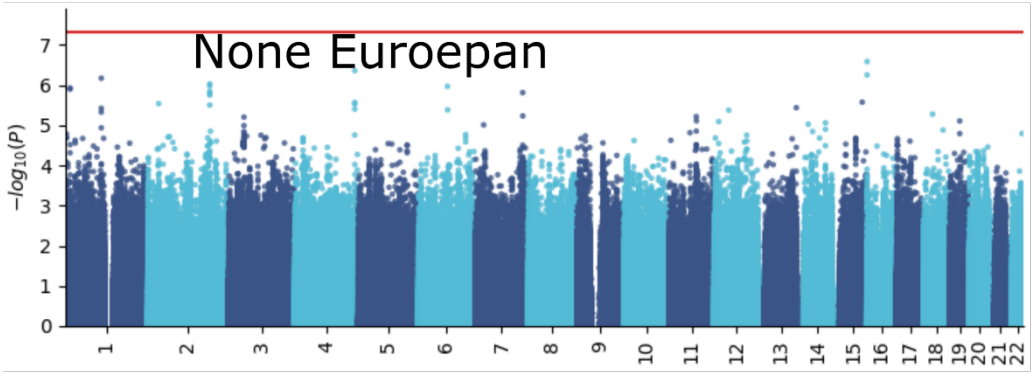

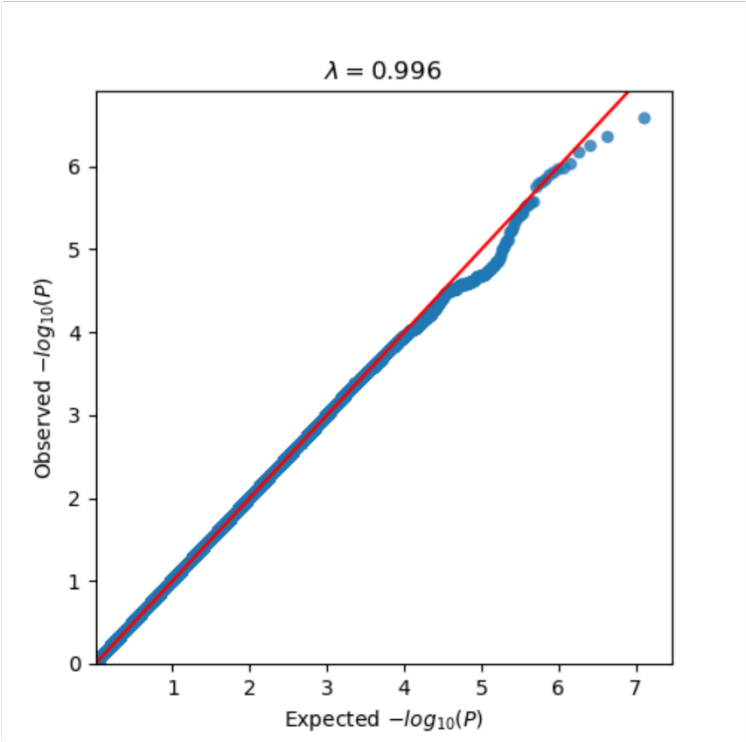

D

Manhattan and QQ plots, along with genomic inflation factors and LDSC intercepts, are displayed for the primary GWAS conducted on individuals of European ancestry (*N*=30,062) using PLINK and fastGWA (**A**). Additionally, results are presented for split-sample GWAS (split1 and split2, **B**), sex-stratified GWAS (female and male, **C**), and GWAS involving non-European ancestry populations (*N*=4465, **D**). All P-values were two-sided, and a genome-wide P-values threshold was used.

390 **Supplementary Figure 2: GWAS Manhattan plots for the cardiovascular BAG**

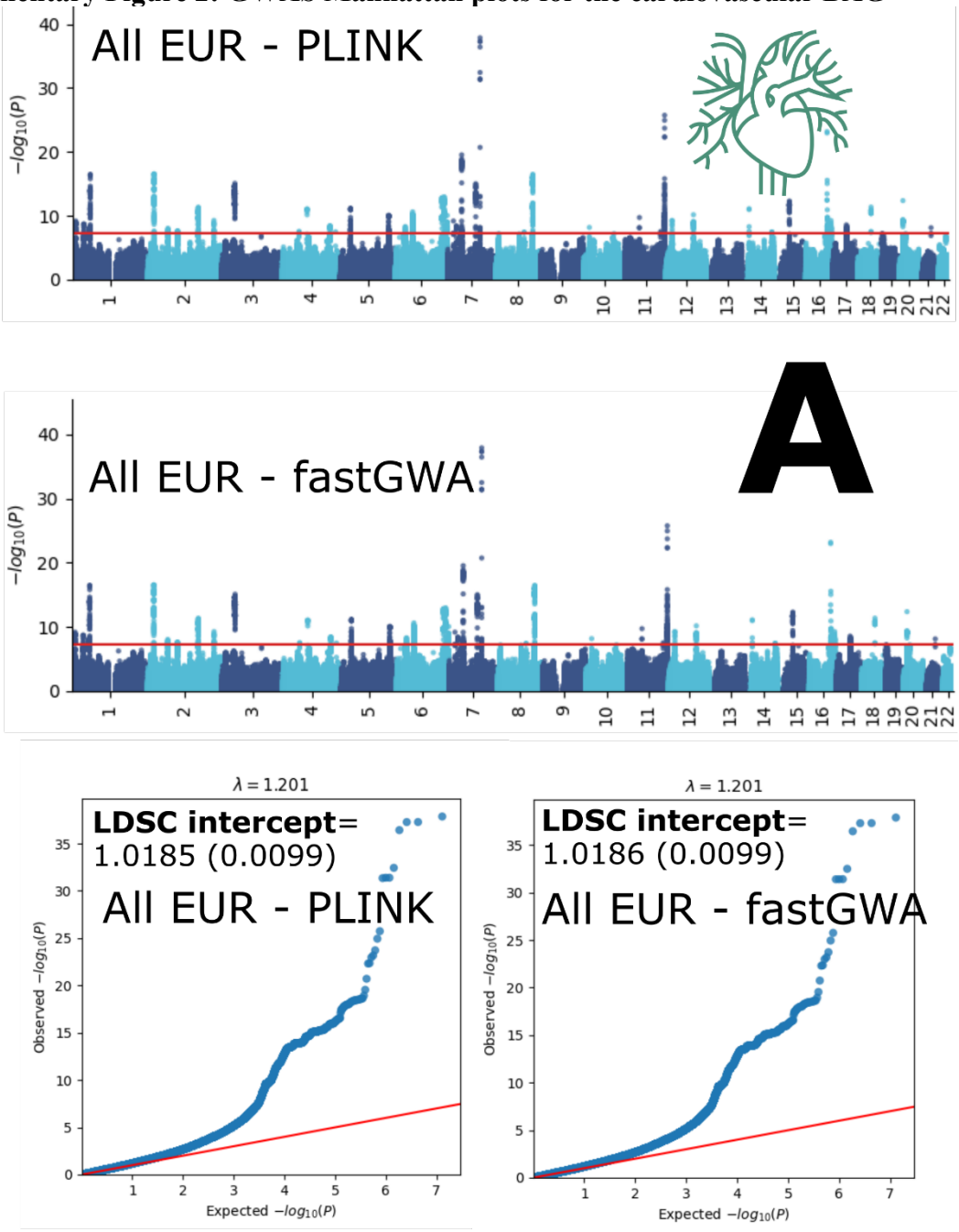

391

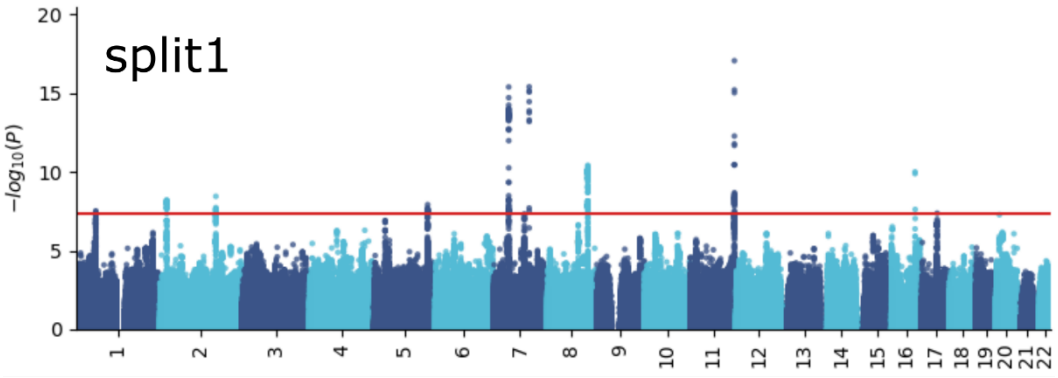
split1
$-log_{10}(P)$
20
15
10
5
0
1
2
3
4
5
6
7
8
9
10
11
12
13
14
15
16
17
18
19
20
21
22

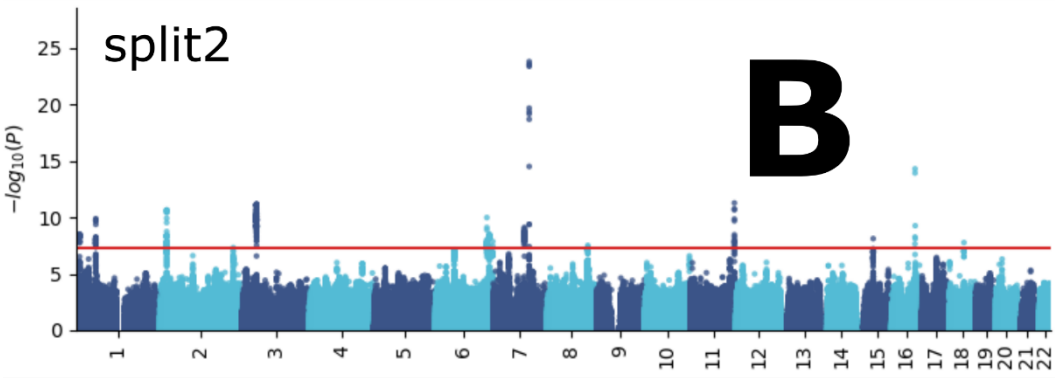
split2
B
$-log_{10}(P)$
25
20
15
10
5
0
1
2
3
4
5
6
7
8
9
10
11
12
13
14
15
16
17
18
19
20
21
22

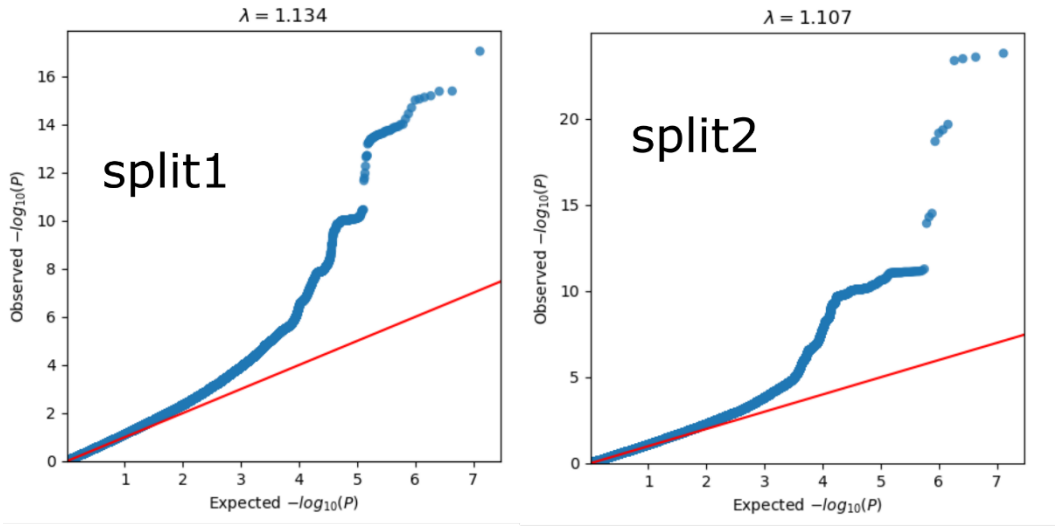
$\lambda = 1.134$
split1
Observed $-log_{10}(P)$
Expected $-log_{10}(P)$
$\lambda = 1.107$
split2
Observed $-log_{10}(P)$
Expected $-log_{10}(P)$

392

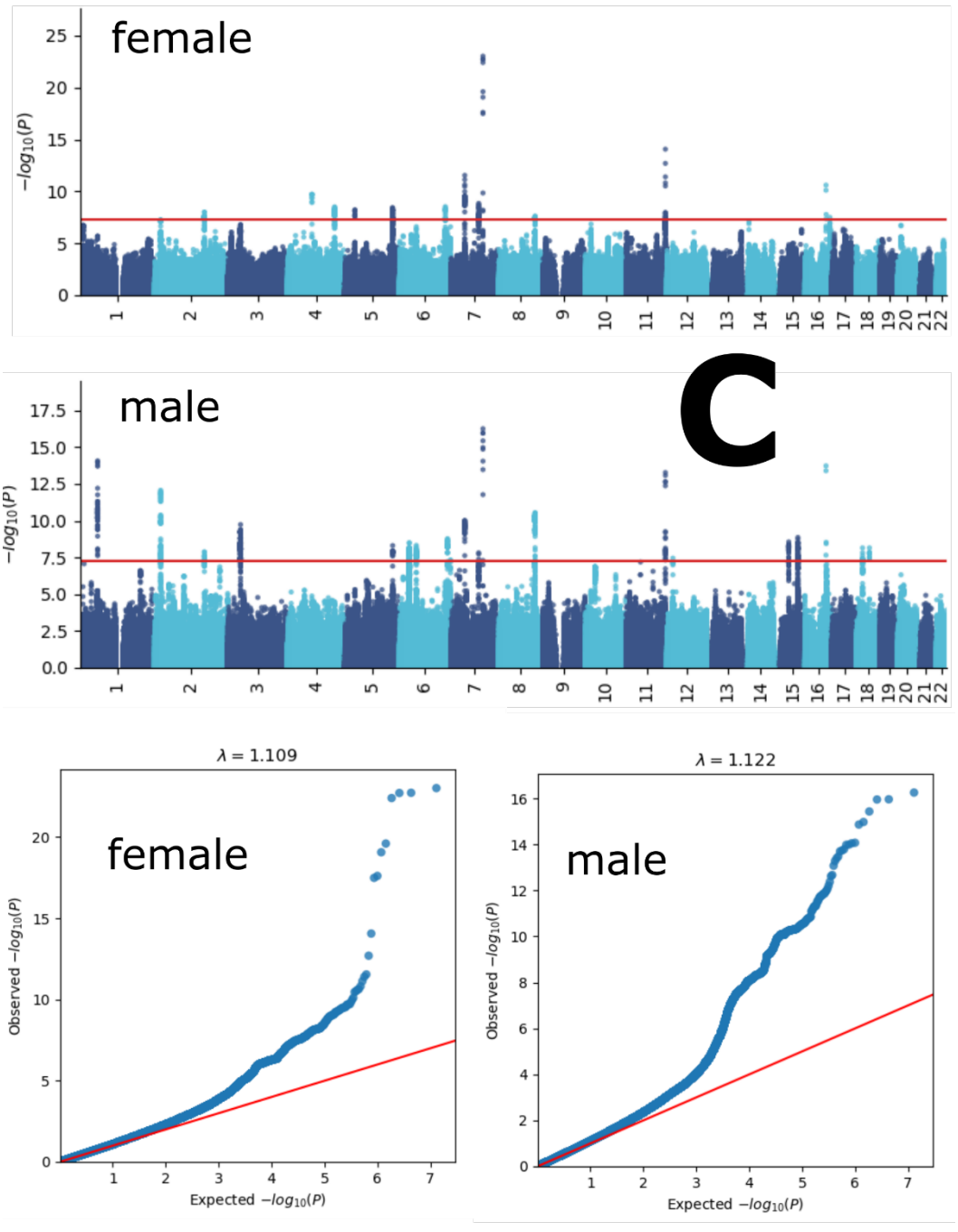
female
male
C
$-log_{10}(P)$
$\lambda = 1.109$
$\lambda = 1.122$
Observed $-log_{10}(P)$
Expected $-log_{10}(P)$

393

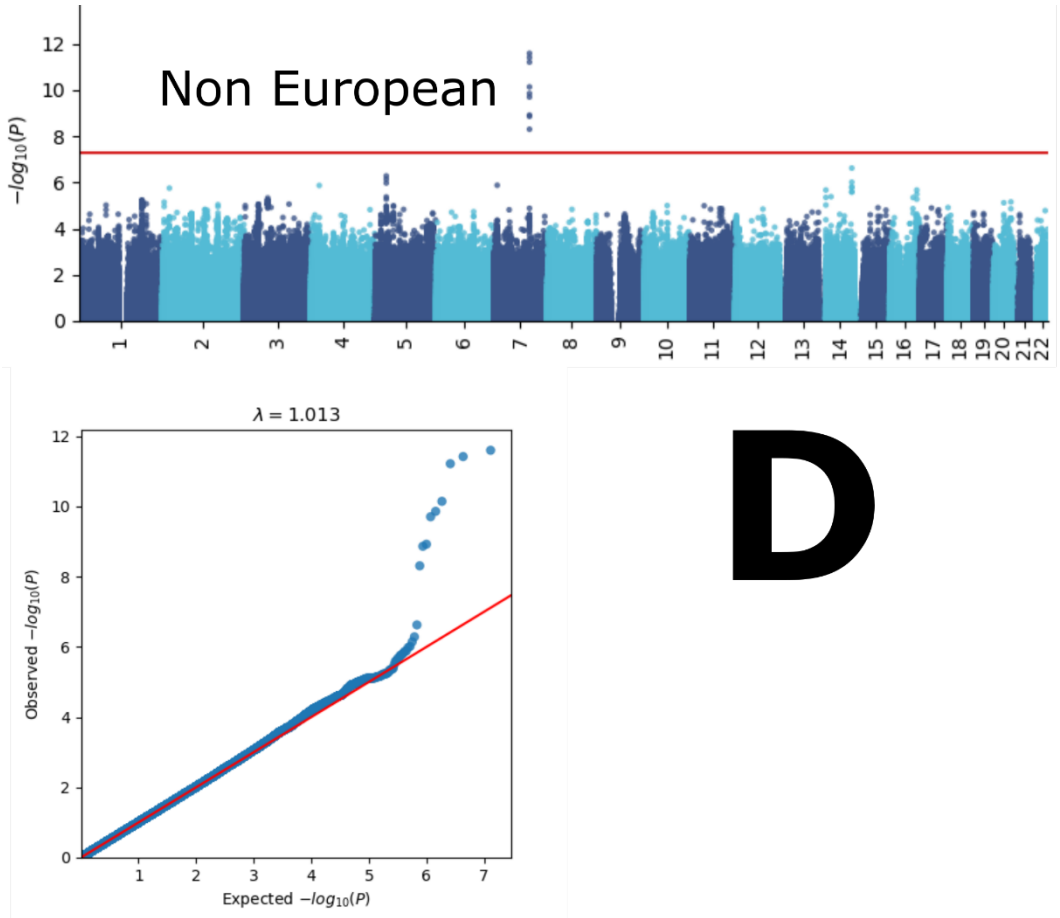

Manhattan and QQ plots, along with genomic inflation factors and LDSC intercepts, are displayed for the primary GWAS conducted on individuals of European ancestry (*N*=111,386) using PLINK and fastGWA (**A**). Additionally, results are presented for split-sample GWAS (split1 and split2, **B**), sex-stratified GWAS (female and male, **C**), and GWAS involving non-European ancestry populations (*N*=20,408, **D**). All P-values were two-sided, and a genome-wide P-values threshold was used.

Supplementary Figure 3: GWAS Manhattan plots for the eye BAG

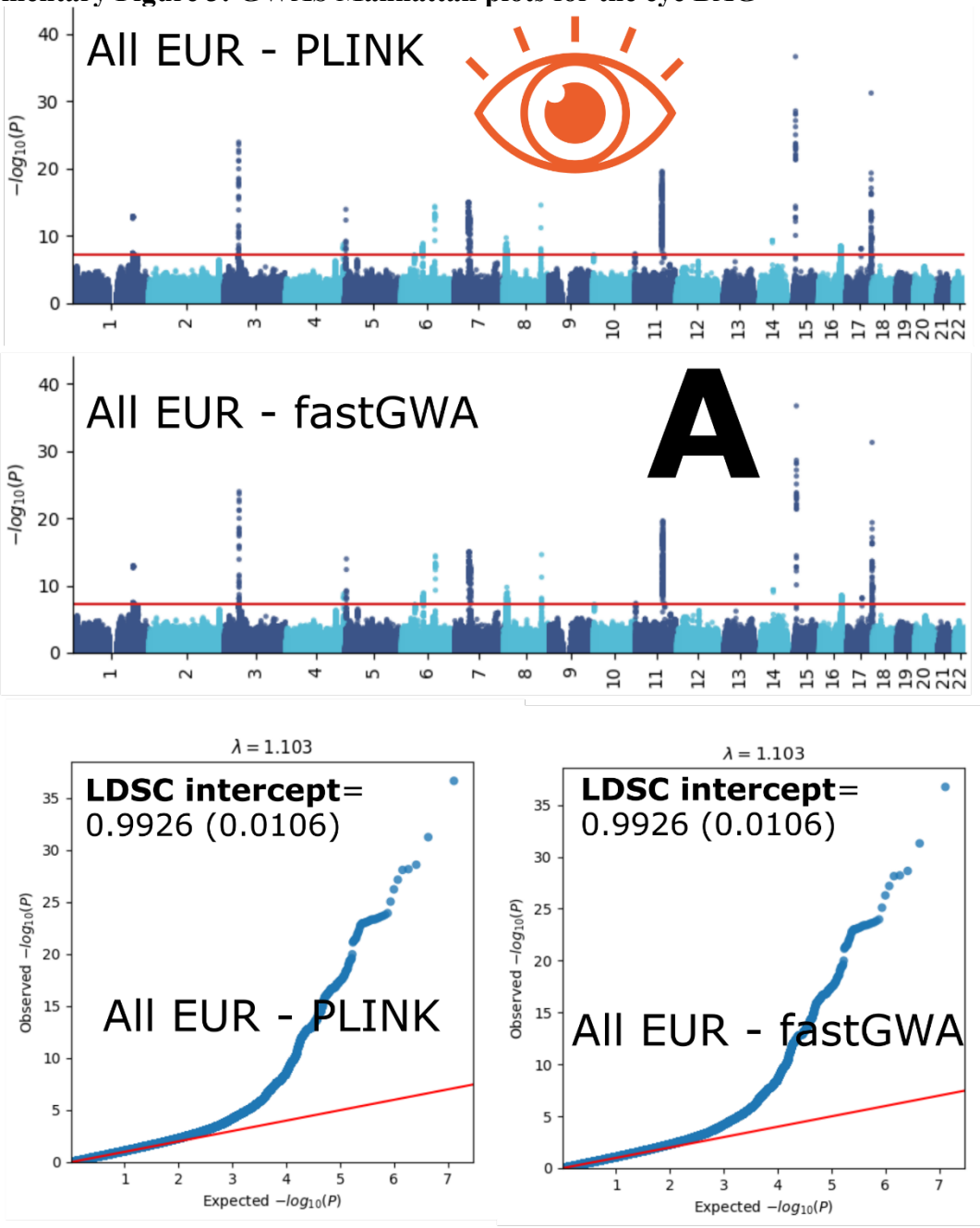

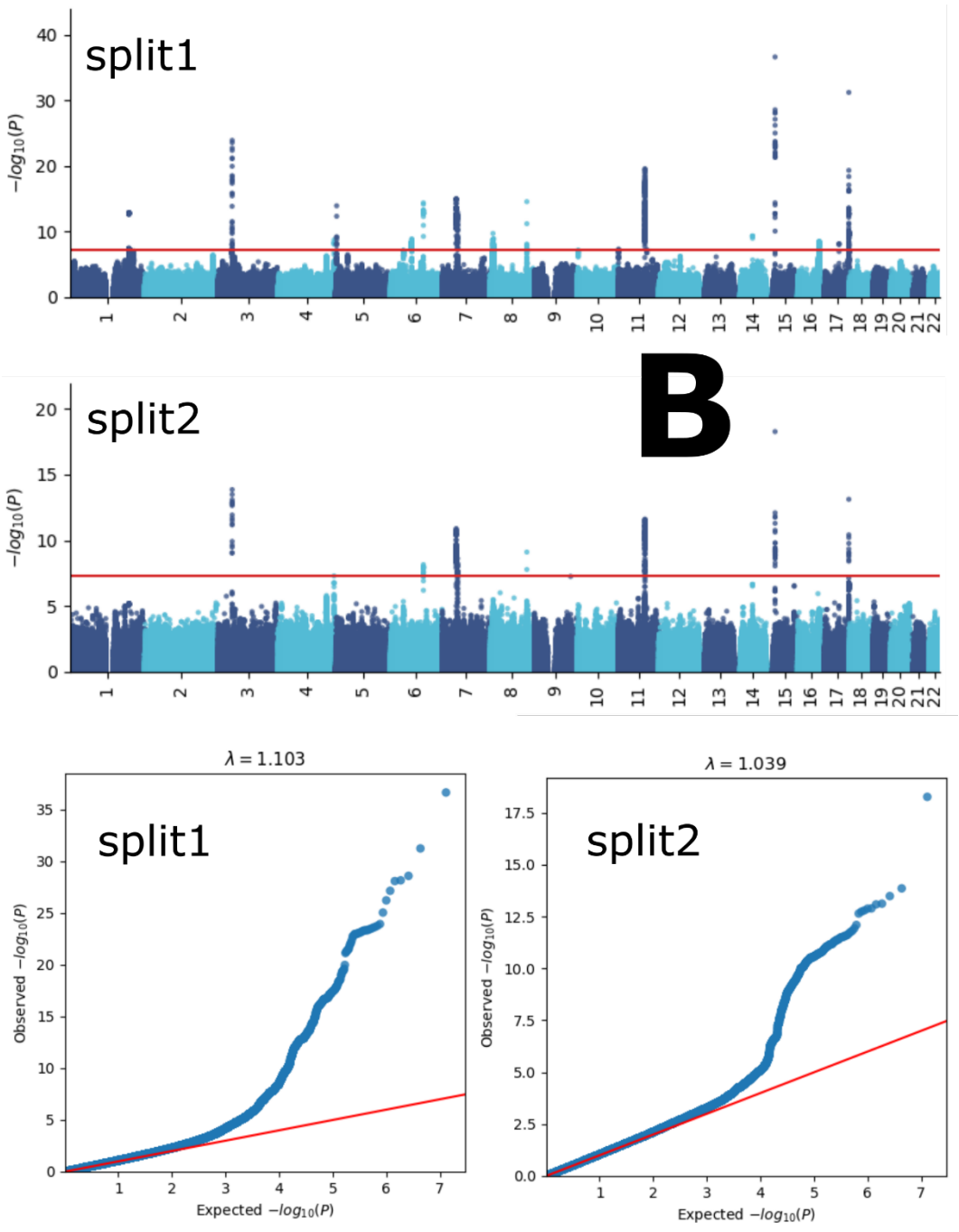
split1
split2
B
$-log_{10}(P)$
λ = 1.103
λ = 1.039
Observed $-log_{10}(P)$
Expected $-log_{10}(P)$

403

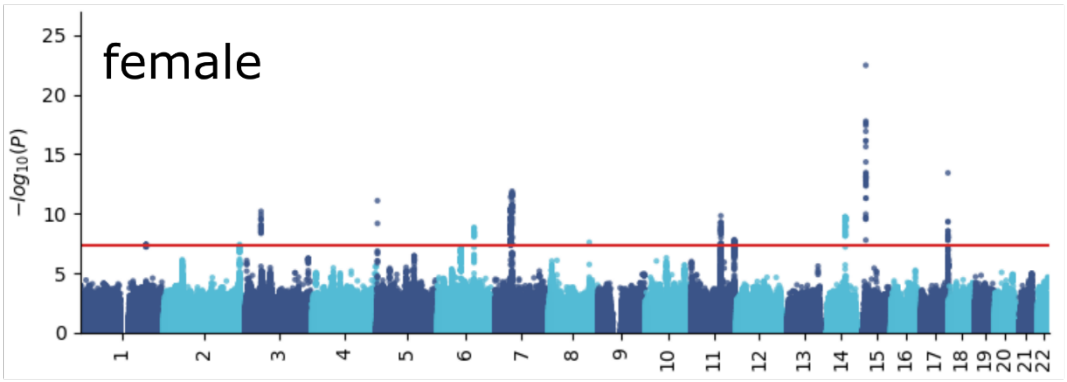
female
$-log_{10}(P)$
25
20
15
10
5
0
1 2 3 4 5 6 7 8 9 10 11 12 13 14 15 16 17 18 19 20 21 22

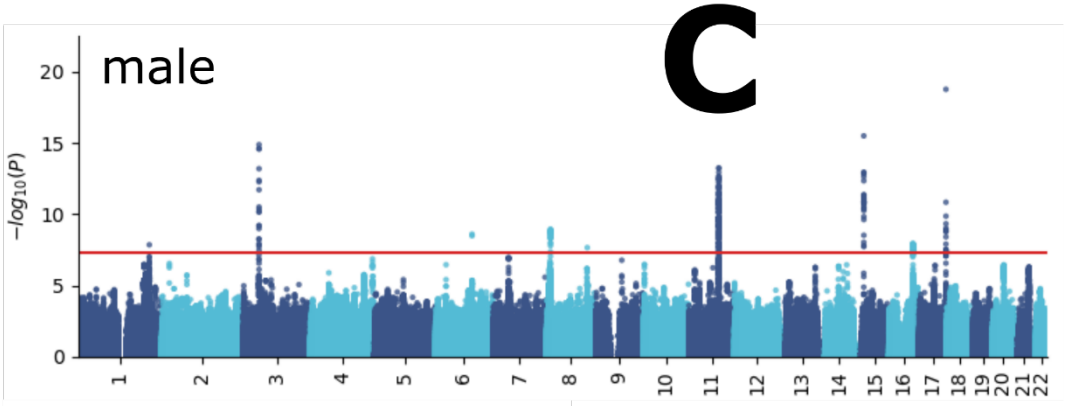
male
C
$-log_{10}(P)$
20
15
10
5
0
1 2 3 4 5 6 7 8 9 10 11 12 13 14 15 16 17 18 19 20 21 22

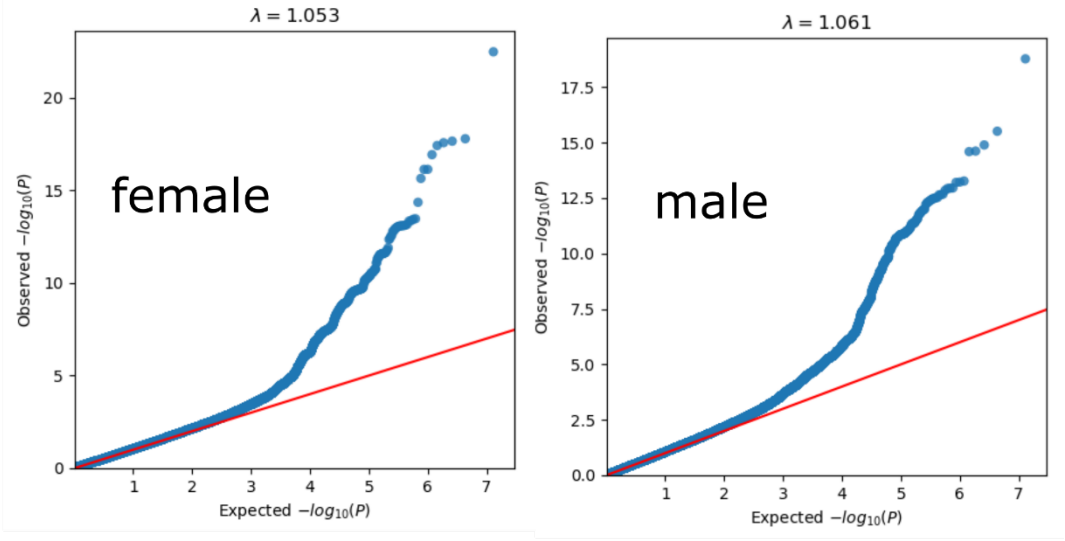
$\lambda = 1.053$
female
Observed $-log_{10}(P)$
Expected $-log_{10}(P)$
$\lambda = 1.061$
male
Observed $-log_{10}(P)$
Expected $-log_{10}(P)$

404

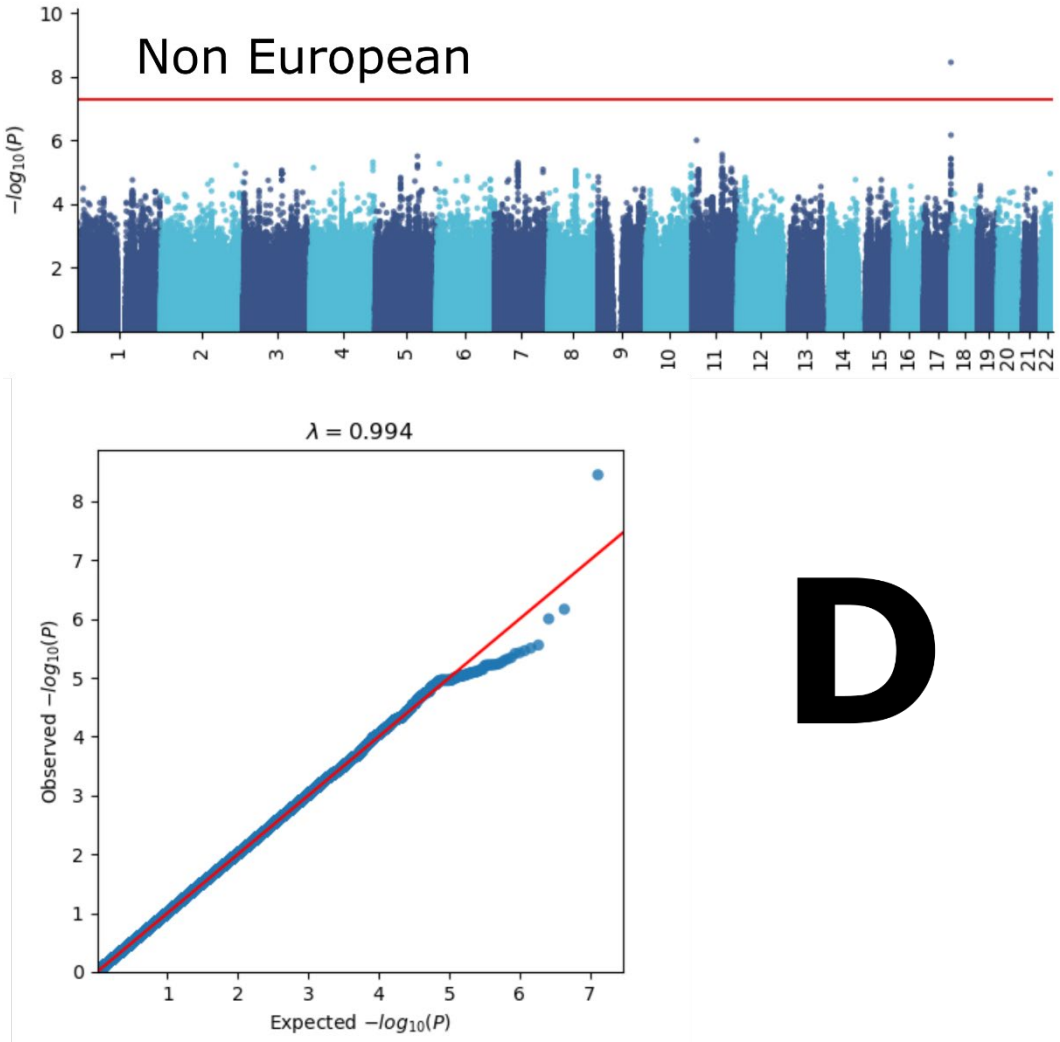

Manhattan and QQ plots, along with genomic inflation factors and LDSC intercepts, are displayed for the primary GWAS conducted on individuals of European ancestry (*N*=36,004) using PLINK and fastGWA (**A**). Additionally, results are presented for split-sample GWAS (split1 and split2, **B**), sex-stratified GWAS (female and male, **C**), and GWAS involving non-European ancestry populations (*N*=3407, **D**). All P-values were two-sided, and a genome-wide P-values threshold was used.

Supplementary Figure 4: GWAS Manhattan plots for the hepatic BAG

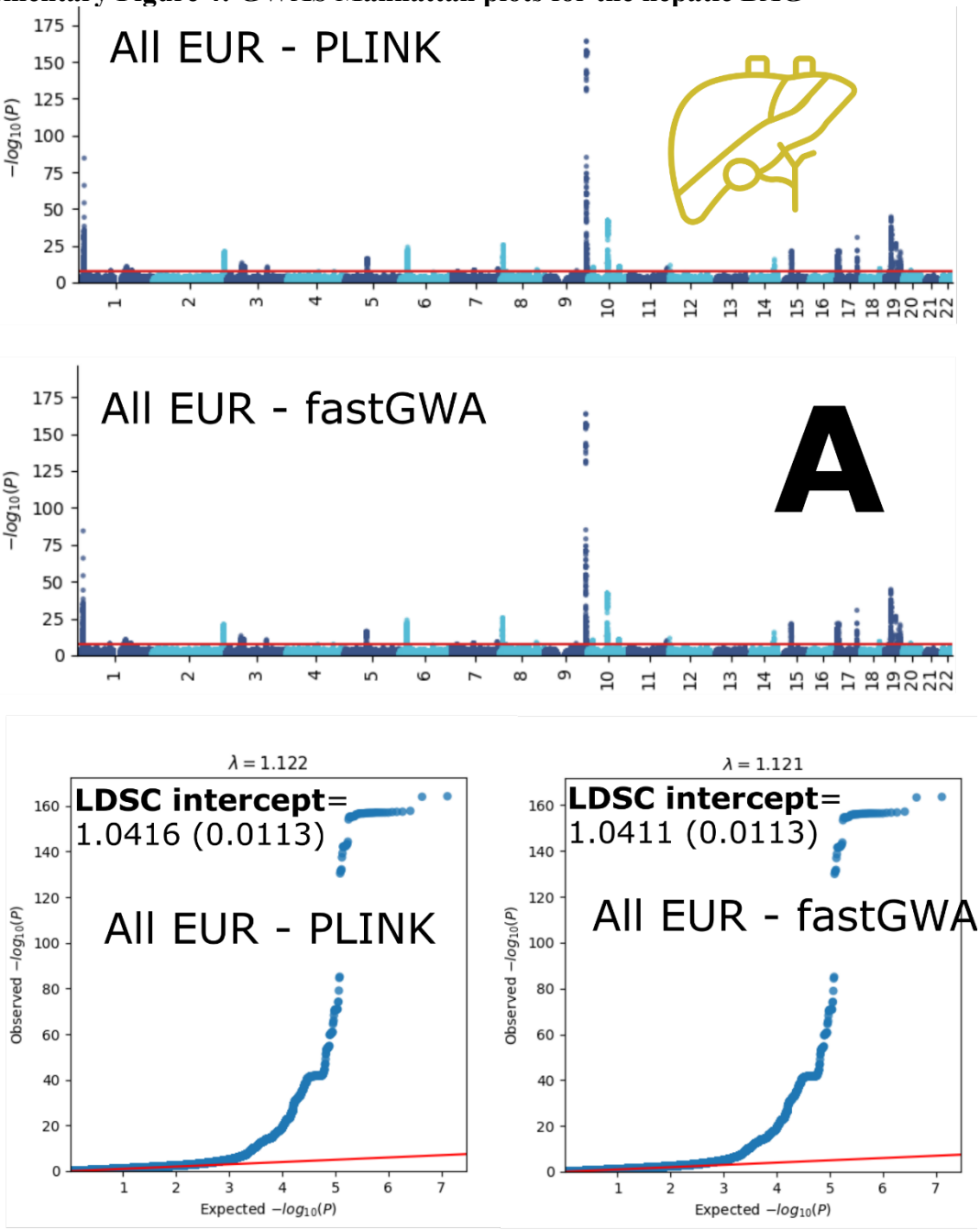

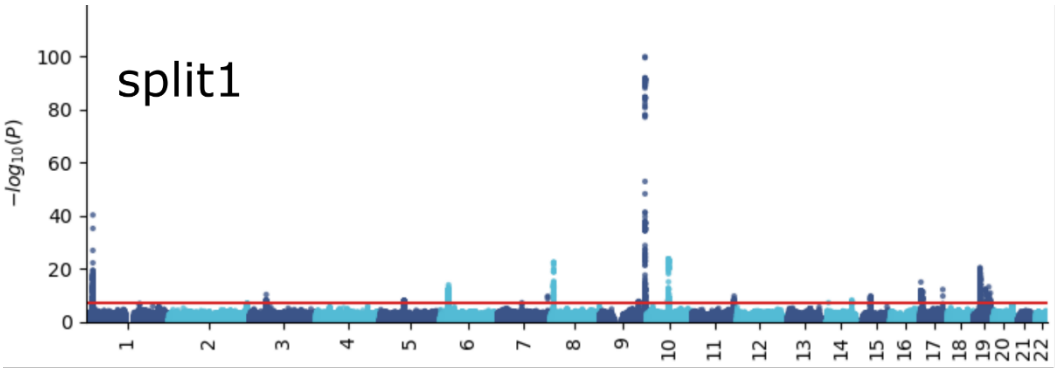
split1
$-log_{10}(P)$
100
80
60
40
20
0
1
2
3
4
5
6
7
8
9
10
11
12
13
14
15
16
17
18
19
20
21
22

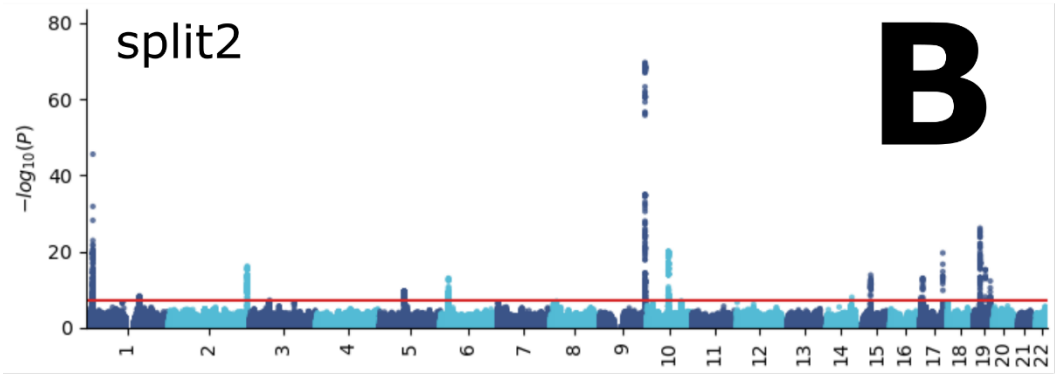
split2
B
$-log_{10}(P)$
80
60
40
20
0
1
2
3
4
5
6
7
8
9
10
11
12
13
14
15
16
17
18
19
20
21
22

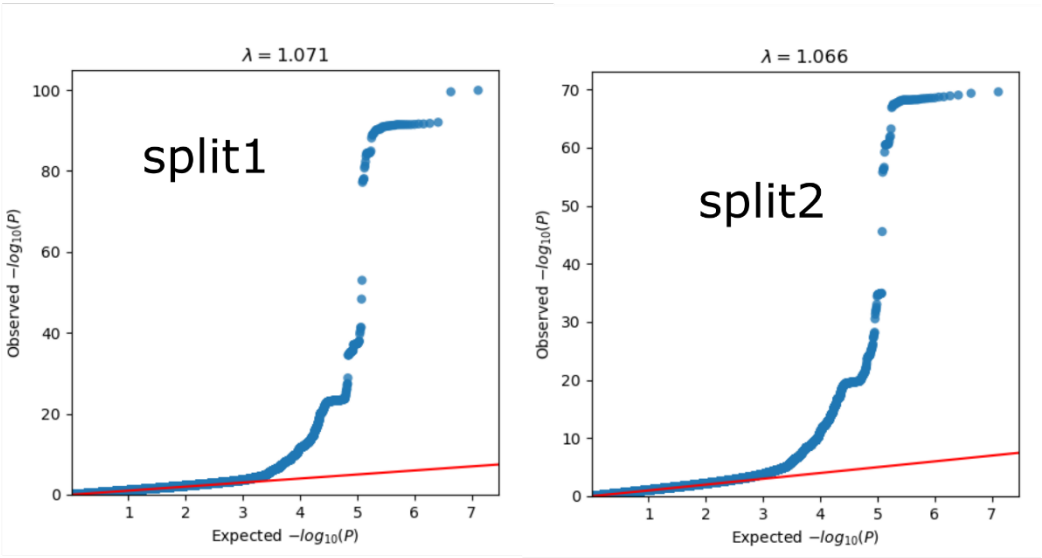
$\lambda = 1.071$
split1
Observed $-log_{10}(P)$
Expected $-log_{10}(P)$
$\lambda = 1.066$
split2
Observed $-log_{10}(P)$
Expected $-log_{10}(P)$

414

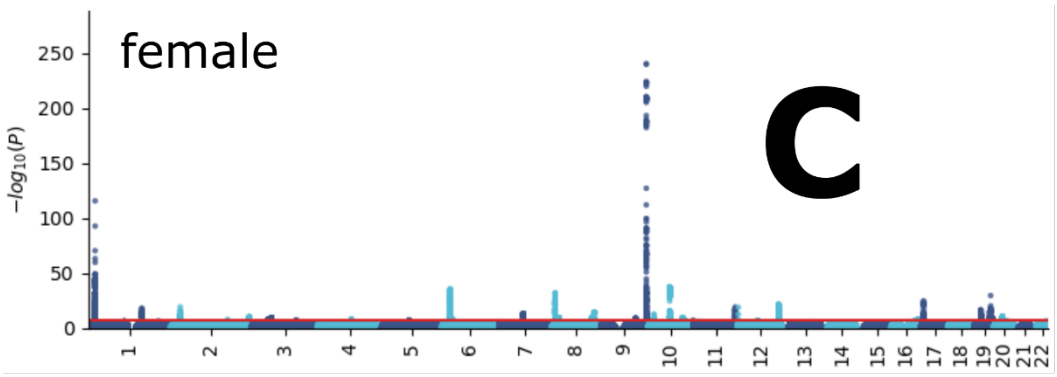
female
C
$-log_{10}(P)$
250
200
150
100
50
0
1
2
3
4
5
6
7
8
9
10
11
12
13
14
15
16
17
18
19
20
21
22

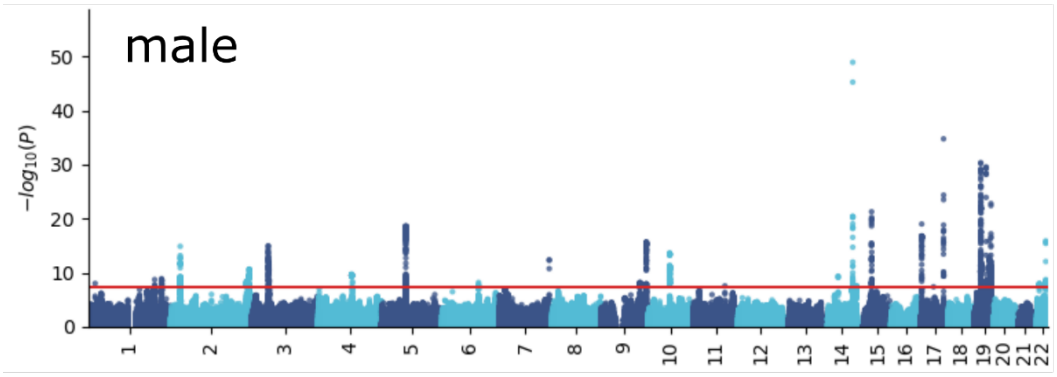
male
$-log_{10}(P)$
50
40
30
20
10
0
1
2
3
4
5
6
7
8
9
10
11
12
13
14
15
16
17
18
19
20
21
22

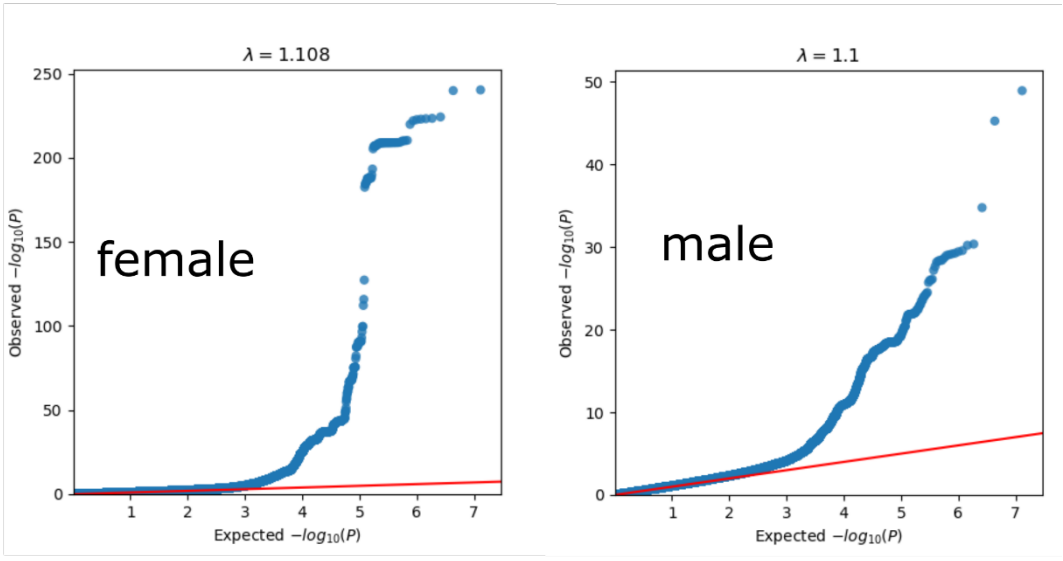
$\lambda = 1.108$
female
Observed $-log_{10}(P)$
Expected $-log_{10}(P)$
250
200
150
100
50
0
1
2
3
4
5
6
7
$\lambda = 1.1$
male
Observed $-log_{10}(P)$
Expected $-log_{10}(P)$
50
40
30
20
10
0
1
2
3
4
5
6
7

415

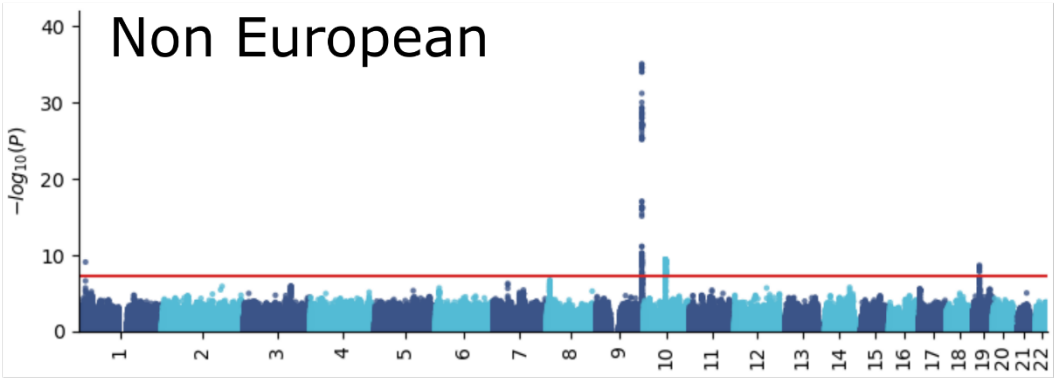

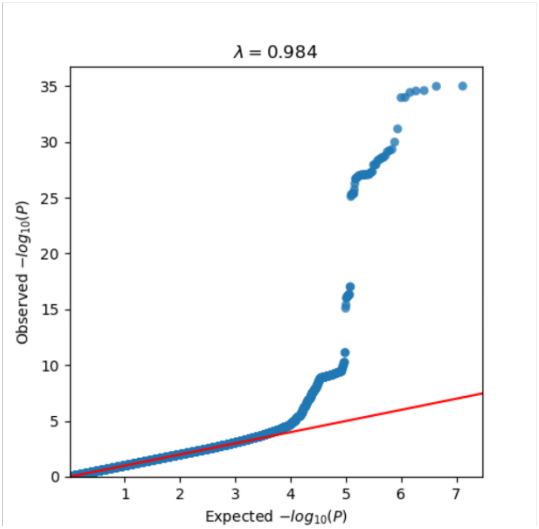

D

Manhattan and QQ plots, along with genomic inflation factors and LDSC intercepts, are displayed for the primary GWAS conducted on individuals of European ancestry (*N*=111,386) using PLINK and fastGWA (**A**). Additionally, results are presented for split-sample GWAS (split1 and split2, **B**), sex-stratified GWAS (female and male, **C**), and GWAS involving non-European ancestry populations (*N*=20,408, **D**). All P-values were two-sided, and a genome-wide P-values threshold was used.

Supplementary Figure 5: GWAS Manhattan plots for the immune BAG

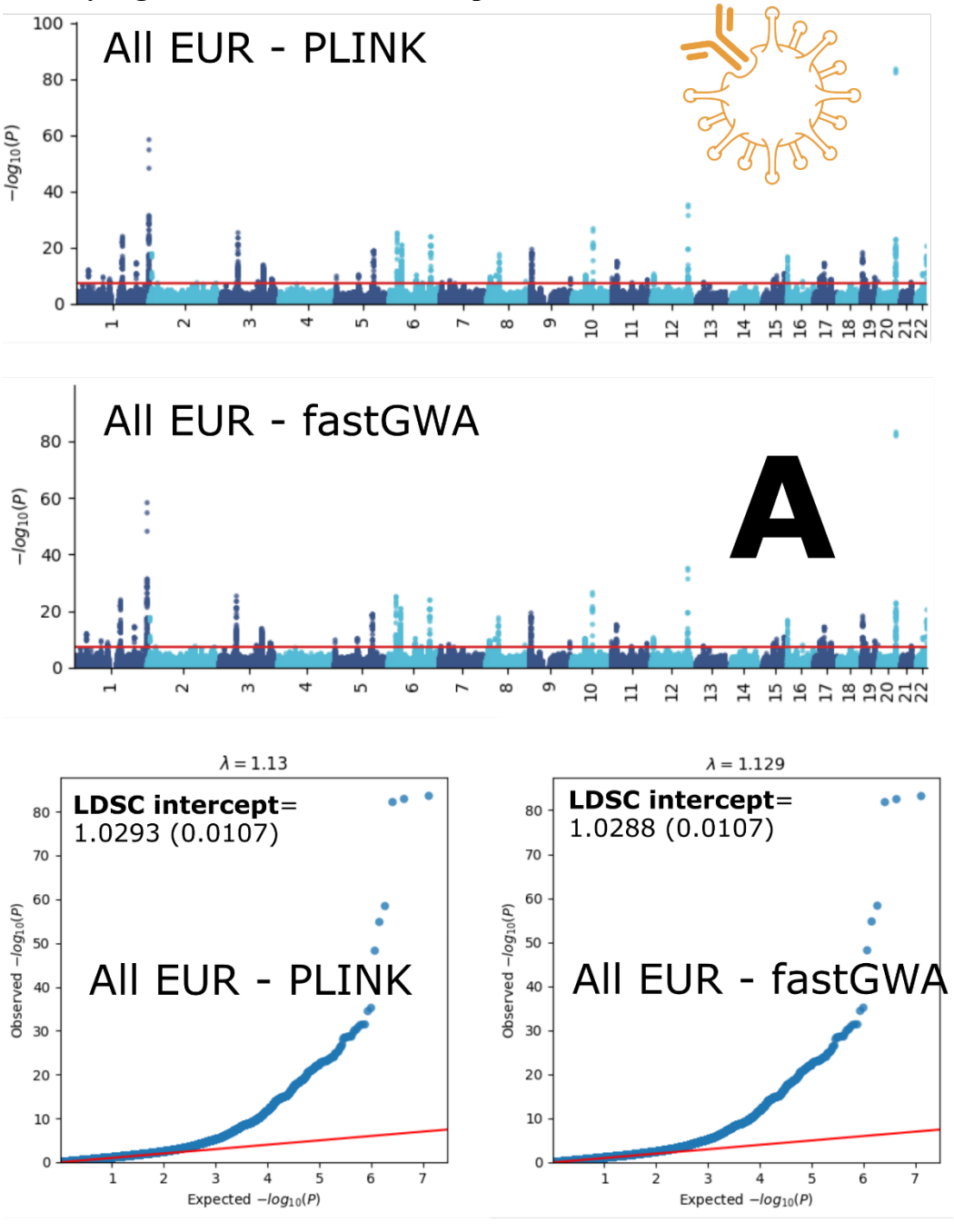

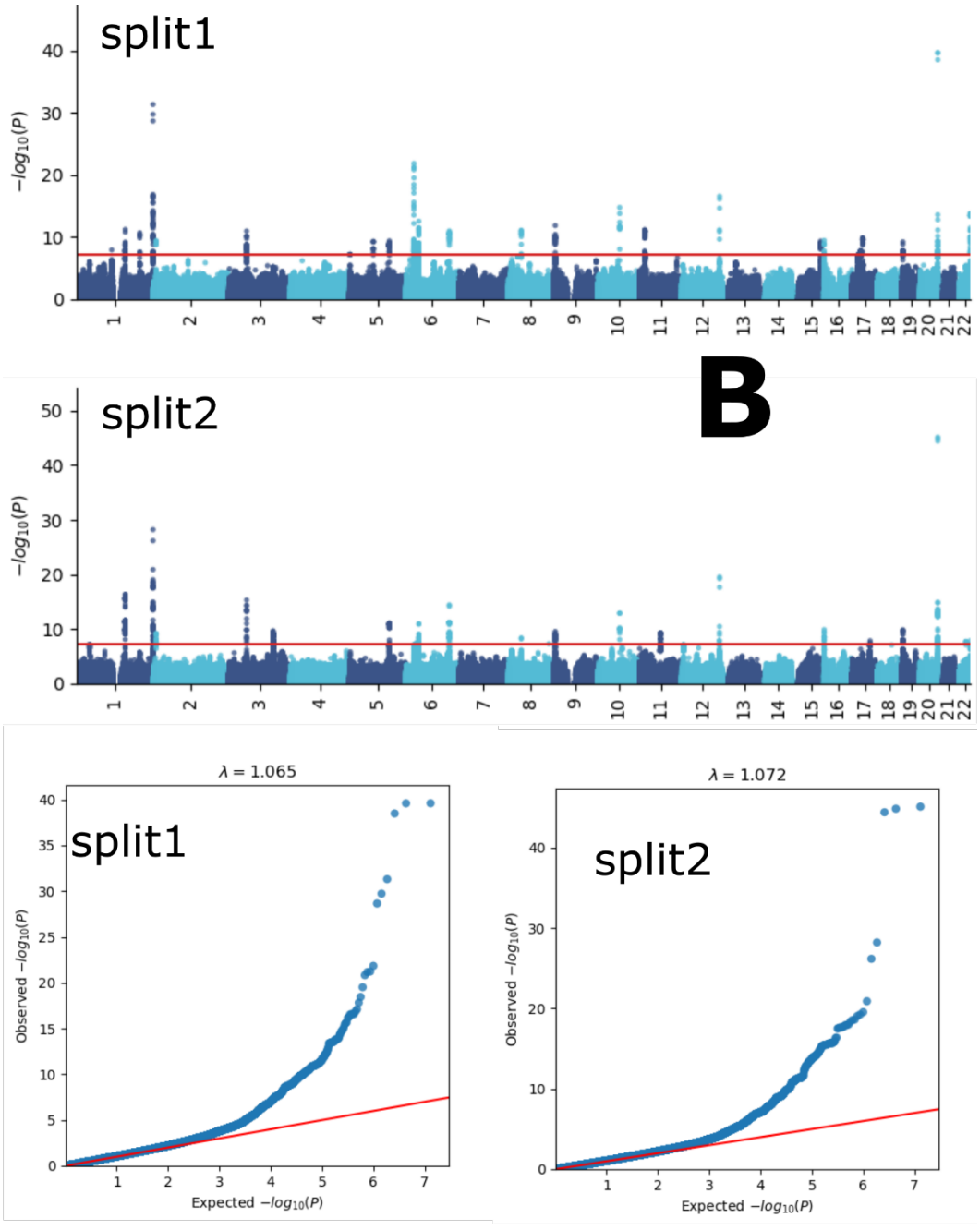
split1
split2
B
$-log_{10}(P)$
λ = 1.065
λ = 1.072
Observed $-log_{10}(P)$
Expected $-log_{10}(P)$

425

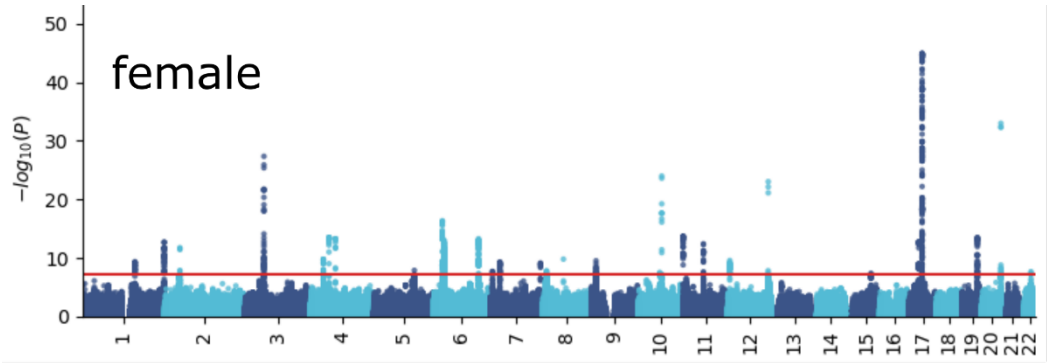
female
$-log_{10}(P)$
50
40
30
20
10
0
1
2
3
4
5
6
7
8
9
10
11
12
13
14
15
16
17
18
19
20
21
22

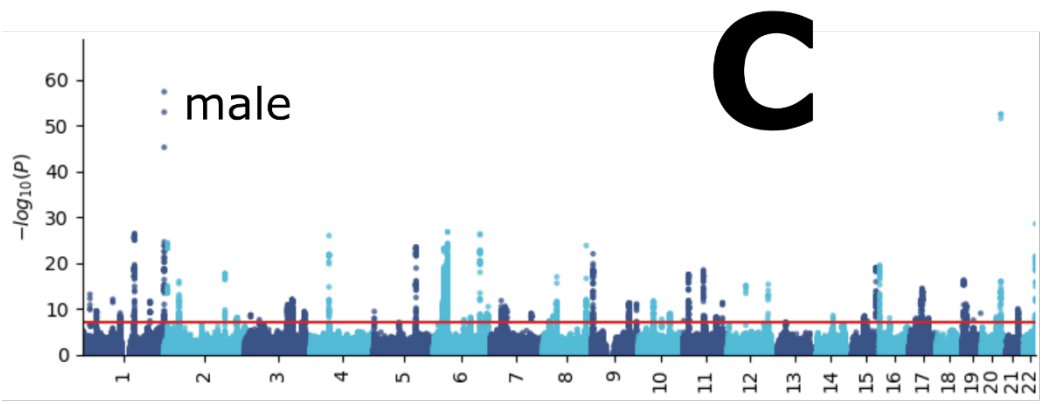
C
male
$-log_{10}(P)$
60
50
40
30
20
10
0
1
2
3
4
5
6
7
8
9
10
11
12
13
14
15
16
17
18
19
20
21
22

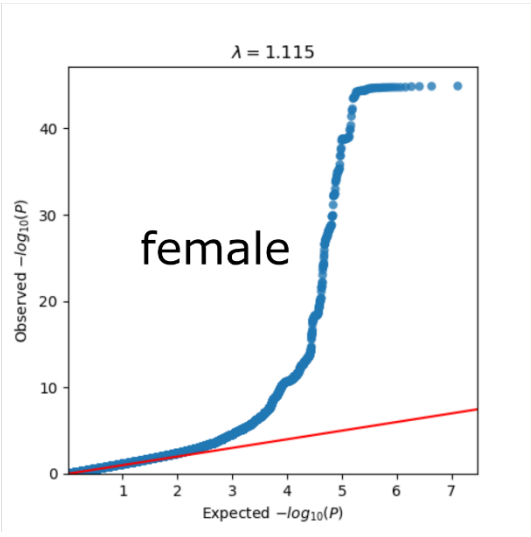
$\lambda = 1.115$
female
Observed $-log_{10}(P)$
Expected $-log_{10}(P)$
0
10
20
30
40
1
2
3
4
5
6
7

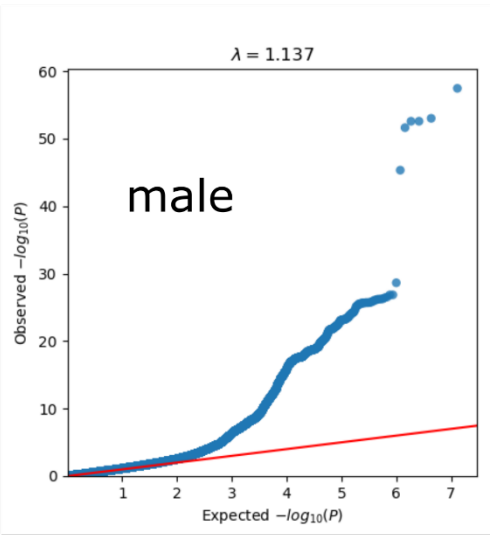
$\lambda = 1.137$
male
Observed $-log_{10}(P)$
Expected $-log_{10}(P)$
0
10
20
30
40
50
60
1
2
3
4
5
6
7

426

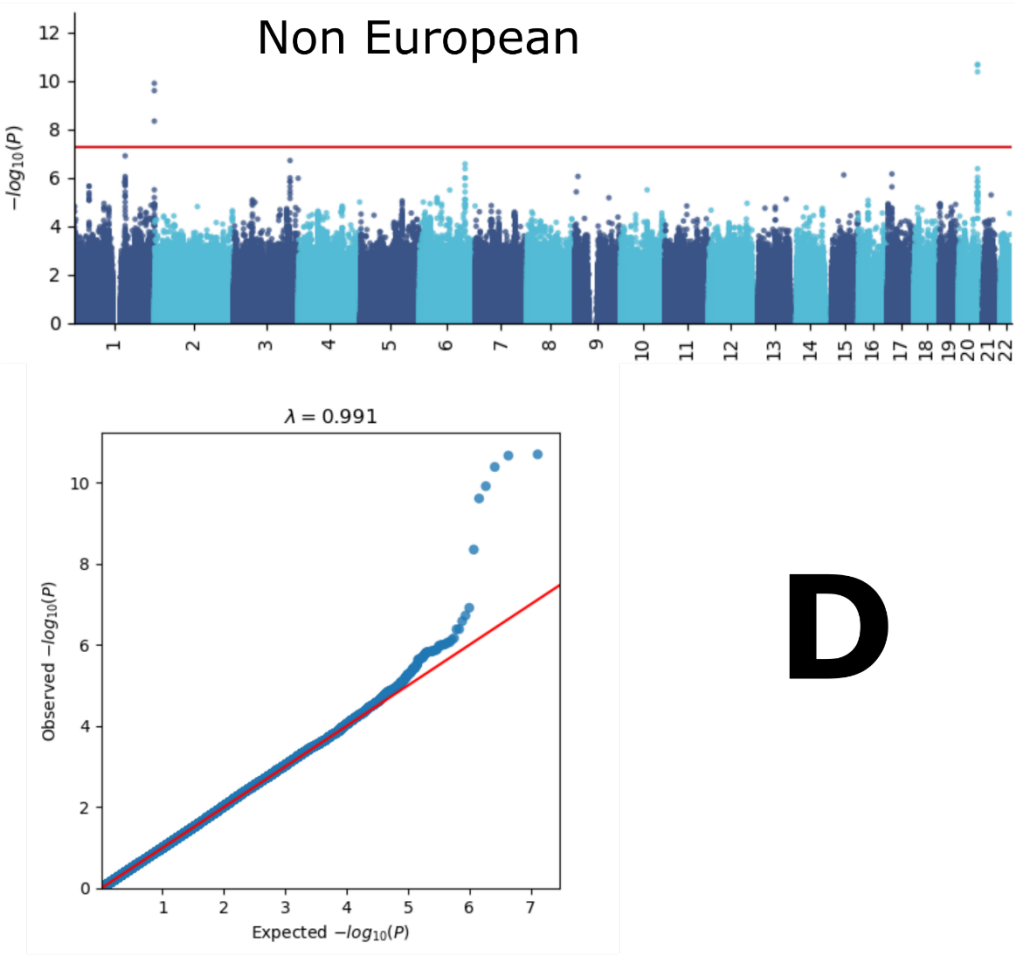

Manhattan and QQ plots, along with genomic inflation factors and LDSC intercepts, are displayed for the primary GWAS conducted on individuals of European ancestry (*N*=111,386) using PLINK and fastGWA (**A**). Additionally, results are presented for split-sample GWAS (split1 and split2, **B**), sex-stratified GWAS (female and male, **C**), and GWAS involving non-European ancestry populations (*N*=20,408, **D**). All P-values were two-sided, and a genome-wide P-values threshold was used.

Supplementary Figure 6: GWAS Manhattan plots for the metabolic BAG

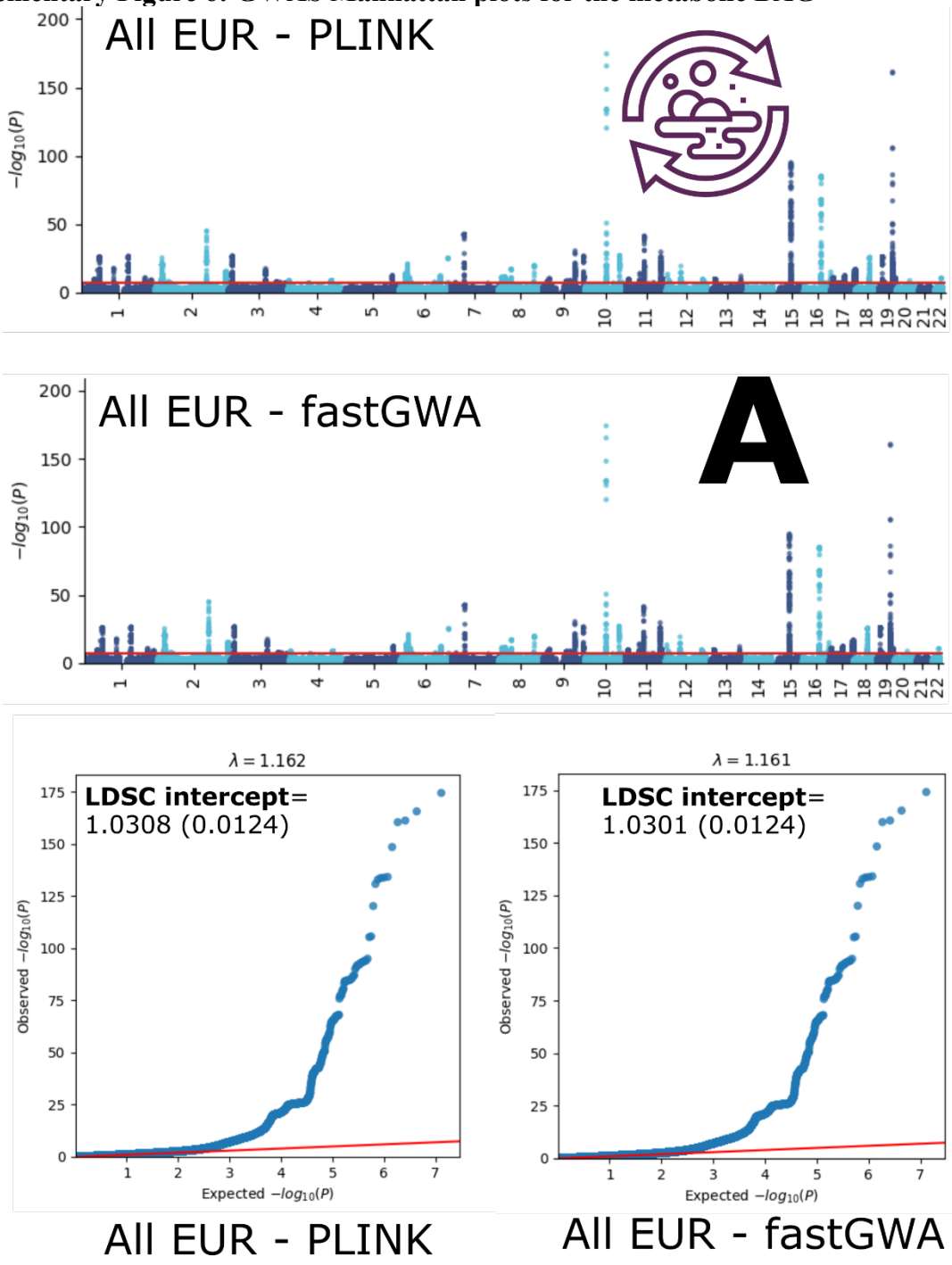

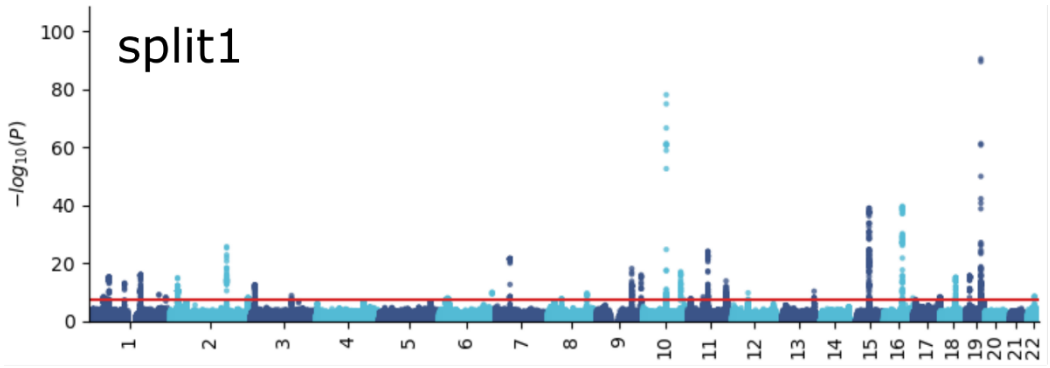
split1
$-log_{10}(P)$
100
80
60
40
20
0
1 2 3 4 5 6 7 8 9 10 11 12 13 14 15 16 17 18 19 20 21 22

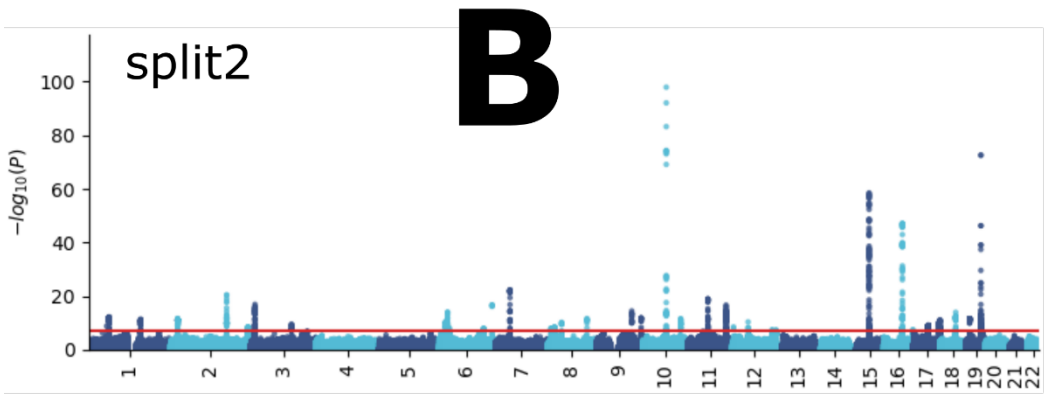
split2
B
$-log_{10}(P)$
100
80
60
40
20
0
1 2 3 4 5 6 7 8 9 10 11 12 13 14 15 16 17 18 19 20 21 22

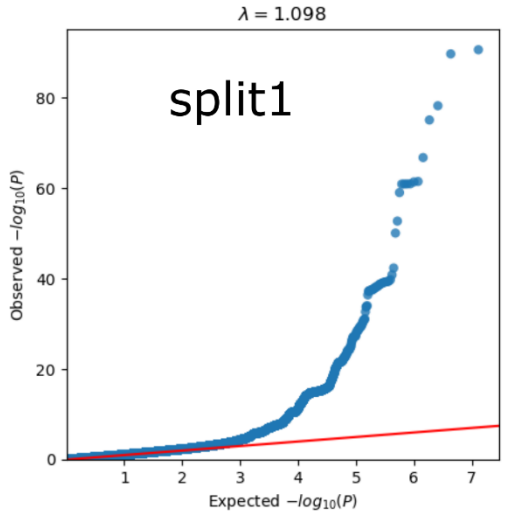
$\lambda = 1.098$
split1
Observed $-log_{10}(P)$
Expected $-log_{10}(P)$
0
20
40
60
80
1 2 3 4 5 6 7

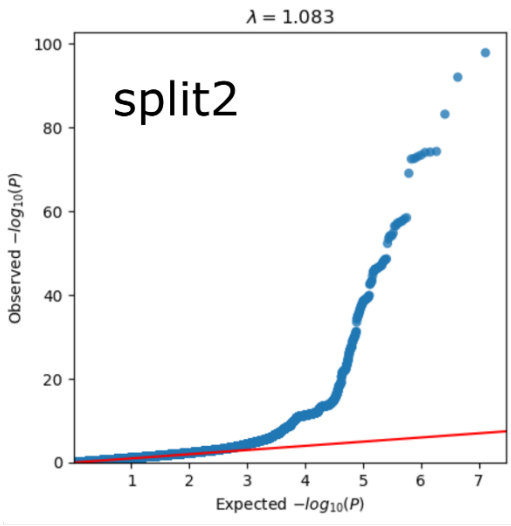
$\lambda = 1.083$
split2
Observed $-log_{10}(P)$
Expected $-log_{10}(P)$
0
20
40
60
80
100
1 2 3 4 5 6 7

436

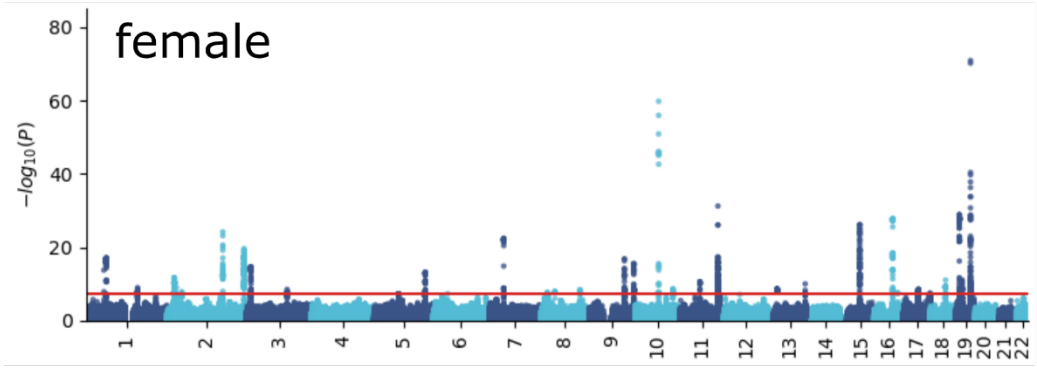
female
$-log_{10}(P)$
0
20
40
60
80
1
2
3
4
5
6
7
8
9
10
11
12
13
14
15
16
17
18
19
20
21
22

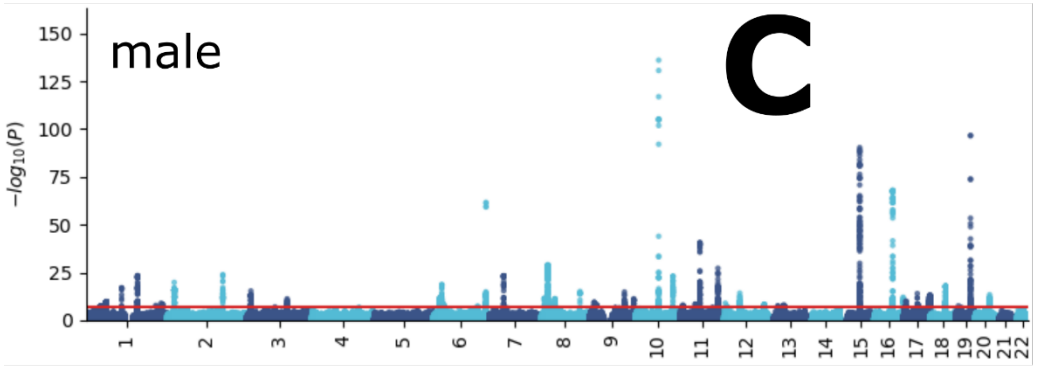
male
C
$-log_{10}(P)$
0
25
50
75
100
125
150
1
2
3
4
5
6
7
8
9
10
11
12
13
14
15
16
17
18
19
20
21
22

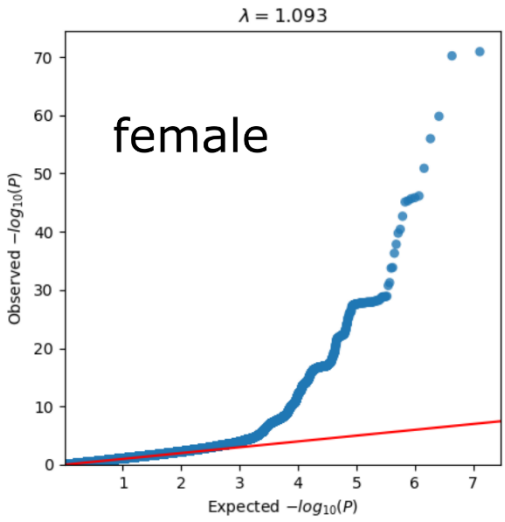
$\lambda = 1.093$
female
Observed $-log_{10}(P)$
Expected $-log_{10}(P)$
0
10
20
30
40
50
60
70
1
2
3
4
5
6
7

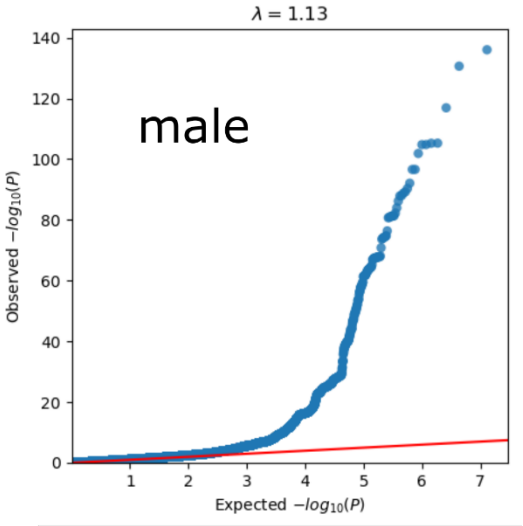
$\lambda = 1.13$
male
Observed $-log_{10}(P)$
Expected $-log_{10}(P)$
0
20
40
60
80
100
120
140
1
2
3
4
5
6
7

437

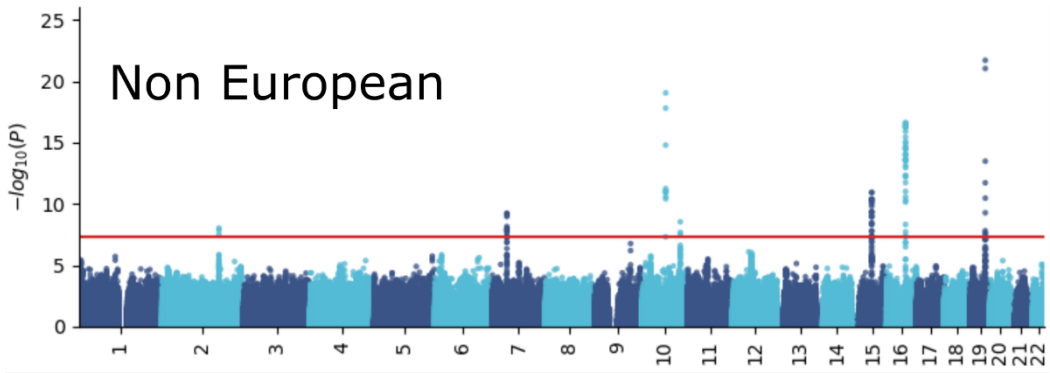

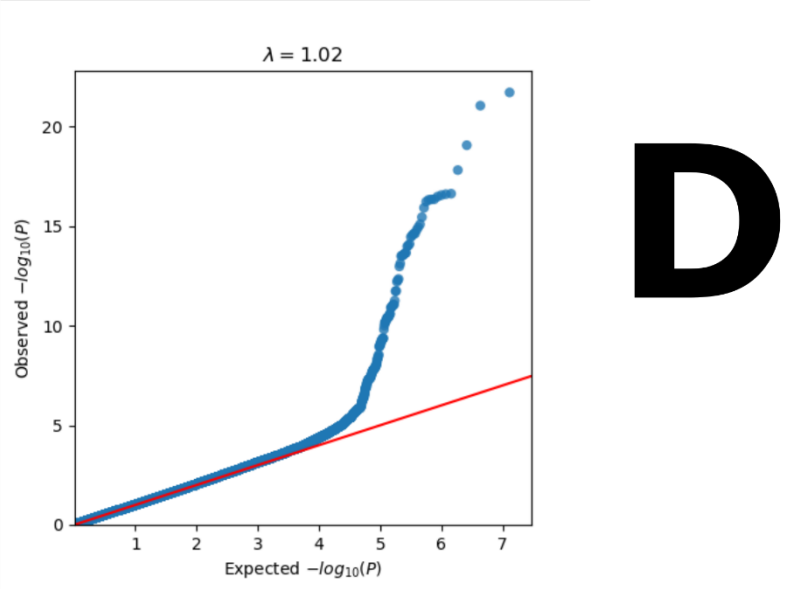

D

Manhattan and QQ plots, along with genomic inflation factors and LDSC intercepts, are displayed for the primary GWAS conducted on individuals of European ancestry (*N*=111,386) using PLINK and fastGWA (**A**). Additionally, results are presented for split-sample GWAS (split1 and split2, **B**), sex-stratified GWAS (female and male, **C**), and GWAS involving non-European ancestry populations (*N*=20,408, **D**). All P-values were two-sided, and a genome-wide P-values threshold was used.

Supplementary Figure 7: GWAS Manhattan plots for the musculoskeletal BAG

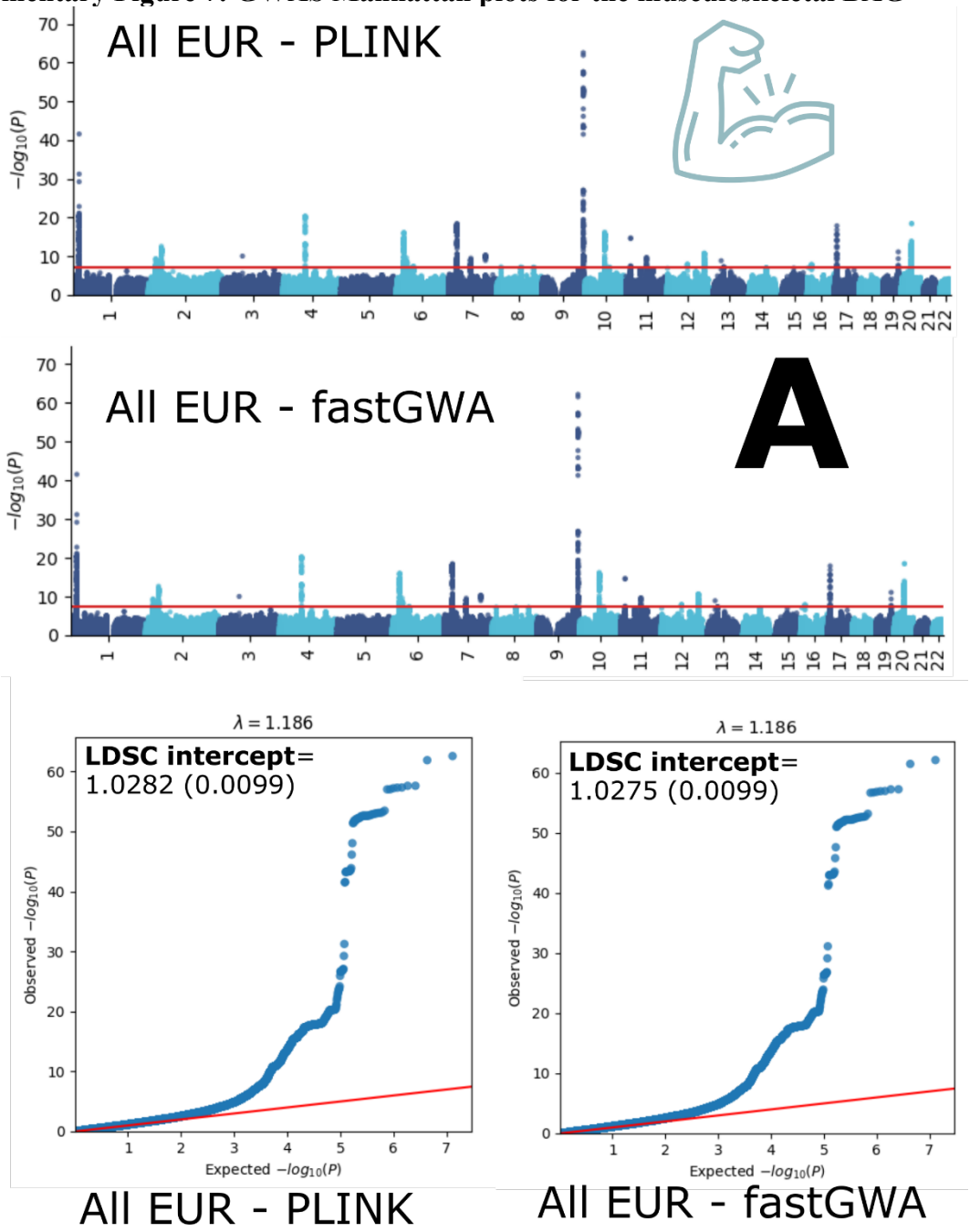

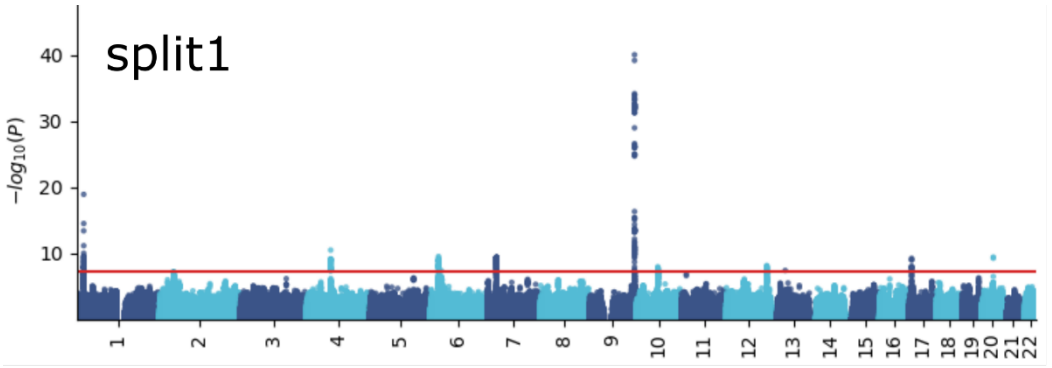
split1
$-log_{10}(P)$
40
30
20
10
1
2
3
4
5
6
7
8
9
10
11
12
13
14
15
16
17
18
19
20
21
22

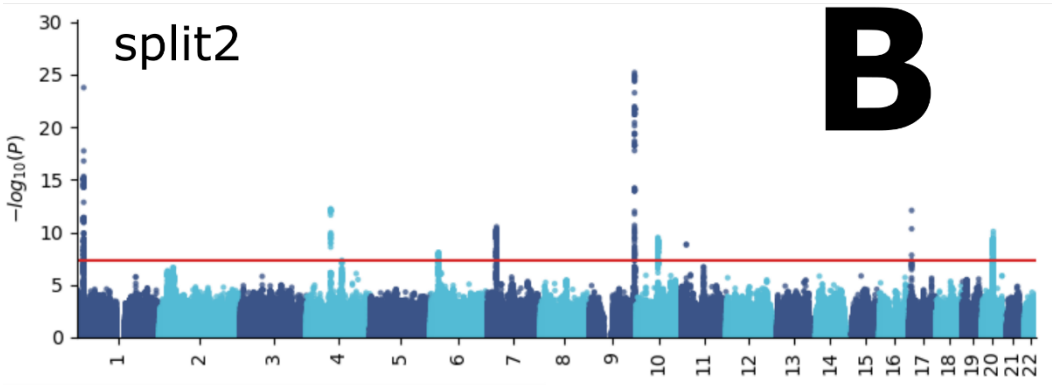
split2
B
$-log_{10}(P)$
30
25
20
15
10
5
0
1
2
3
4
5
6
7
8
9
10
11
12
13
14
15
16
17
18
19
20
21
22

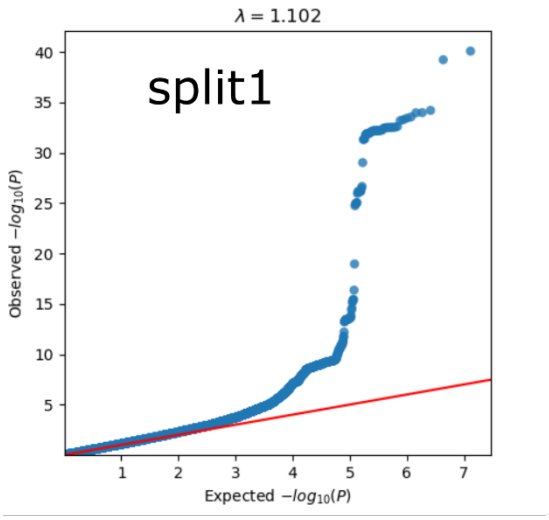
$\lambda = 1.102$
split1
Observed $-log_{10}(P)$
Expected $-log_{10}(P)$
40
35
30
25
20
15
10
5
1
2
3
4
5
6
7

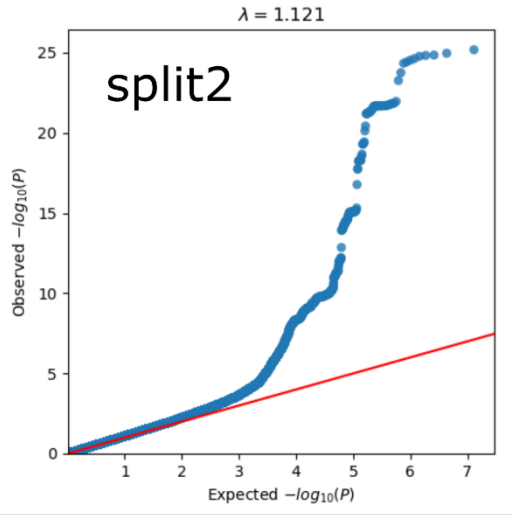
$\lambda = 1.121$
split2
Observed $-log_{10}(P)$
Expected $-log_{10}(P)$
25
20
15
10
5
0
1
2
3
4
5
6
7

447

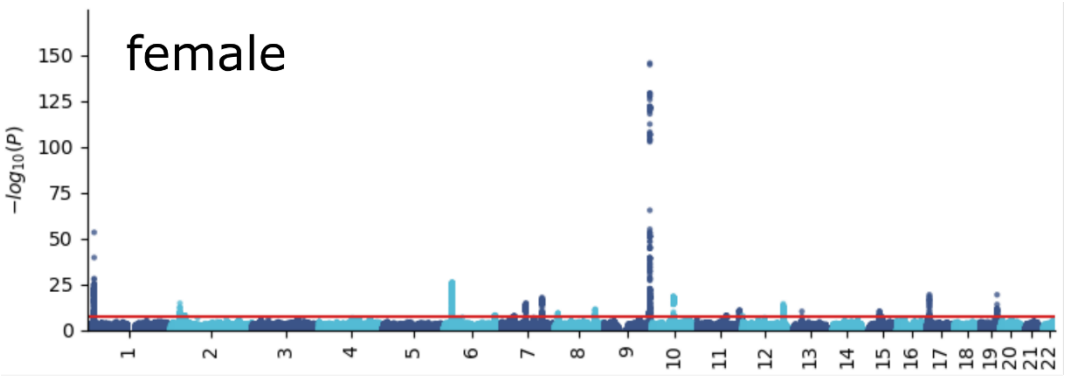
female
$-log_{10}(P)$
150
125
100
75
50
25
0
1
2
3
4
5
6
7
8
9
10
11
12
13
14
15
16
17
18
19
20
21
22

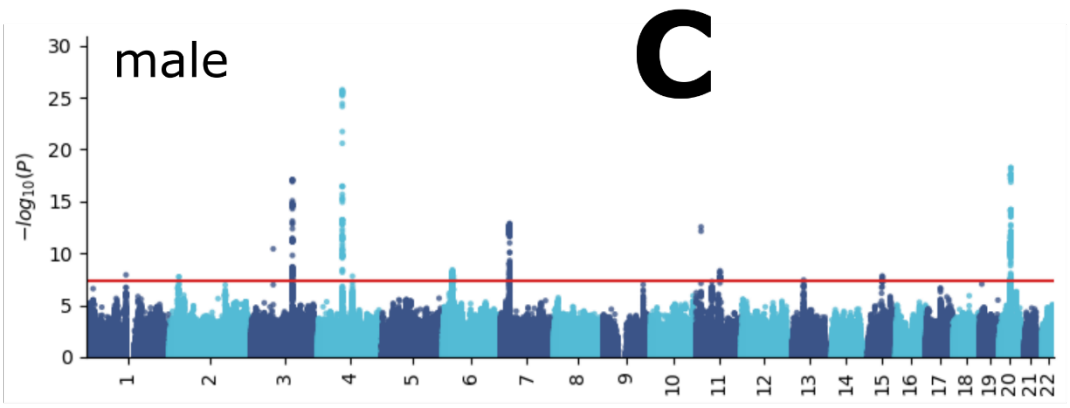
male
C
$-log_{10}(P)$
30
25
20
15
10
5
0
1
2
3
4
5
6
7
8
9
10
11
12
13
14
15
16
17
18
19
20
21
22

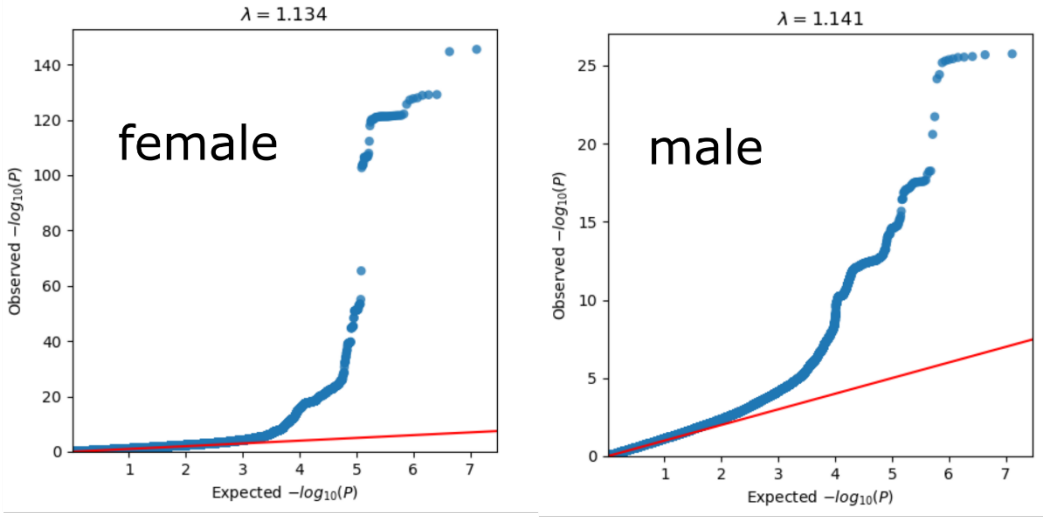
$\lambda = 1.134$
female
Observed $-log_{10}(P)$
Expected $-log_{10}(P)$
$\lambda = 1.141$
male
Observed $-log_{10}(P)$
Expected $-log_{10}(P)$

448

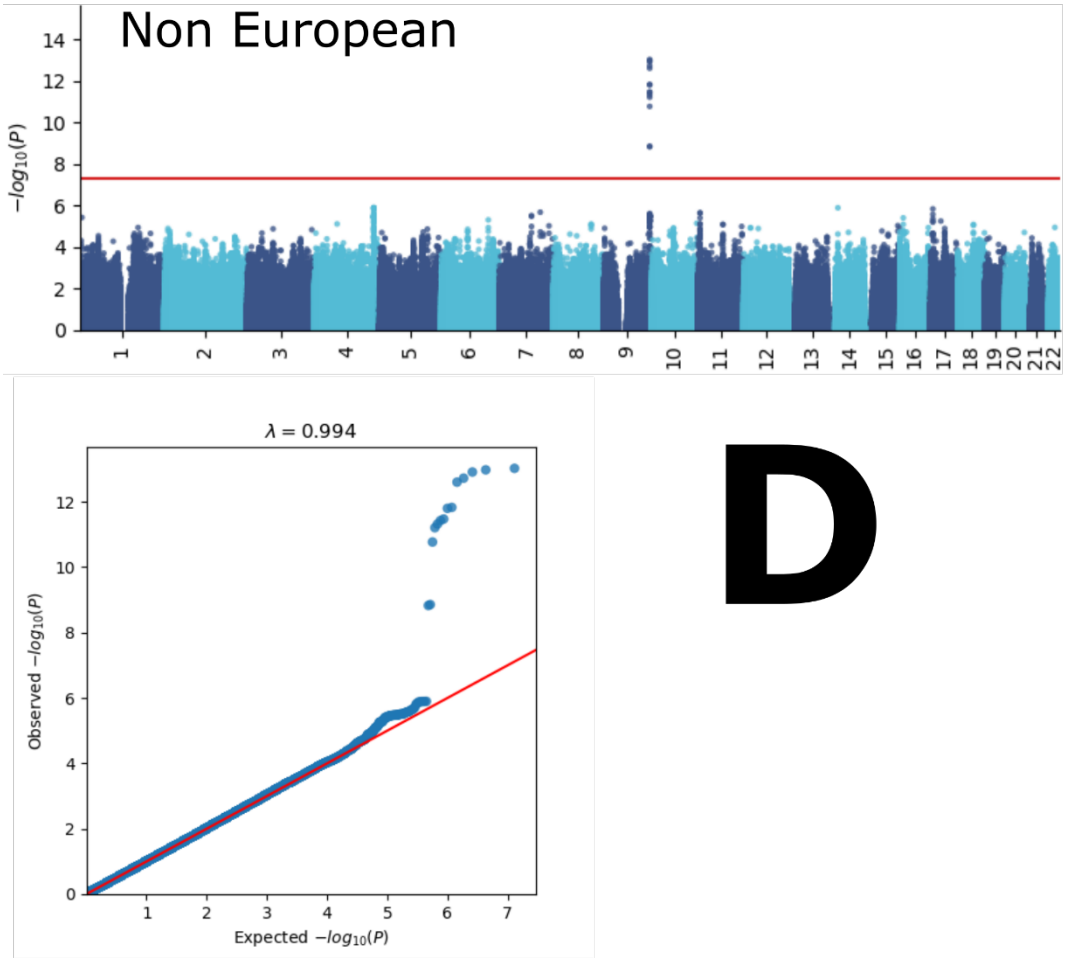

Manhattan and QQ plots, along with genomic inflation factors and LDSC intercepts, are displayed for the primary GWAS conducted on individuals of European ancestry (*N*=111,386) using PLINK and fastGWA (**A**). Additionally, results are presented for split-sample GWAS (split1 and split2, **B**), sex-stratified GWAS (female and male, **C**), and GWAS involving non-European ancestry populations (*N*=20,408, **D**). All P-values were two-sided, and a genome-wide P-values threshold was used.

Supplementary Figure 8: GWAS Manhattan plots for the pulmonary BAG

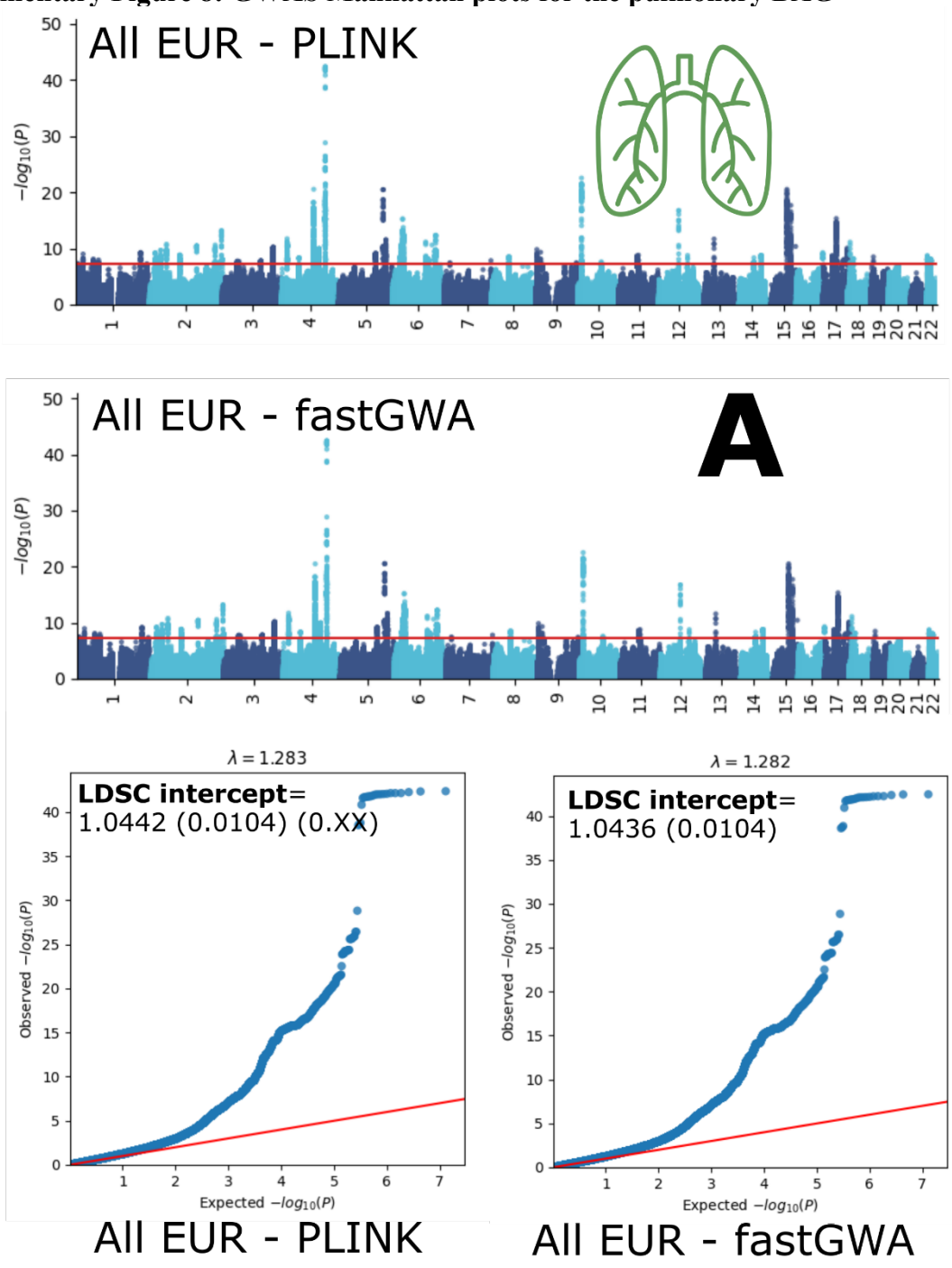

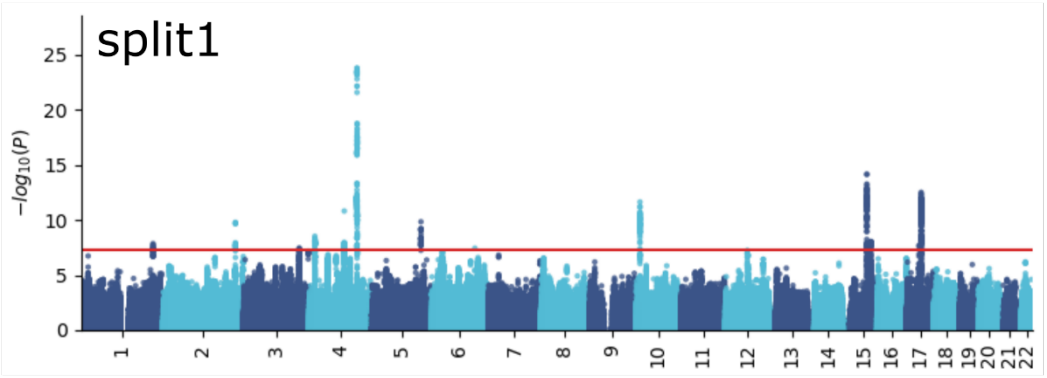
split1
$-log_{10}(P)$

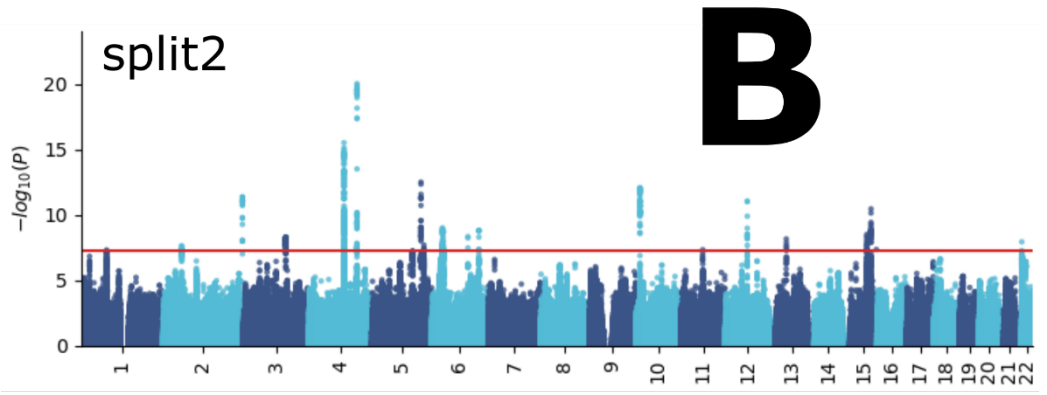
split2
B
$-log_{10}(P)$

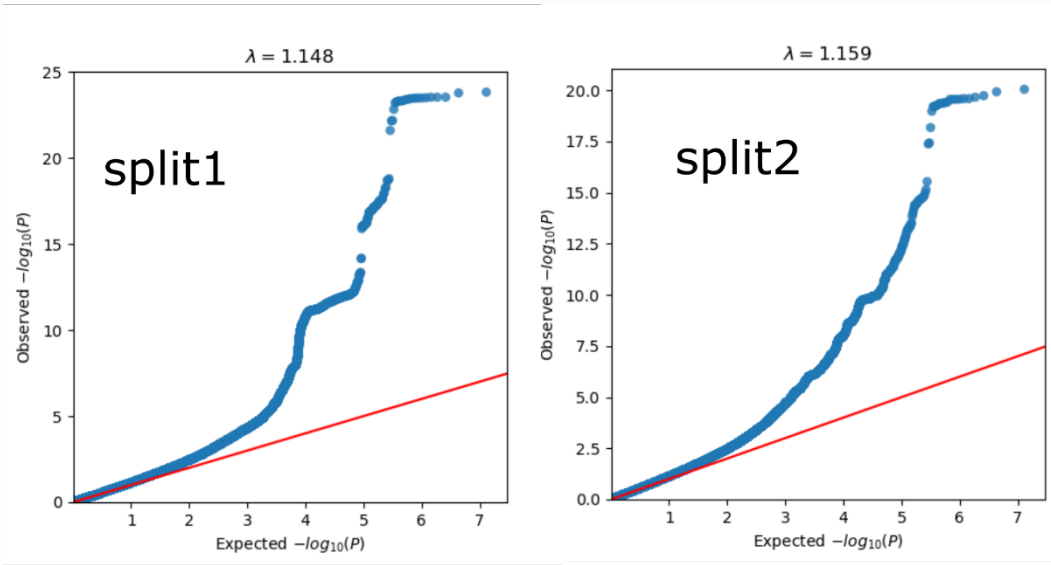
$\lambda = 1.148$
split1
Observed $-log_{10}(P)$
Expected $-log_{10}(P)$
$\lambda = 1.159$
split2
Observed $-log_{10}(P)$
Expected $-log_{10}(P)$

458

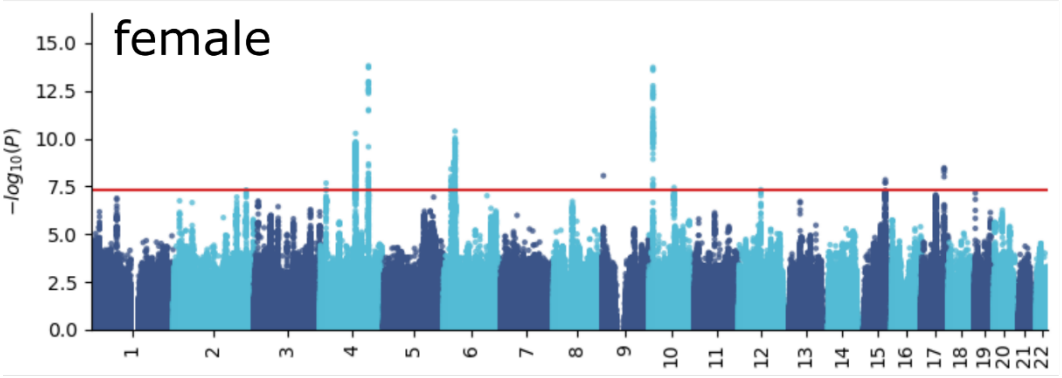
female
$-log_{10}(P)$
15.0
12.5
10.0
7.5
5.0
2.5
0.0
1 2 3 4 5 6 7 8 9 10 11 12 13 14 15 16 17 18 19 20 21 22

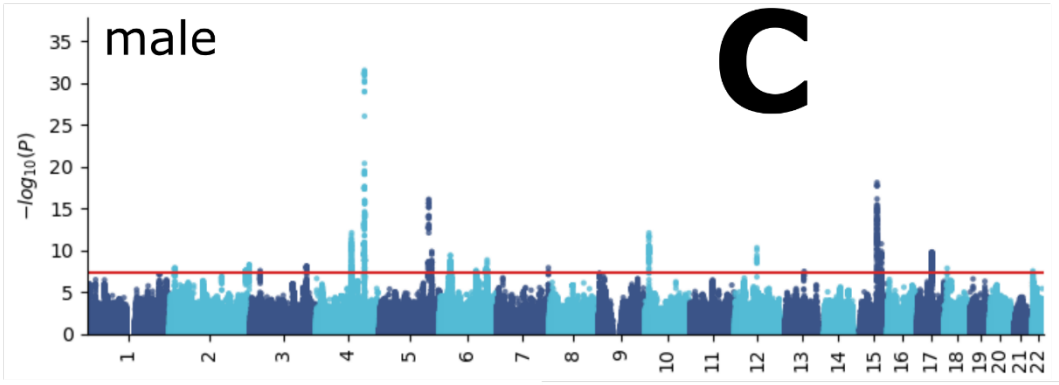
male
C
$-log_{10}(P)$
35
30
25
20
15
10
5
0
1 2 3 4 5 6 7 8 9 10 11 12 13 14 15 16 17 18 19 20 21 22

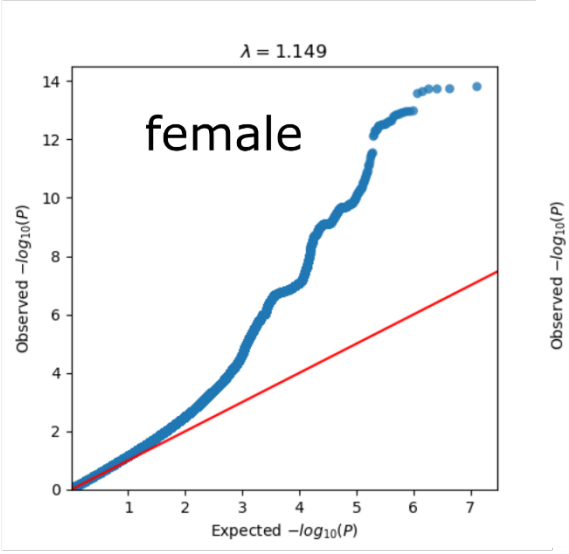
$\lambda = 1.149$
female
Observed $-log_{10}(P)$
Expected $-log_{10}(P)$
0 2 4 6 8 10 12 14
1 2 3 4 5 6 7

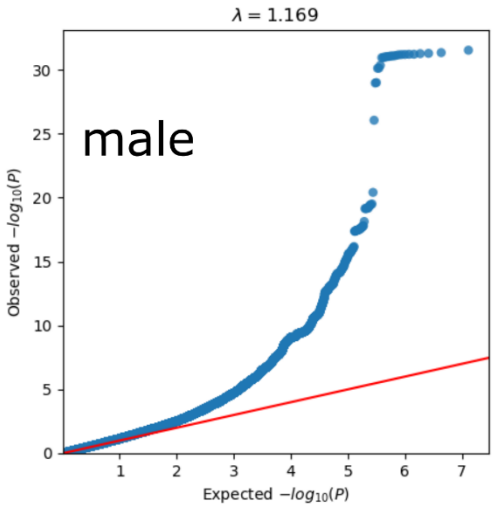
$\lambda = 1.169$
male
Observed $-log_{10}(P)$
Expected $-log_{10}(P)$
0 5 10 15 20 25 30
1 2 3 4 5 6 7

459

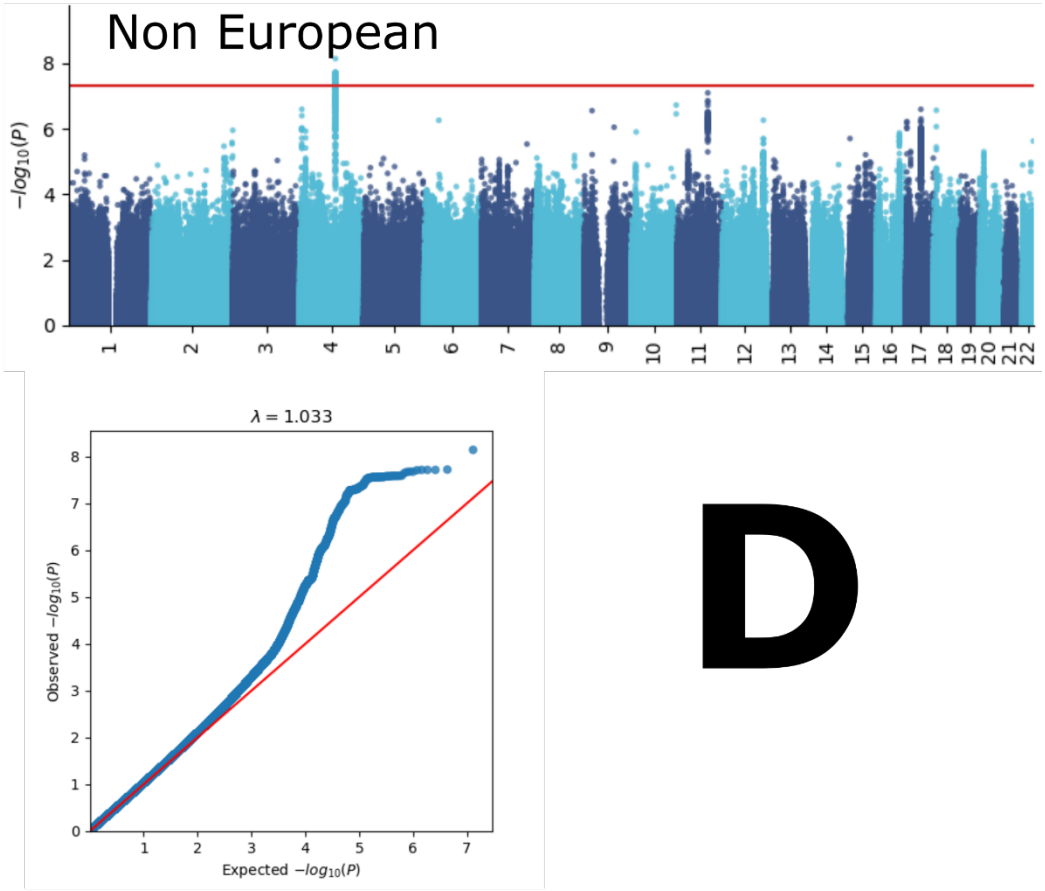

Manhattan and QQ plots, along with genomic inflation factors and LDSC intercepts, are displayed for the primary GWAS conducted on individuals of European ancestry (*N*=111,386) using PLINK and fastGWA (**A**). Additionally, results are presented for split-sample GWAS (split1 and split2, **B**), sex-stratified GWAS (female and male, **C**), and GWAS involving non-European ancestry populations (*N*=20,408, **D**). All P-values were two-sided, and a genome-wide P-values threshold was used.

Supplementary Figure 9: GWAS Manhattan plots for the renal BAG

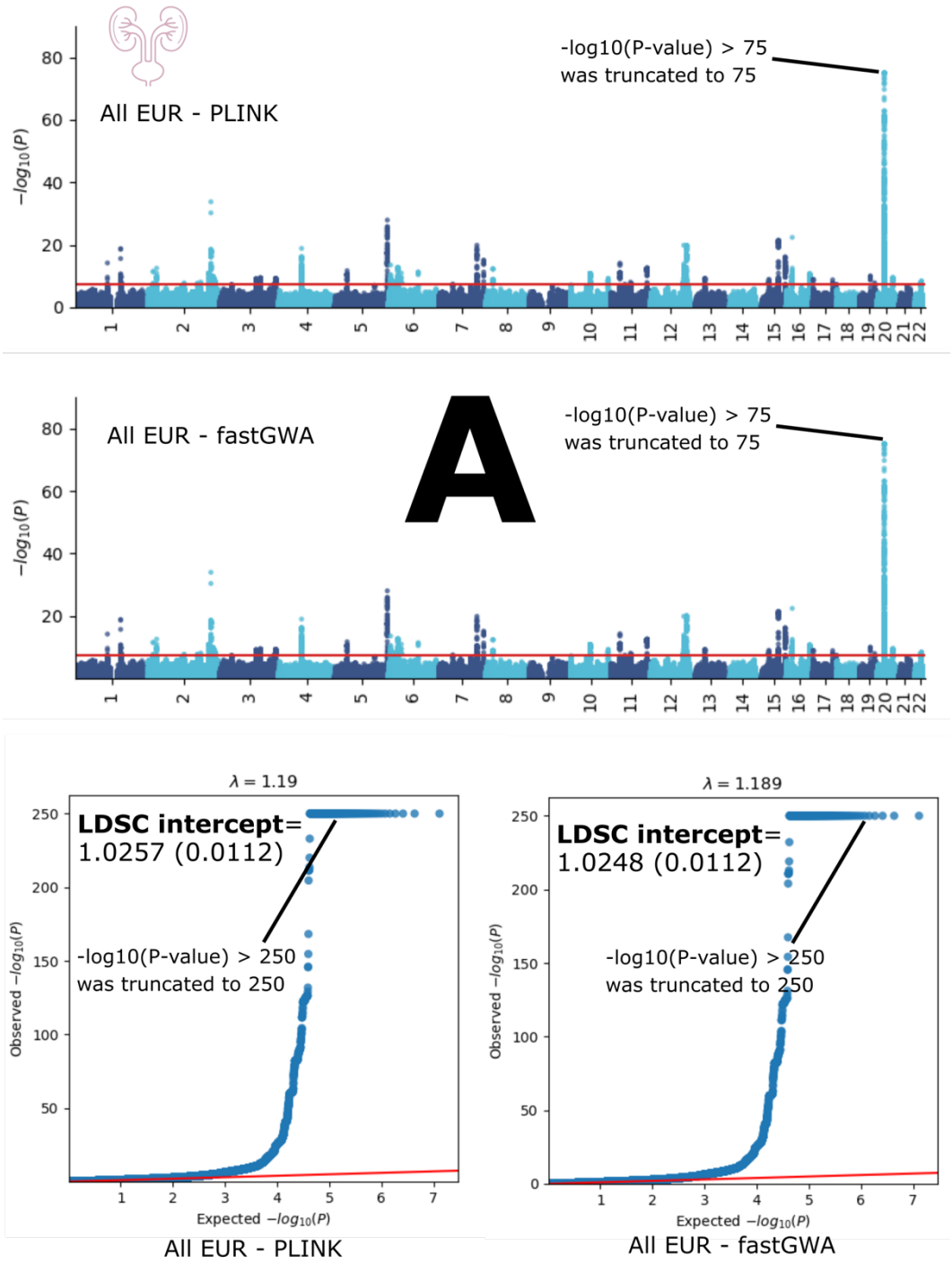

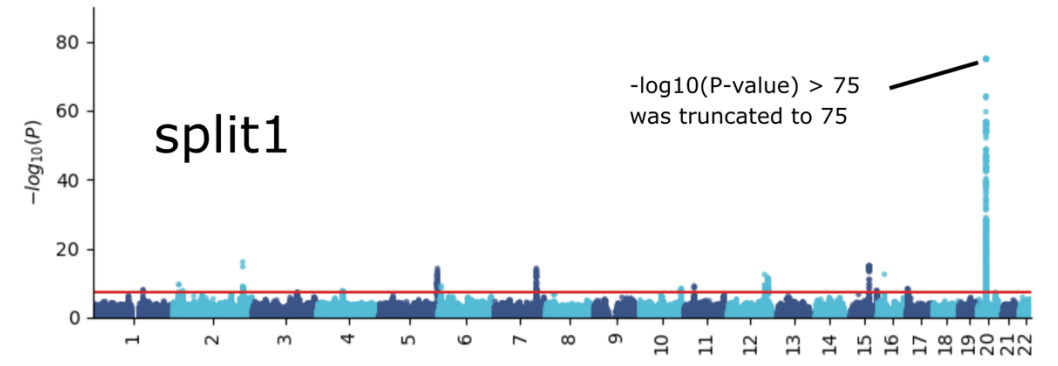
split1
-log10(P-value) > 75
was truncated to 75
$-log_{10}(P)$

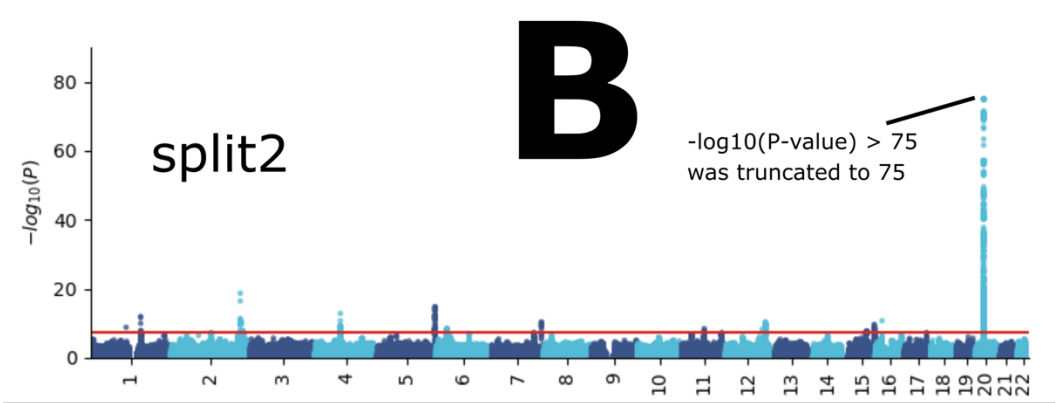
B
split2
-log10(P-value) > 75
was truncated to 75
$-log_{10}(P)$

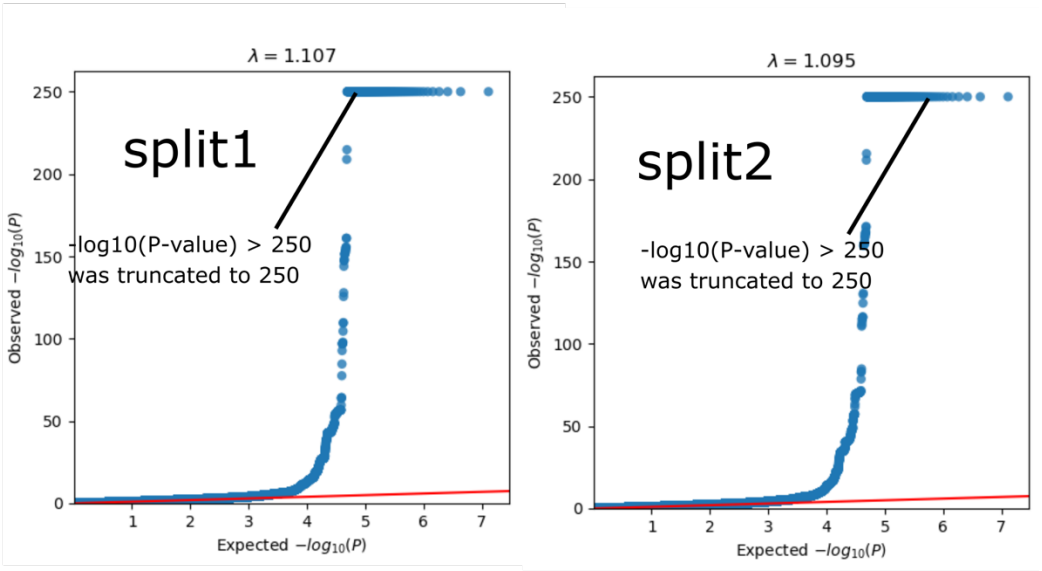
$\lambda = 1.107$
split1
-log10(P-value) > 250
was truncated to 250
Observed $-log_{10}(P)$
Expected $-log_{10}(P)$
$\lambda = 1.095$
split2
-log10(P-value) > 250
was truncated to 250
Observed $-log_{10}(P)$
Expected $-log_{10}(P)$

469

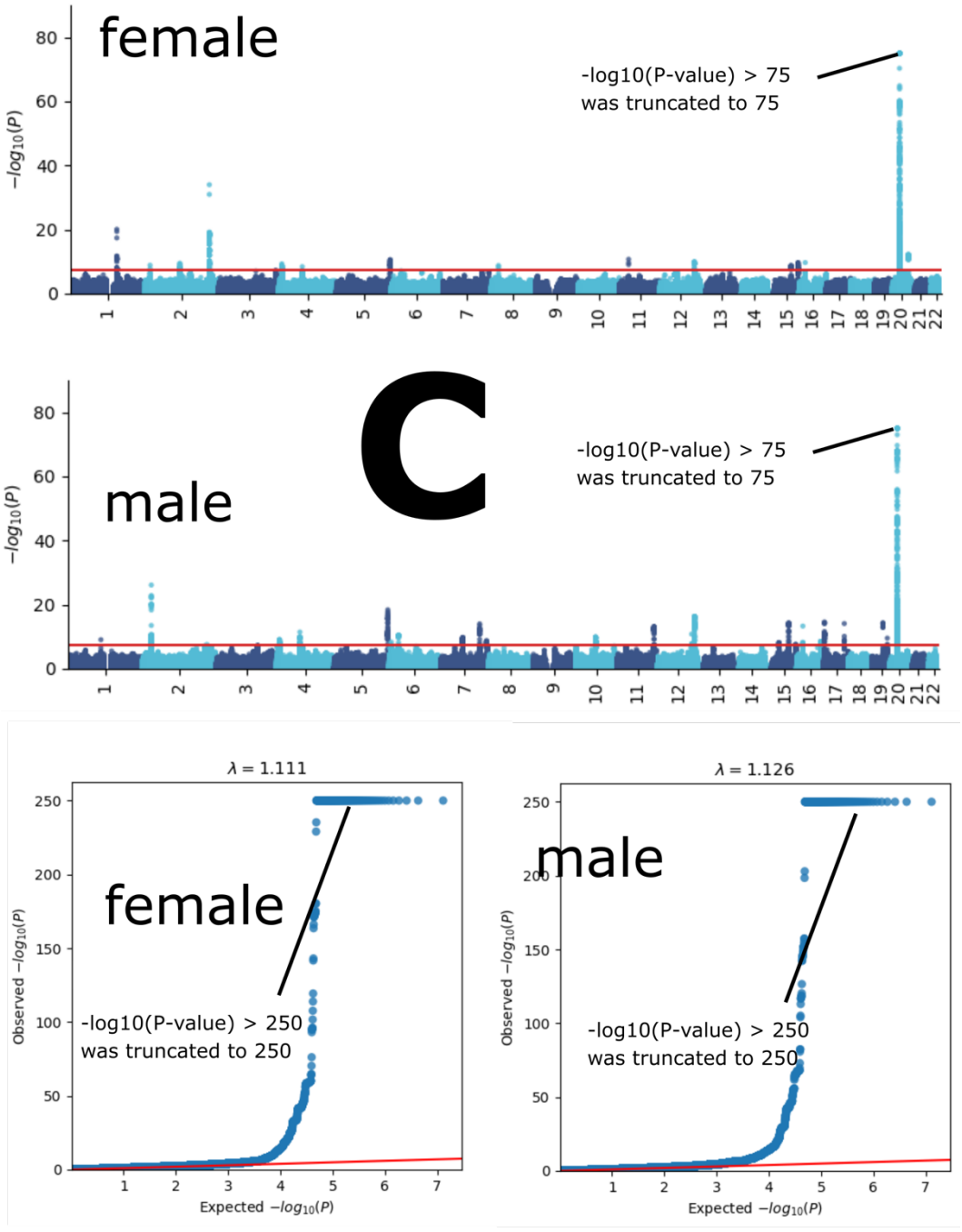
female
-log10(P-value) > 75
was truncated to 75
male
C
-log10(P-value) > 75
was truncated to 75
λ = 1.111
female
-log10(P-value) > 250
was truncated to 250
λ = 1.126
male
-log10(P-value) > 250
was truncated to 250
Observed −log10(P)
Expected −log10(P)

470

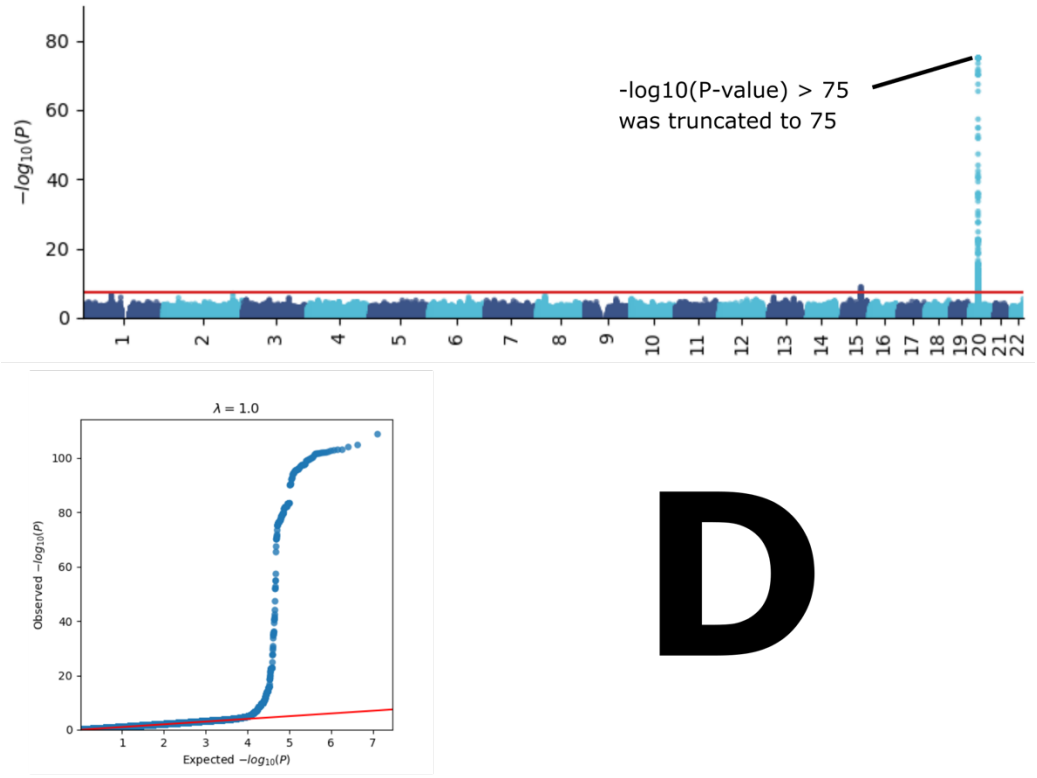

Manhattan and QQ plots, along with genomic inflation factors and LDSC intercepts, are displayed for the primary GWAS conducted on individuals of European ancestry (*N*=111,386) using PLINK and fastGWA (**A**). Additionally, results are presented for split-sample GWAS (split1 and split2, **B**), sex-stratified GWAS (female and male, **C**), and GWAS involving non-European ancestry populations (*N*=20,408, **D**). For visualization purposes, we chose to truncate the highly significant P-value (P-value<$1x10^{-300}$) to a lower P-value ($1x10^{-75}$ for Manhattan plots and $1x10^{-250}$ for QQ plots). All P-values were two-sided, and a genome-wide P-values threshold was used.

Supplementary Figure 10: Bayesian colocalization analysis for the locus on chromosome 6 between the hepatic and musculoskeletal BAGs

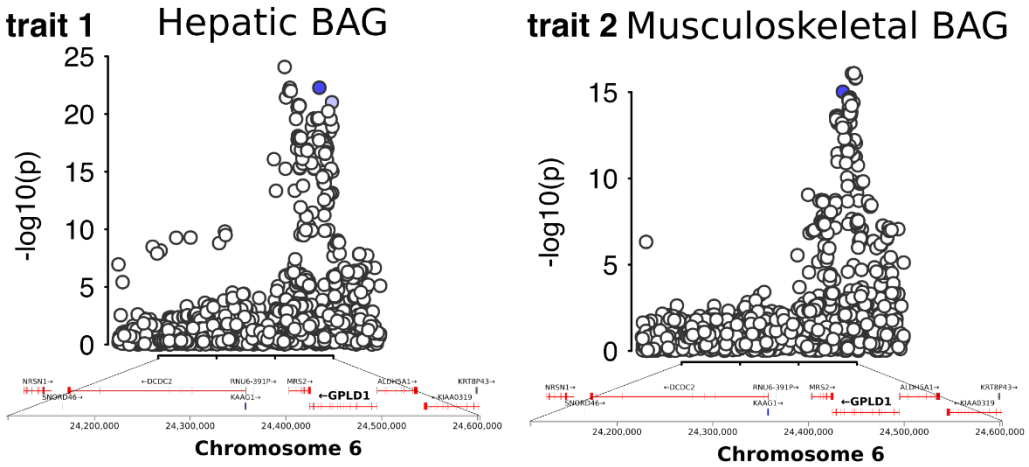

We conducted a Bayesian colocalization analysis using Bayes factors to investigate shared causal variants in a specific locus on chromosome 6 for the hepatic and musculoskeletal BAGs. The analysis tested five hypotheses, denoted by their posterior probabilities: H0 (no association with either trait), H1 (association with trait 1 but not trait 2), H2 (association with trait 2 but not trait 1), H3 (association with both traits but with separate causal variants), and H4 (association with both traits with a shared causal variant). The potential causal variants for both traits are indicated by blue-colored SNPs, assuming each locus contains at most one causal variant. The gene mapped to this locus (*GPLD1*) is shown in bold based on physical positions. All P-values were two-sided.

Supplementary Figure 11: Exemplary genomic locus for each BAG in the nine human organ systems

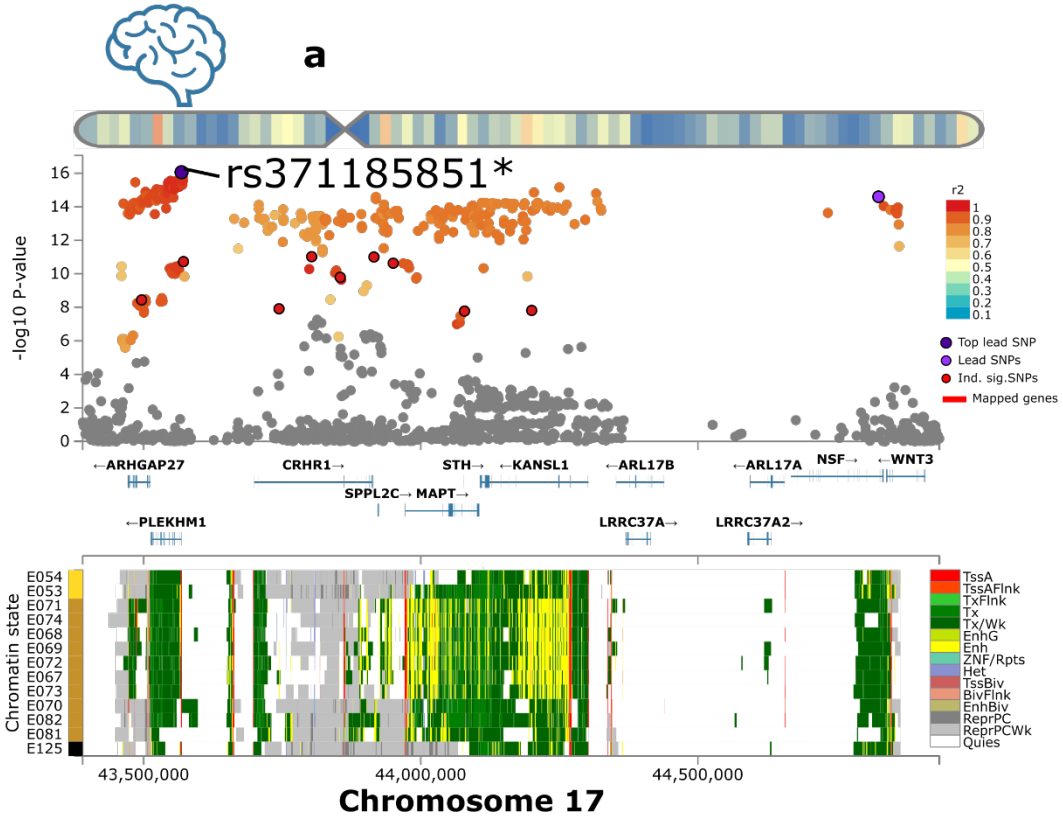

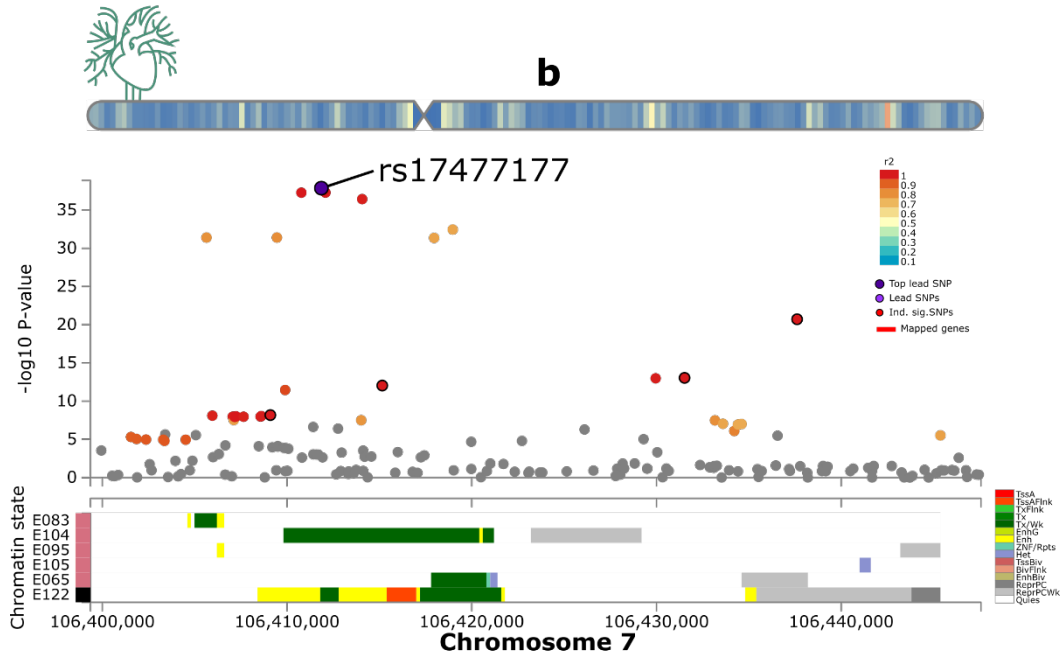

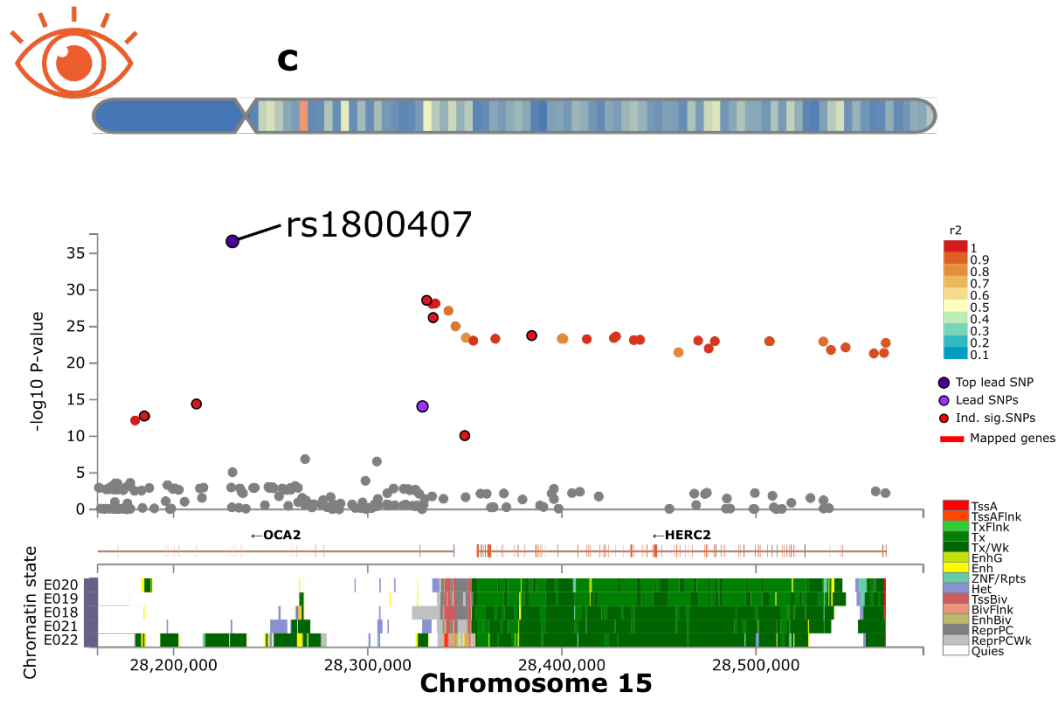
c
rs1800407
-log10 P-value
r2
Top lead SNP
Lead SNPs
Ind. sig.SNPs
Mapped genes
←OCA2
←HERC2
Chromatin state
E020
E019
E018
E021
E022
28,200,000
28,300,000
28,400,000
28,500,000
Chromosome 15

497

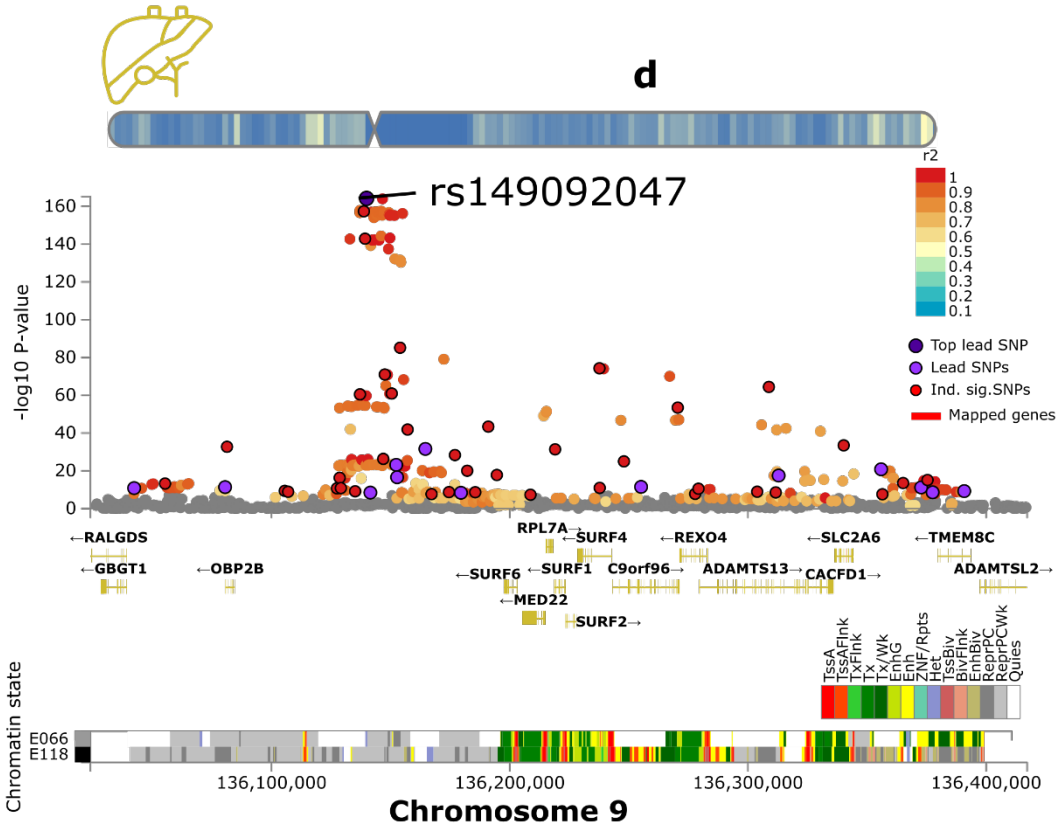
d
rs149092047
-log10 P-value
r2
Top lead SNP
Lead SNPs
Ind. sig.SNPs
Mapped genes
←RALGDS
←GBGT1
←OBP2B
RPL7A→
←SURF4
←REXO4
←SLC2A6
←TMEM8C
←SURF6
←SURF1
C9orf96→
ADAMTS13→
CACFD1→
ADAMTSL2→
←MED22
SURF2→
Chromatin state
E066
E118
136,100,000
136,200,000
136,300,000
136,400,000
Chromosome 9

498

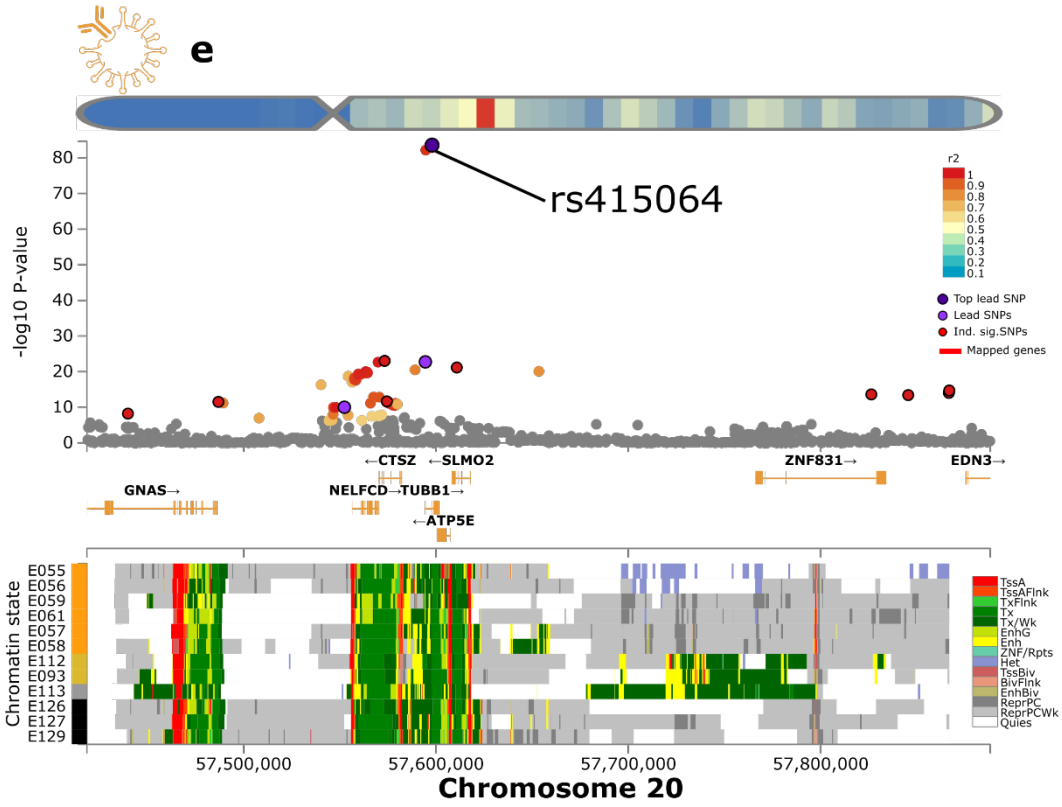
e
rs415064
-log10 P-value
r2
Top lead SNP
Lead SNPs
Ind. sig.SNPs
Mapped genes
←CTSZ
←SLMO2
ZNF831→
EDN3→
GNAS→
NELFCD→TUBB1→
←ATP5E
Chromatin state
E055
E056
E059
E061
E057
E058
E112
E093
E113
E126
E127
E129
TssA
TssAFlnk
TxFlnk
Tx
Tx/Wk
EnhG
Enh
ZNF/Rpts
Het
TssBiv
BivFlnk
EnhBiv
ReprPC
ReprPCWk
Quies
57,500,000
57,600,000
57,700,000
57,800,000
Chromosome 20

499

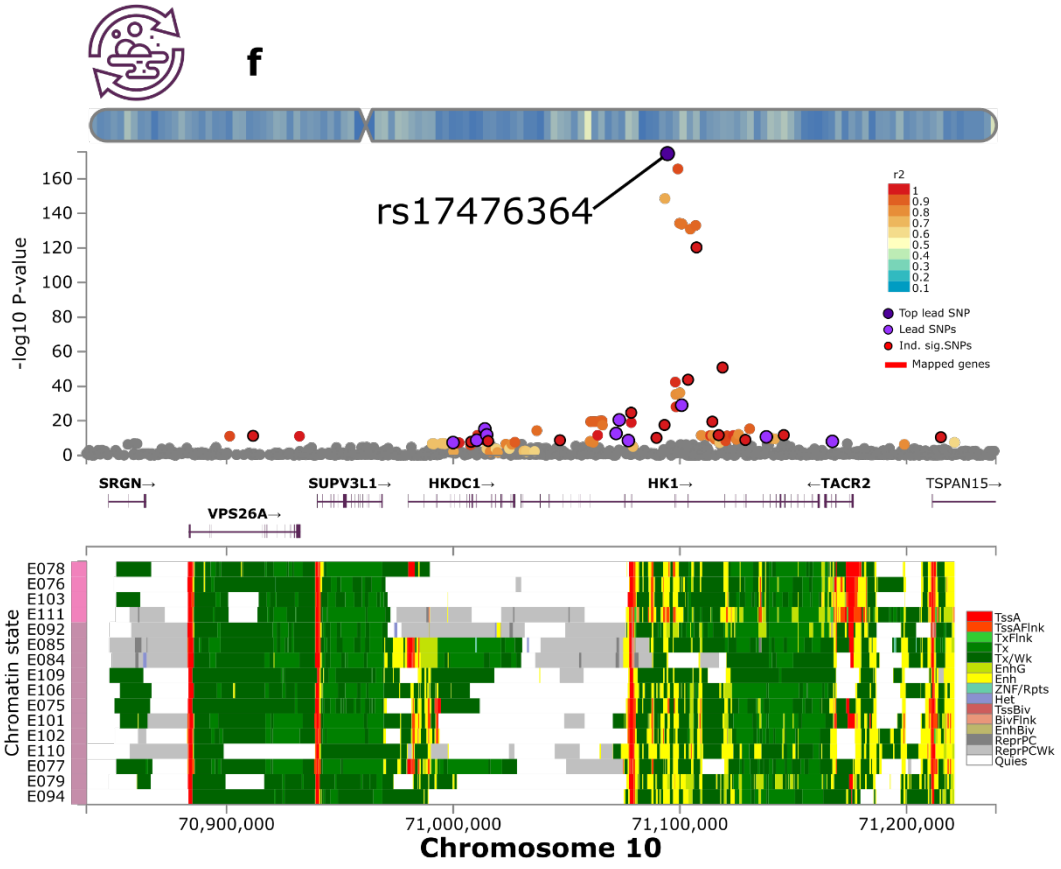
f
rs17476364
-log10 P-value
r2
Top lead SNP
Lead SNPs
Ind. sig.SNPs
Mapped genes
SRGN→
SUPV3L1→
HKDC1→
HK1→
←TACR2
TSPAN15→
VPS26A→
Chromatin state
E078
E076
E103
E111
E092
E085
E084
E109
E106
E075
E101
E102
E110
E077
E079
E094
TssA
TssAFlnk
TxFlnk
Tx
Tx/Wk
EnhG
Enh
ZNF/Rpts
Het
TssBiv
BivFlnk
EnhBiv
ReprPC
ReprPCWk
Quies
70,900,000
71,000,000
71,100,000
71,200,000
Chromosome 10

500

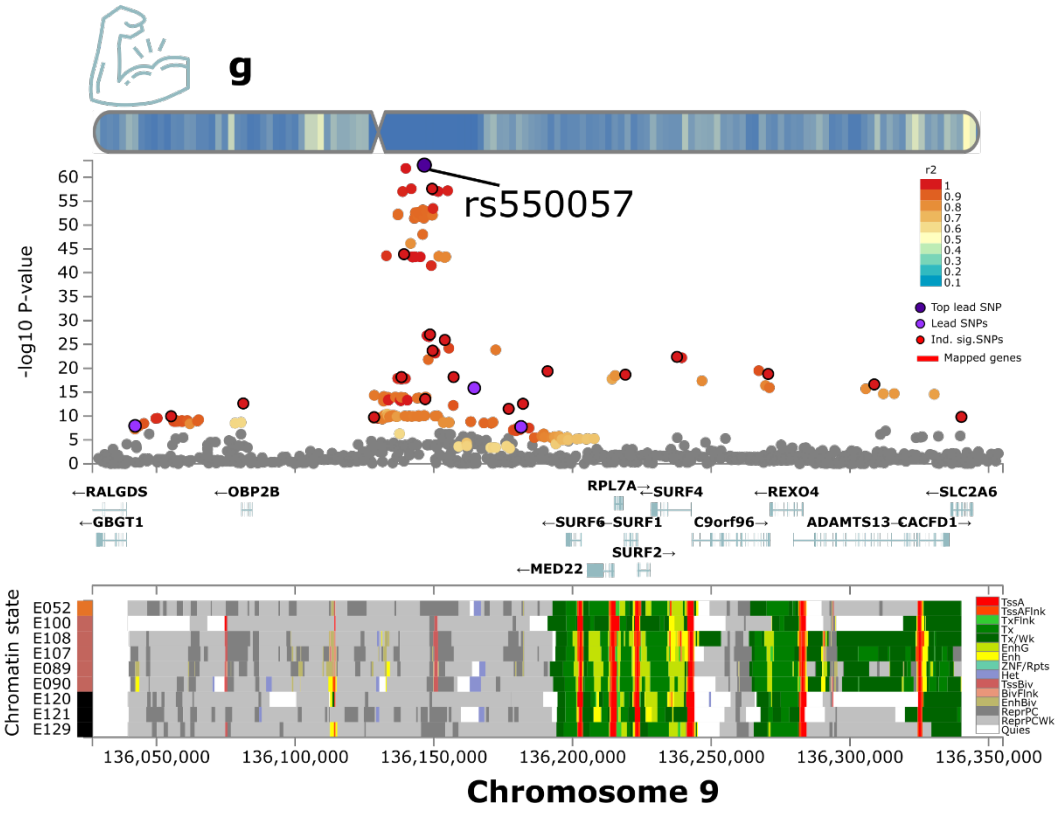
g
rs550057
-log10 P-value
r2
Top lead SNP
Lead SNPs
Ind. sig.SNPs
Mapped genes
←RALGDS
←OBP2B
←GBGT1
RPL7A→
←SURF4
←REXO4
←SLC2A6
←SURF6
SURF1
C9orf96→
ADAMTS13
CACFD1→
SURF2→
←MED22
Chromatin state
E052
E100
E108
E107
E089
E090
E120
E121
E129
136,050,000
136,100,000
136,150,000
136,200,000
136,250,000
136,300,000
136,350,000
Chromosome 9

501

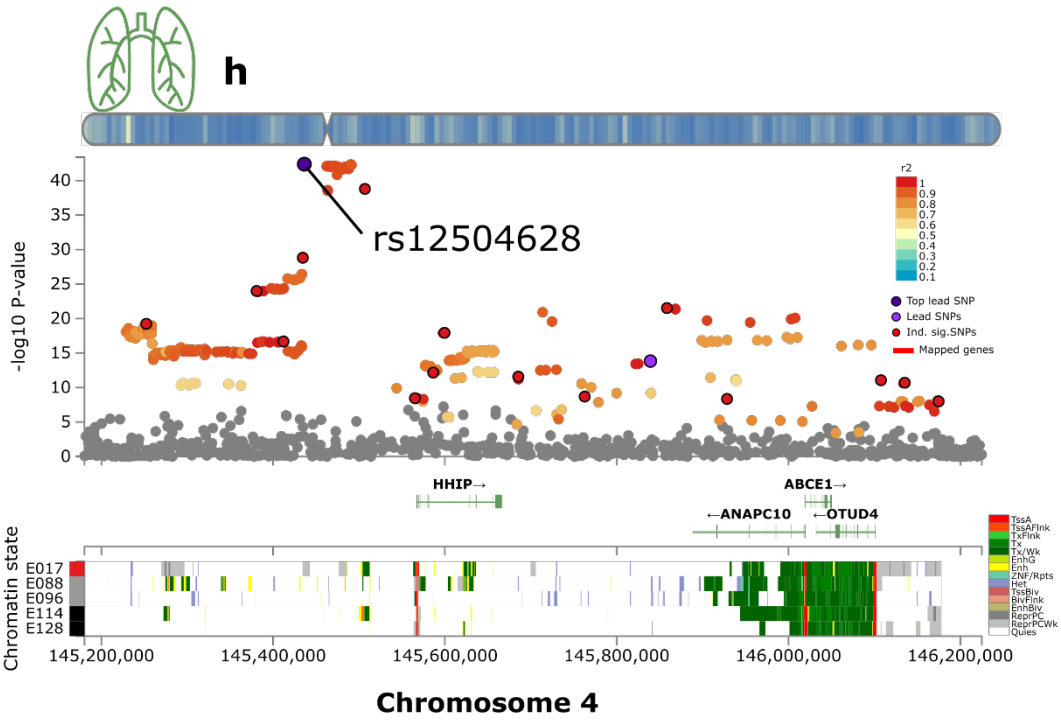
h
rs12504628
-log10 P-value
r2
Top lead SNP
Lead SNPs
Ind. sig.SNPs
Mapped genes
HHIP→
ABCE1→
←ANAPC10
←OTUD4
Chromatin state
E017
E088
E096
E114
E128
145,200,000
145,400,000
145,600,000
145,800,000
146,000,000
146,200,000
Chromosome 4

502

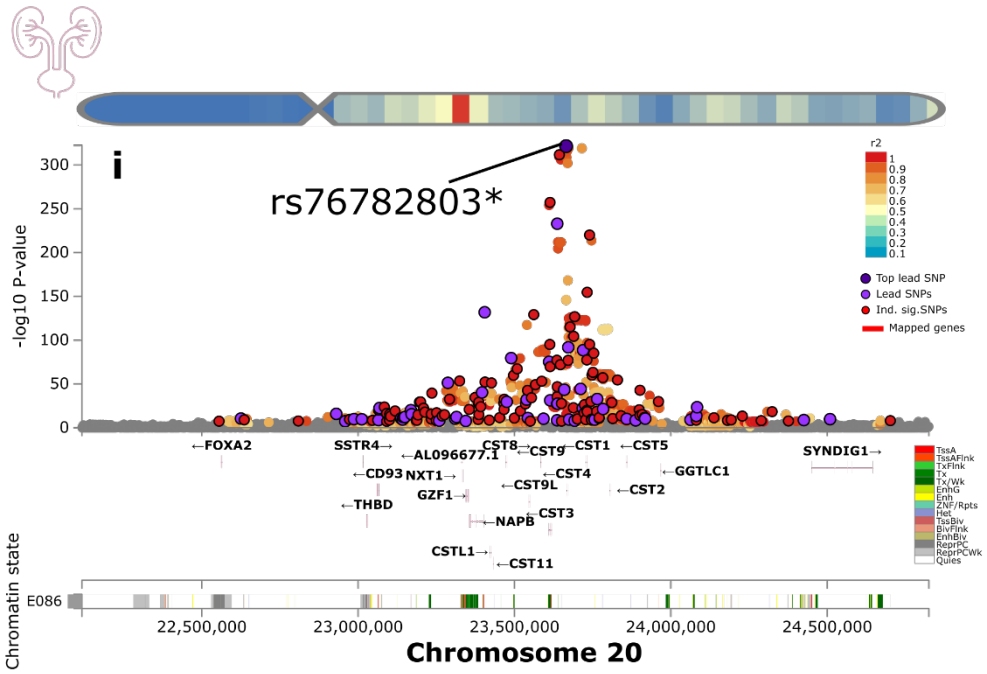

a-i) The exemplary genomic locus with the most significant signals for the brain, cardiovascular, eye, hepatic, immune, metabolic, musculoskeletal, pulmonary, and renal BAGs. The top lead SNP, lead SNPs, and independent significant SNPs are annotated within each locus. We mapped the SNPs to the genes and predicted their chromatin states in specific tissues, including the brain for the brain BAG, the heart and vascular tissues for the cardiovascular BAG, the iPSC for the eye BAG, the liver for the hepatic BAG, the spleen, bone, skin, and thymus tissues for the immune BAG, the gastrointestinal tissue for the metabolic BAG, the muscle and bone tissues for the musculoskeletal BAG, the lung tissue for the pulmonary BAG, and the kidney for the renal BAG, respectively. All P-values were two-sided, and a genome-wide P-values threshold was used.

Supplementary Figure 12. Phenome-wide association query of the identified genomic loci in the GWAS Atlas platforms.

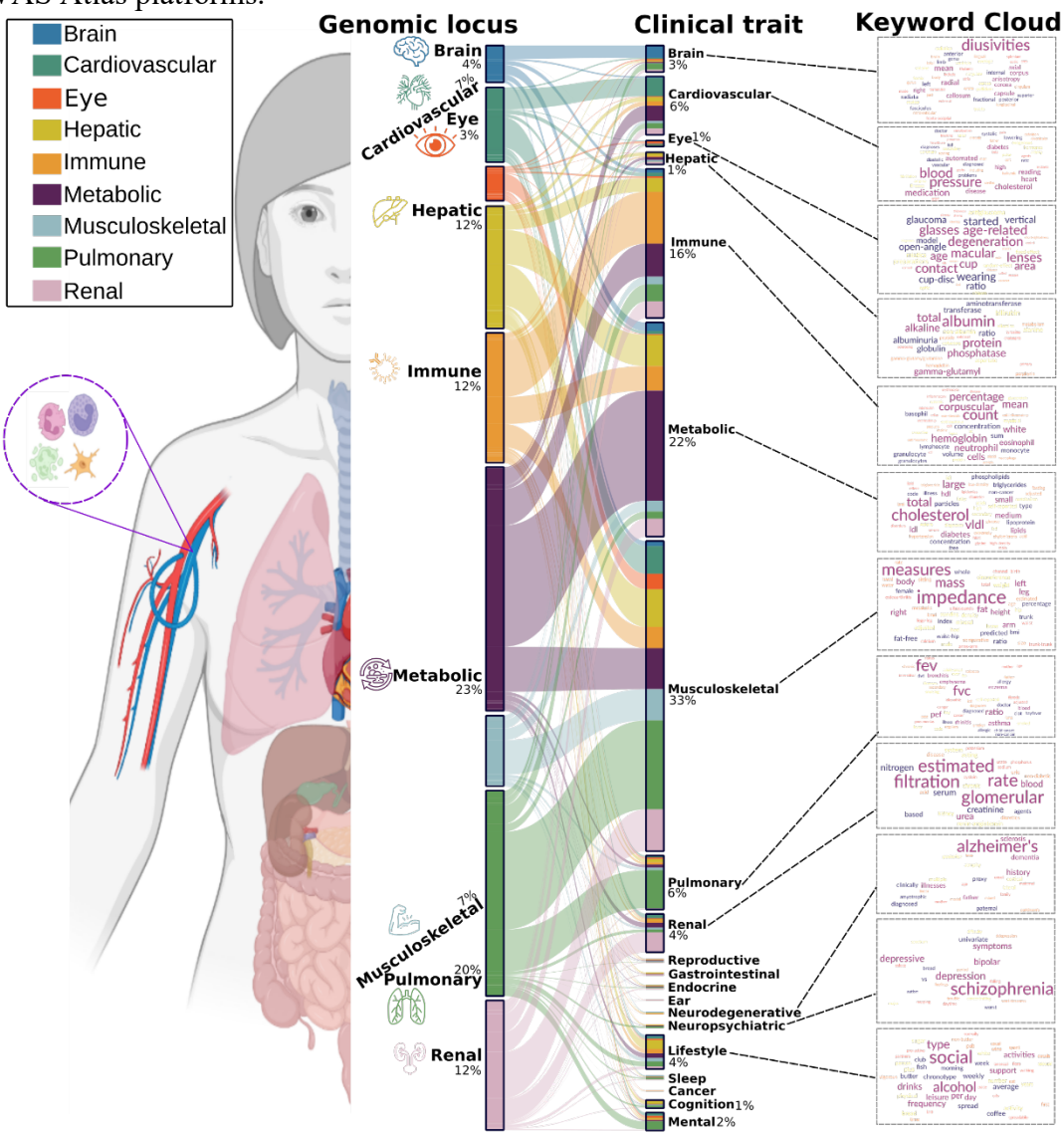

By examining the independent significant SNPs considering linkage disequilibrium within each genomic locus, we linked them to various clinical traits. These traits were categorized into high-level groups encompassing different organ systems, neurodegenerative and neuropsychiatric disorders, and lifestyle factors. To visually represent the findings, we generated keyword cloud plots based on the frequency of these clinical traits within each BAG. The length of each rectangle block indicates the number of associations concerning the genomic loci in our analysis and clinical traits in the literature. The individual disease traits were categorized within their respective organ systems. However, this categorization doesn't imply that the sum of these diseases exclusively represents the entirety of the organ system or that these diseases are solely associated with one specific organ system.

Supplementary Figure 13: Manhattan and QQ plots for the four pulmonary features used to compute the pulmonary BAG

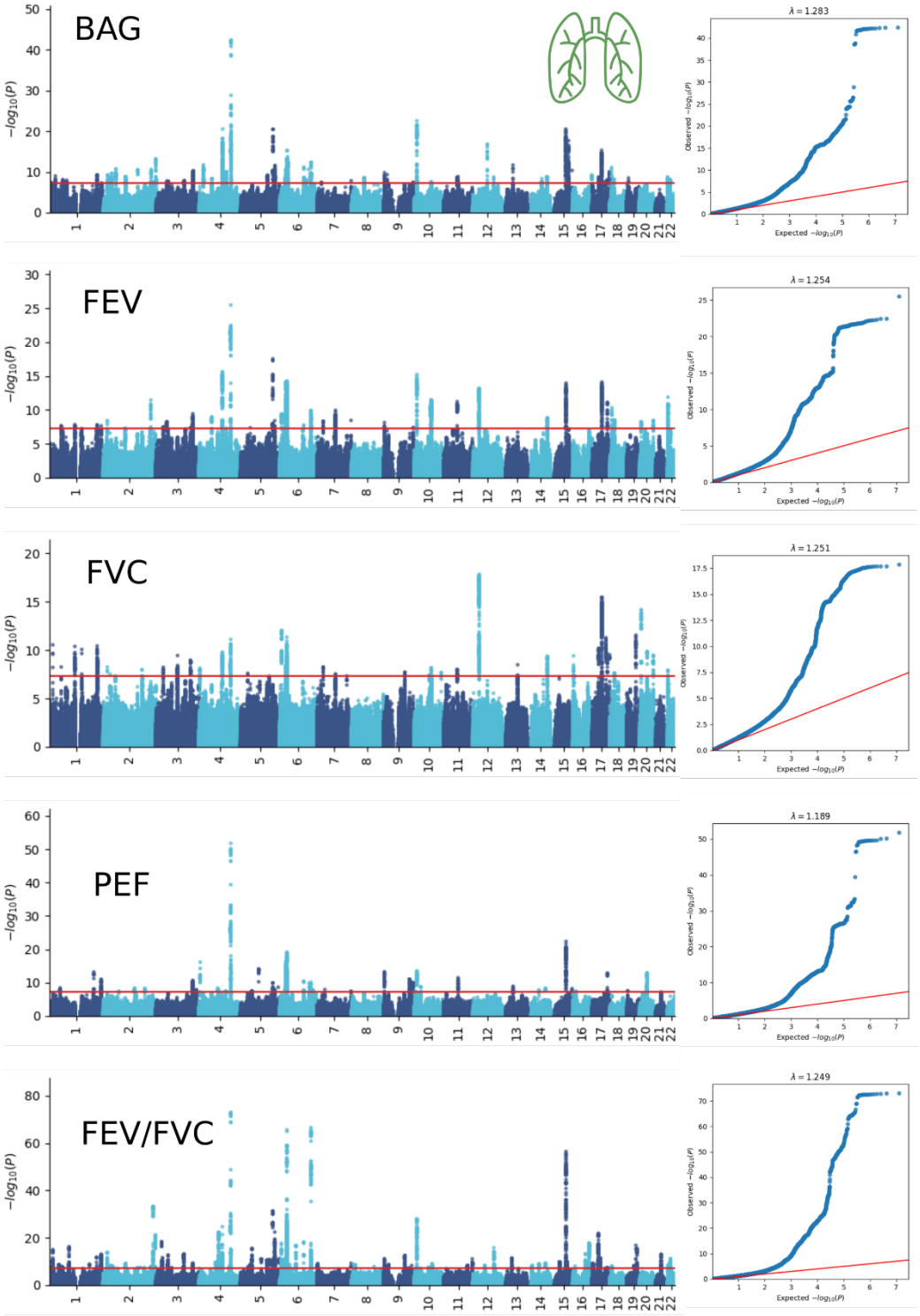

The Manhattan and QQ plots for the pulmonary BAG vs. its four features used to compute the BAG: forced vital capacity (FVC), forced expiratory volume (FEV), peak expiratory flow (PEF), and the ratio of forced expiratory volume to forced vital capacity (FEV/FVC). All P-values were two-sided.

536

Supplementary Figure 14: Beta coefficients of the significant colocalization signal between the pulmonary BAG and the four pulmonary features

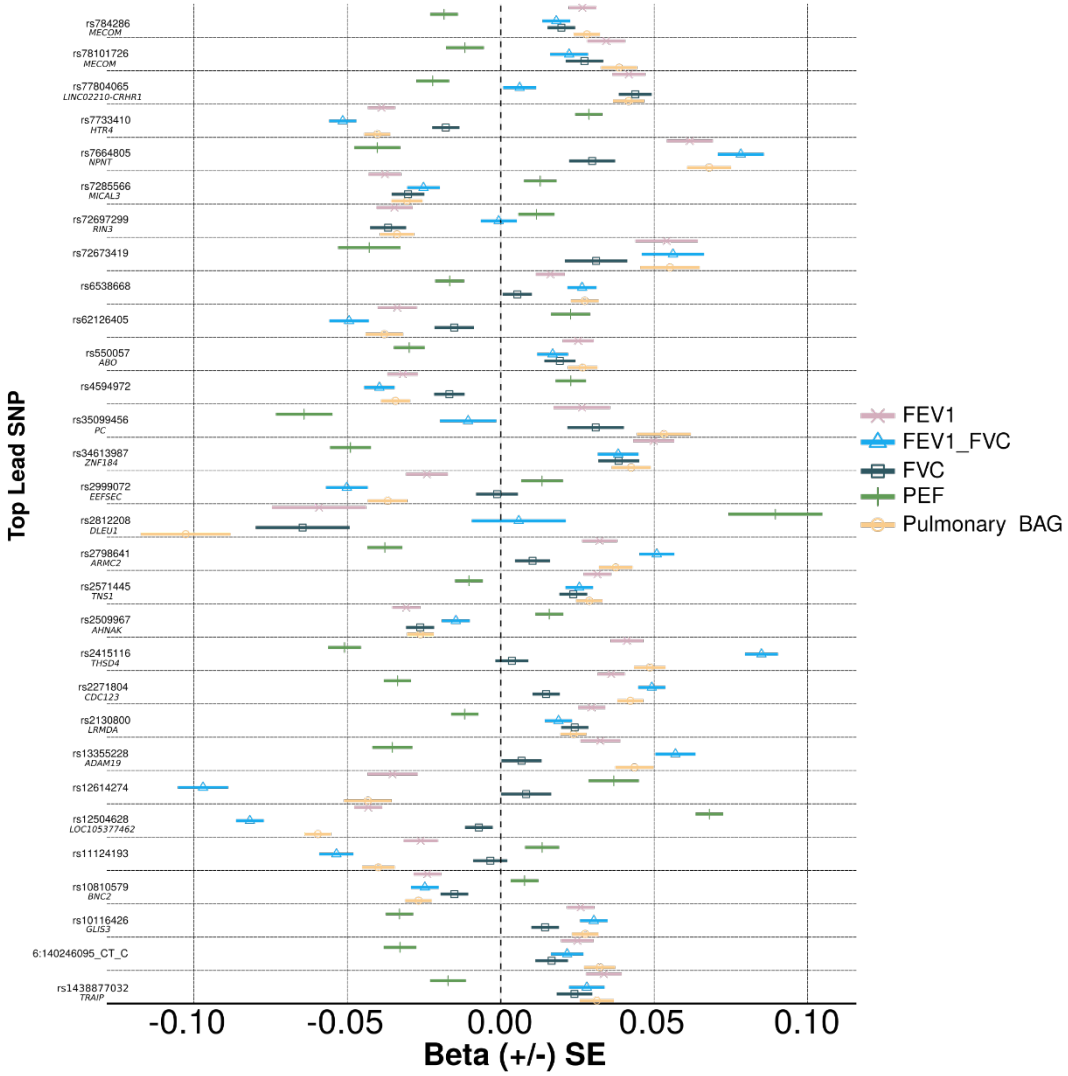

We show the beta coefficients of the significant colocalization signals between the pulmonary BAG and its underlying four pulmonary features. We ensured that at least one of the four pulmonary features achieved the genome-wide P-value threshold, totaling 48 loci (represented by its top lead SNP). We also showed the mapped gene when available. All P-values were two-sided.

Supplementary Figure 15: Mendelian randomization sensitivity check for the hepatic BAG on the musculoskeletal BAG

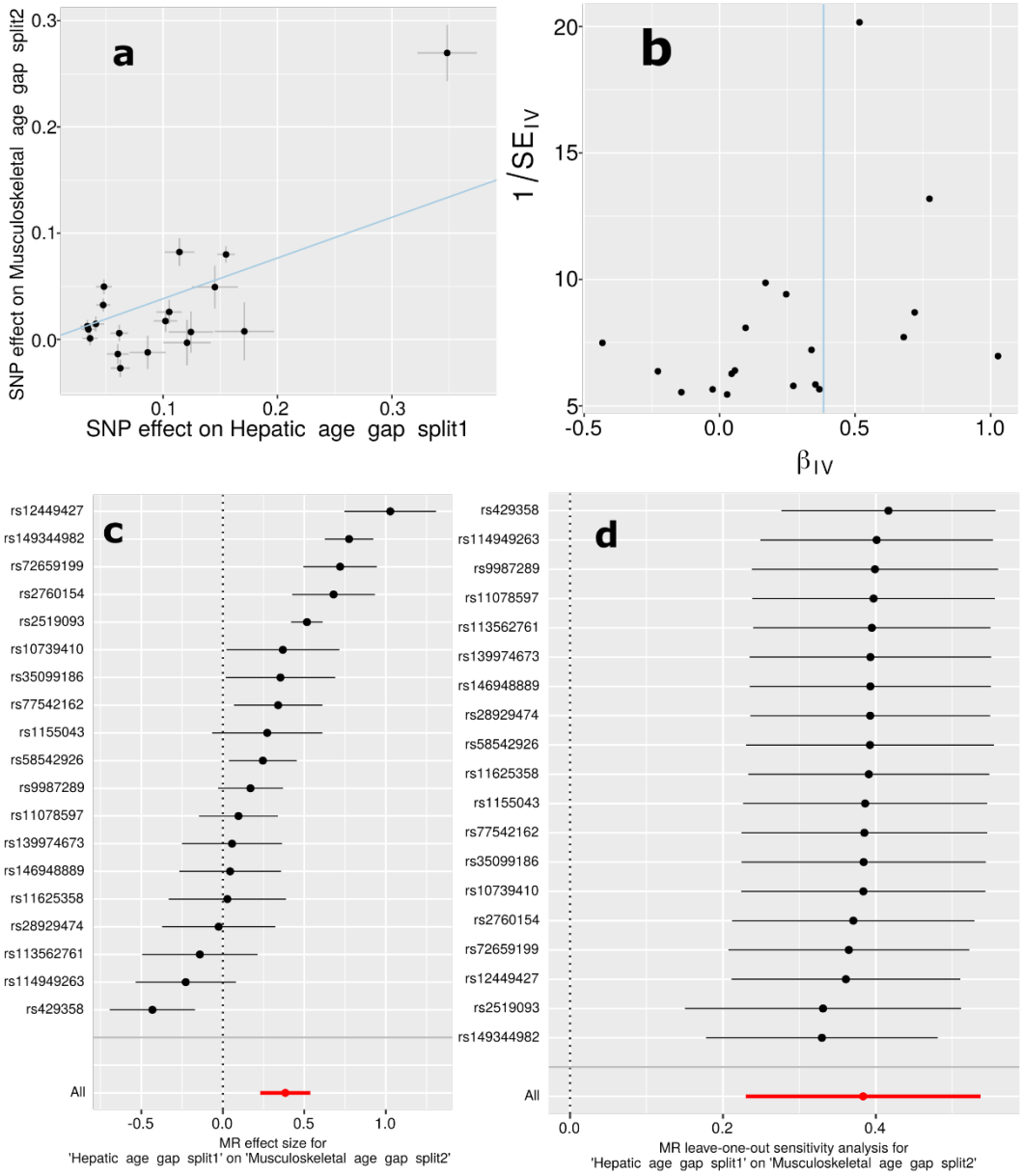

a) Scatter plot for the MR effect sizes of the exposure variable (hepatic BAG, *x*-axis, SD units) and the outcome variable (musculoskeletal BAG, *y*-axis, log OR) with standard error bars. The slopes of the regression line correspond to the causal effect sizes estimated by the IVW estimator. **b**) Funnel plot for the relationship between the causal effect of the exposure variable on the outcome variable. Each dot represents MR effect sizes estimated using each SNP as a separate instrument against the inverse of the standard error of the causal estimate. The vertical red line shows the MR estimates using all SNPs. **c**) Forest plot for the single-SNP MR results. Each line represents the MR effect (log OR) for the exposure variable on the outcome variable using only one SNP; the red line shows the MR effect using all SNPs together. **d**) Leave-one-out analysis of the exposure variable on the outcome variable. Each row represents the MR effect

(log OR) and the 95% CI by excluding that SNP from the analysis. The red line depicts the IVW estimator using all SNPs. The sample size of the BAGs is indicated in the GWAS summary statistics publicly shared on the MEDICINE portal. The measure of the center for the error bars represents the inferred statistics.

Supplementary Figure 16: Mendelian randomization sensitivity check for the musculoskeletal BAG on the hepatic BAG

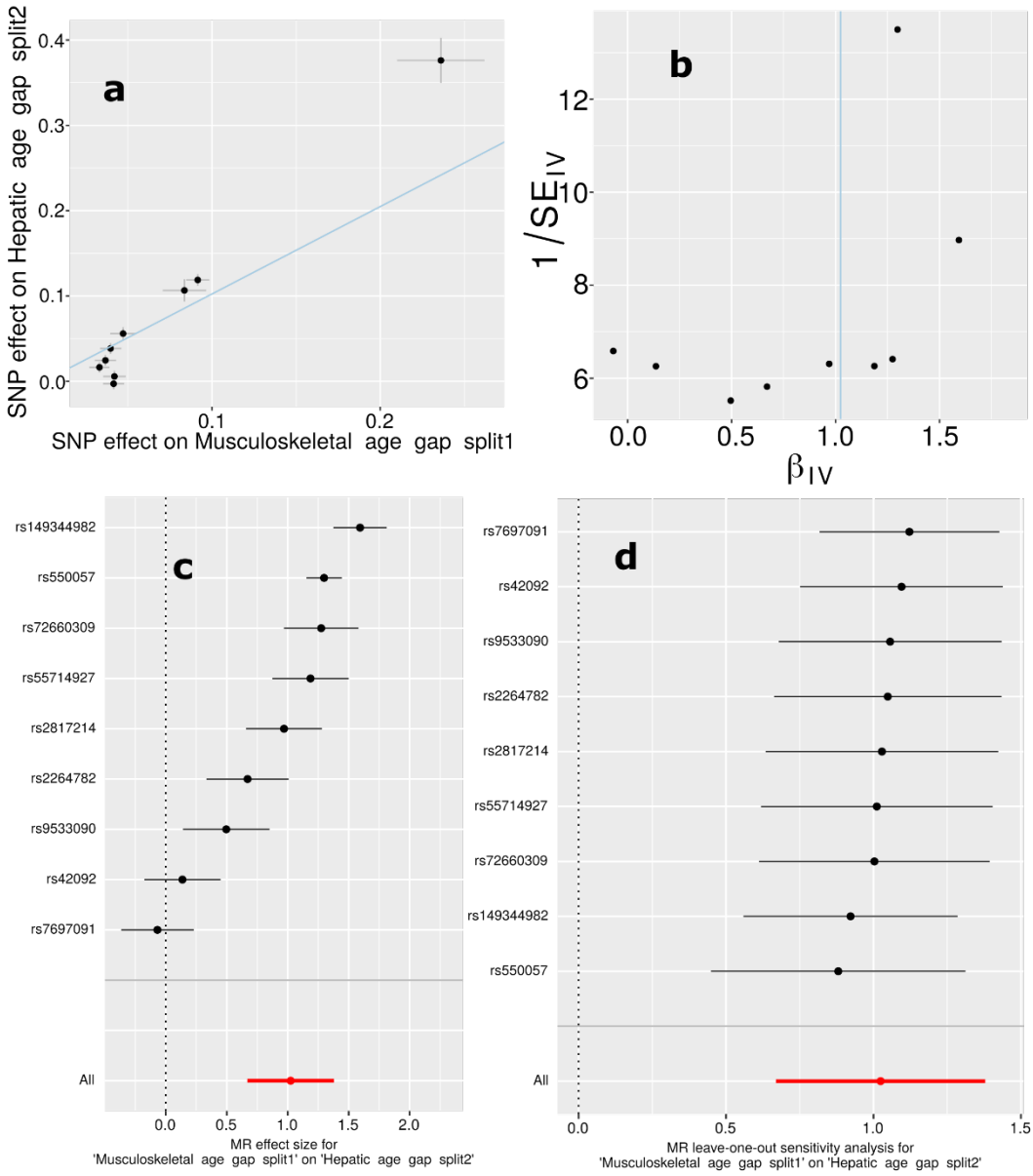

a) Scatter plot for the MR effect sizes of the exposure variable (musculoskeletal BAG, *x*-axis, SD units) and the outcome variable (hepatic BAG, *y*-axis, log OR) with standard error bars. The slopes of the regression line correspond to the causal effect sizes estimated by the IVW estimator. **b**) Funnel plot for the relationship between the causal effect of the exposure variable on the outcome variable. Each dot represents MR effect sizes estimated using each SNP as a separate instrument against the inverse of the standard error of the causal estimate. The vertical red line shows the MR estimates using all SNPs. **c**) Forest plot for the single-SNP MR results. Each line represents the MR effect (log OR) for the exposure variable on the outcome variable using only one SNP; the red line shows the MR effect using all SNPs together. **d**) Leave-one-out analysis of the exposure variable on the outcome variable. Each row represents the MR effect

(log OR) and the 95% CI by excluding that SNP from the analysis. The red line depicts the IVW estimator using all SNPs. The sample size of the BAGs is indicated in the GWAS summary statistics publicly shared on the MEDICINE portal. The measure of the center for the error bars represents the inferred statistics.

582 **Supplementary Figure 17: Mendelian randomization sensitivity check for AD on the brain**
583 **BAG**

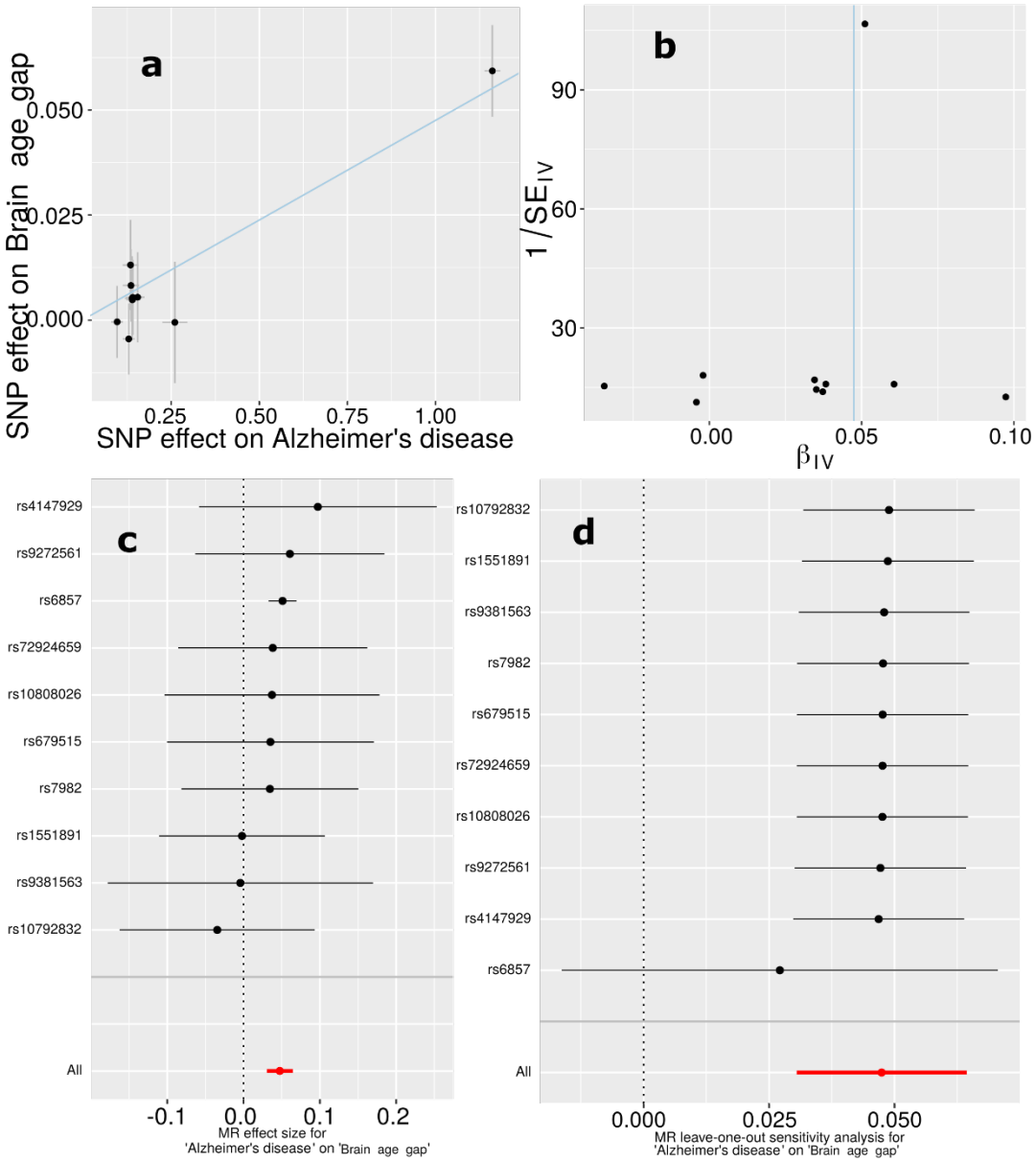

584
585 **a**) Scatter plot for the MR effect sizes of the exposure variable (AD, *x*-axis, SD units) and the
586 outcome variable (brain BAG, *y*-axis, log OR) with standard error bars. The slopes of the
587 regression line correspond to the causal effect sizes estimated by the IVW estimator. **b**) Funnel
588 plot for the relationship between the causal effect of the exposure variable on the outcome
589 variable. Each dot represents MR effect sizes estimated using each SNP as a separate instrument
590 against the inverse of the standard error of the causal estimate. The vertical red line shows the
591 MR estimates using all SNPs. **c**) Forest plot for the single-SNP MR results. Each line represents
592 the MR effect (log OR) for the exposure variable on the outcome variable using only one SNP;
593 the red line shows the MR effect using all SNPs together. **d**) Leave-one-out analysis of the
594 exposure variable on the outcome variable. Each row represents the MR effect (log OR) and the
595 95% CI by excluding that SNP from the analysis. The red line depicts the IVW estimator using

596 all SNPs. The sample size of the BAGs is indicated in the GWAS summary statistics publicly
597 shared on the MEDICINE portal. The measure of the center for the error bars represents the
598 inferred statistics.

Supplementary Figure 18: Mendelian randomization sensitivity check for AD on the hepatic BAG

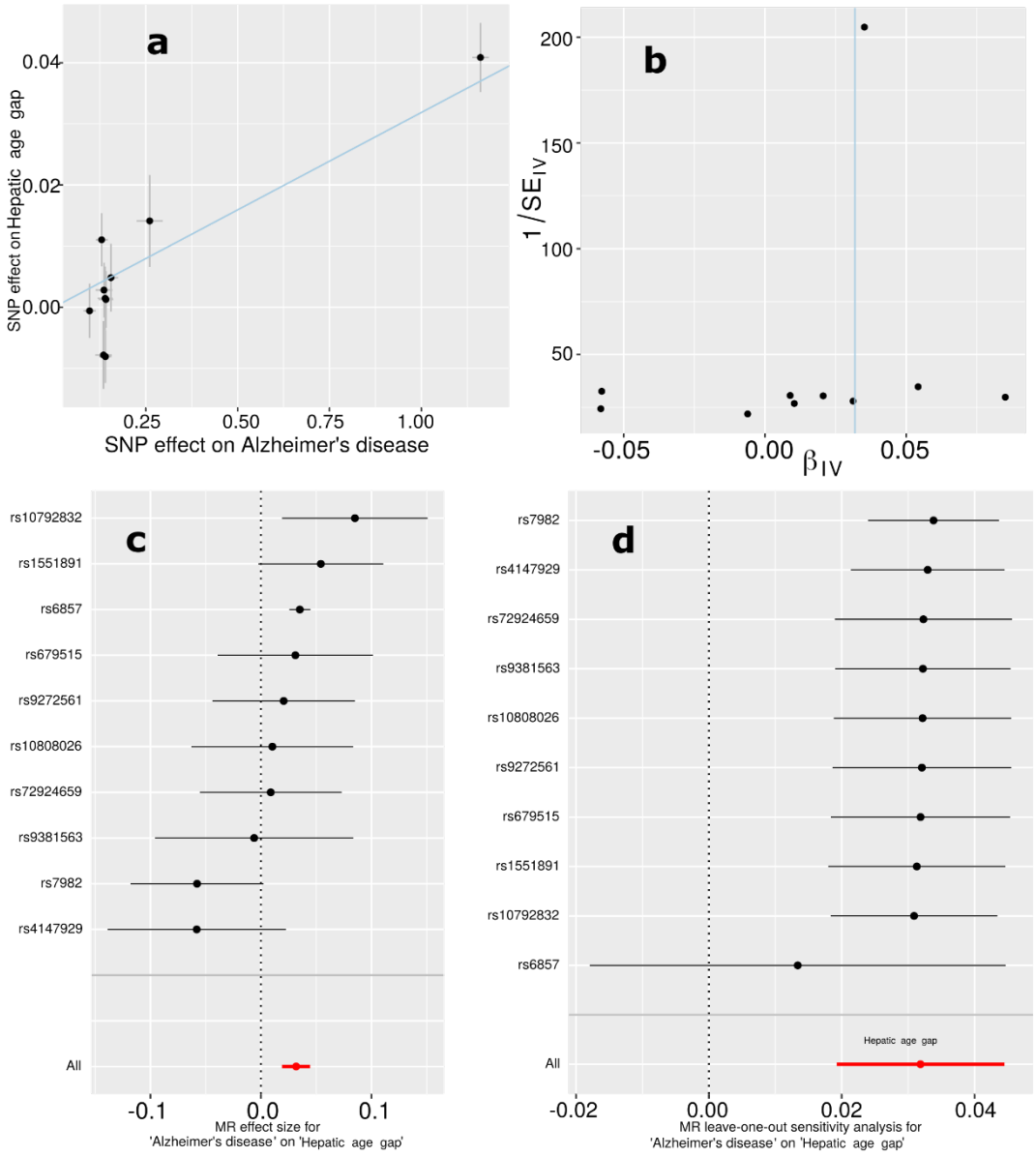

a) Scatter plot for the MR effect sizes of the exposure variable (AD, *x*-axis, SD units) and the outcome variable (hepatic BAG, *y*-axis, log OR) with standard error bars. The slopes of the regression line correspond to the causal effect sizes estimated by the IVW estimator. **b**) Funnel plot for the relationship between the causal effect of the exposure variable on the outcome variable. Each dot represents MR effect sizes estimated using each SNP as a separate instrument against the inverse of the standard error of the causal estimate. The vertical red line shows the MR estimates using all SNPs. **c**) Forest plot for the single-SNP MR results. Each line represents the MR effect (log OR) for the exposure variable on the outcome variable using only one SNP; the red line shows the MR effect using all SNPs together. **d**) Leave-one-out analysis of the exposure variable on the outcome variable. Each row represents the MR effect (log OR) and the 95% CI by excluding that SNP from the analysis. The red line depicts the IVW estimator using

all SNPs. The sample size of the BAGs is indicated in the GWAS summary statistics publicly shared on the MEDICINE portal. The measure of the center for the error bars represents the inferred statistics.

Supplementary Figure 19: Mendelian randomization sensitivity check for Crohn's disease on the hepatic BAG

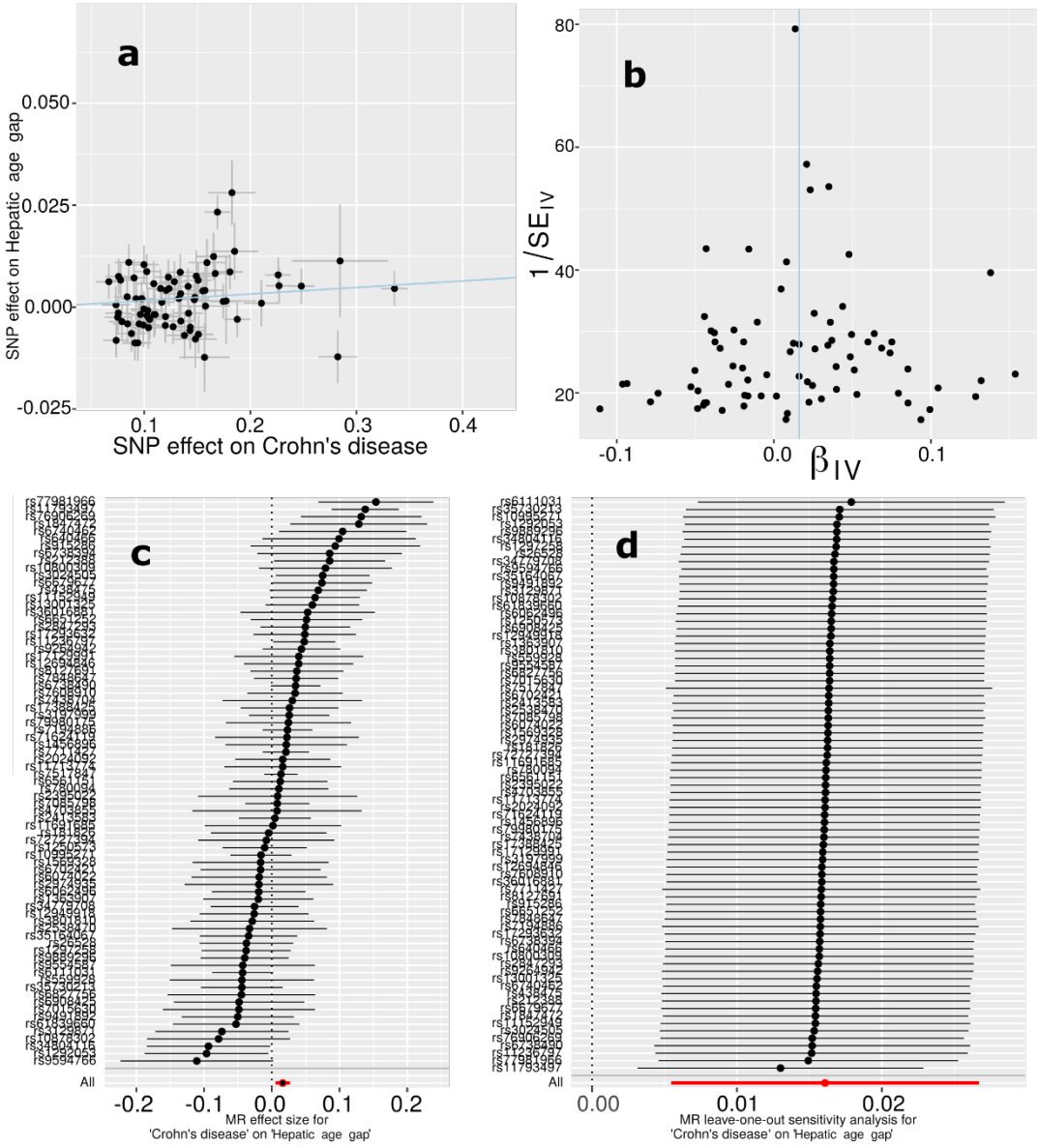

a) Scatter plot for the MR effect sizes of the exposure variable (Crohn's disease, *x*-axis, SD units) and the outcome variable (hepatic BAG, *y*-axis, log OR) with standard error bars. The slopes of the regression line correspond to the causal effect sizes estimated by the IVW estimator. **b**) Funnel plot for the relationship between the causal effect of the exposure variable on the outcome variable. Each dot represents MR effect sizes estimated using each SNP as a separate instrument against the inverse of the standard error of the causal estimate. The vertical red line shows the MR estimates using all SNPs. **c**) Forest plot for the single-SNP MR results. Each line represents the MR effect (log OR) for the exposure variable on the outcome variable using only one SNP; the red line shows the MR effect using all SNPs together. **d**) Leave-one-out analysis of the exposure variable on the outcome variable. Each row represents the MR effect (log OR) and the 95% CI by excluding that SNP from the analysis. The red line depicts the IVW estimator

using all SNPs. The sample size of the BAGs is indicated in the GWAS summary statistics publicly shared on the MEDICINE portal. The measure of the center for the error bars represents the inferred statistics.

Supplementary Figure 20: Mendelian randomization sensitivity check for body weight on the immune BAG

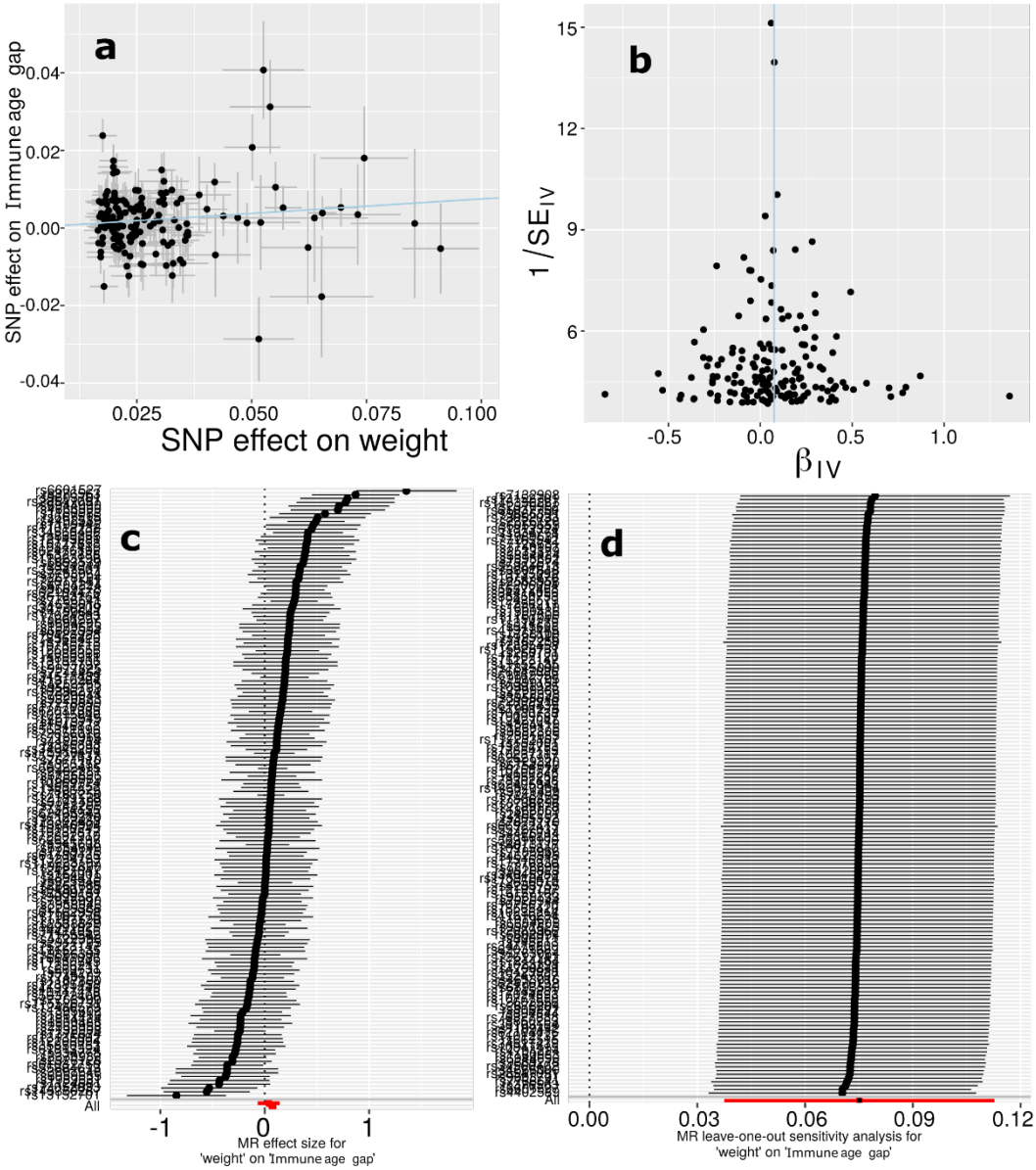

a) Scatter plot for the MR effect sizes of the exposure variable (body weight, *x*-axis, SD units) and the outcome variable (immune BAG, *y*-axis, log OR) with standard error bars. The slopes of the regression line correspond to the causal effect sizes estimated by the IVW estimator. **b**) Funnel plot for the relationship between the causal effect of the exposure variable on the outcome variable. Each dot represents MR effect sizes estimated using each SNP as a separate instrument against the inverse of the standard error of the causal estimate. The vertical red line shows the MR estimates using all SNPs. **c**) Forest plot for the single-SNP MR results. Each line represents the MR effect (log OR) for the exposure variable on the outcome variable using only one SNP; the red line shows the MR effect using all SNPs together. **d**) Leave-one-out analysis of the exposure variable on the outcome variable. Each row represents the MR effect (log OR) and the 95% CI by excluding that SNP from the analysis. The red line depicts the IVW estimator

649 using all SNPs. The sample size of the BAGs is indicated in the GWAS summary statistics
650 publicly shared on the MEDICINE portal. The measure of the center for the error bars represents
651 the inferred statistics.
652

Supplementary Figure 21: Mendelian randomization sensitivity check for type 2 diabetes on the metabolic BAG

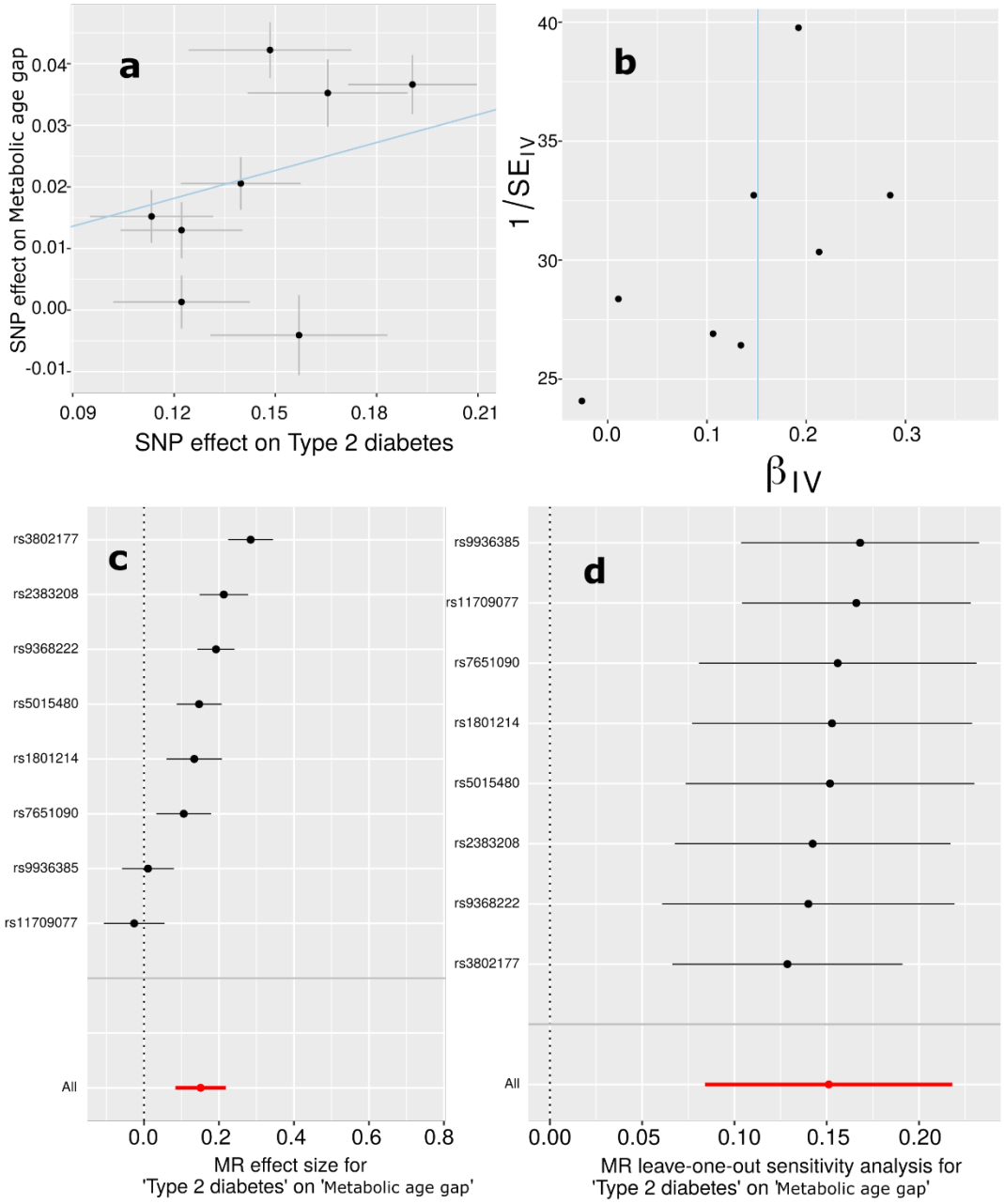

a) Scatter plot for the MR effect sizes of the exposure variable (type 2 diabetes, *x*-axis, SD units) and the outcome variable (metabolic BAG, *y*-axis, log OR) with standard error bars. The slopes of the regression line correspond to the causal effect sizes estimated by the IVW estimator. **b**) Funnel plot for the relationship between the causal effect of the exposure variable on the outcome variable. Each dot represents MR effect sizes estimated using each SNP as a separate instrument against the inverse of the standard error of the causal estimate. The vertical red line shows the MR estimates using all SNPs. **c**) Forest plot for the single-SNP MR results. Each line represents the MR effect (log OR) for the exposure variable on the outcome variable using only

664 one SNP; the red line shows the MR effect using all SNPs together. **d**) Leave-one-out analysis of
665 the exposure variable on the outcome variable. Each row represents the MR effect (log OR) and
666 the 95% CI by excluding that SNP from the analysis. The red line depicts the IVW estimator
667 using all SNPs. The sample size of the BAGs is indicated in the GWAS summary statistics
668 publicly shared on the MEDICINE portal. The measure of the center for the error bars represents
669 the inferred statistics.
670

Supplementary Figure 22: Mendelian randomization sensitivity check for AD on the musculoskeletal BAG

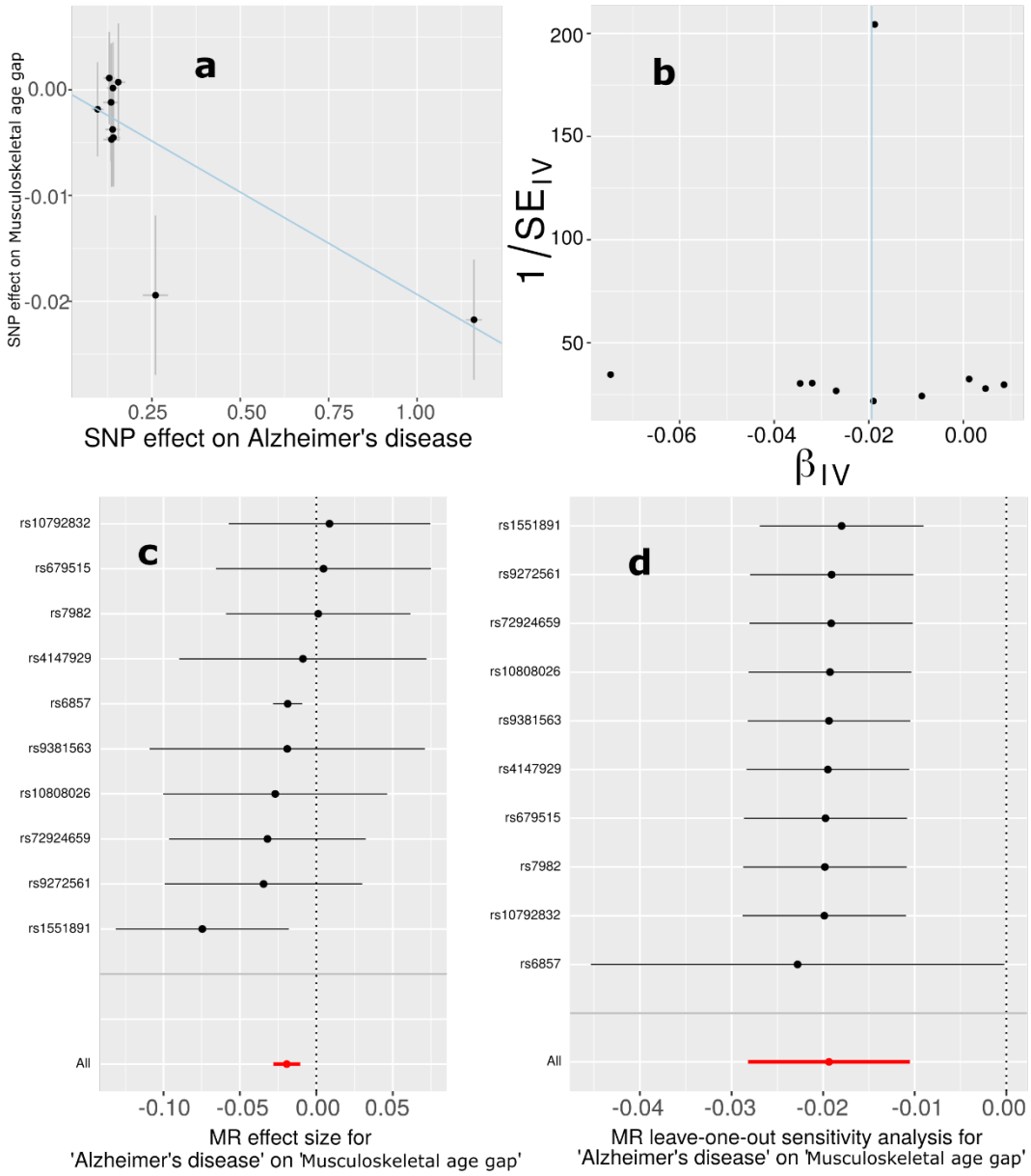

a) Scatter plot for the MR effect sizes of the exposure variable (AD, *x*-axis, SD units) and the outcome variable (musculoskeletal BAG, *y*-axis, log OR) with standard error bars. The slopes of the regression line correspond to the causal effect sizes estimated by the IVW estimator. **b**) Funnel plot for the relationship between the causal effect of the exposure variable on the outcome variable. Each dot represents MR effect sizes estimated using each SNP as a separate instrument against the inverse of the standard error of the causal estimate. The vertical red line shows the MR estimates using all SNPs. **c**) Forest plot for the single-SNP MR results. Each line represents the MR effect (log OR) for the exposure variable on the outcome variable using only one SNP; the red line shows the MR effect using all SNPs together. **d**) Leave-one-out analysis of the exposure variable on the outcome variable. Each row represents the MR effect (log OR) and

684 the 95% CI by excluding that SNP from the analysis. The red line depicts the IVW estimator
685 using all SNPs. The sample size of the BAGs is indicated in the GWAS summary statistics
686 publicly shared on the MEDICINE portal. The measure of the center for the error bars represents
687 the inferred statistics.

Supplementary Figure 23: Mendelian randomization sensitivity check for IBD on the musculoskeletal BAG

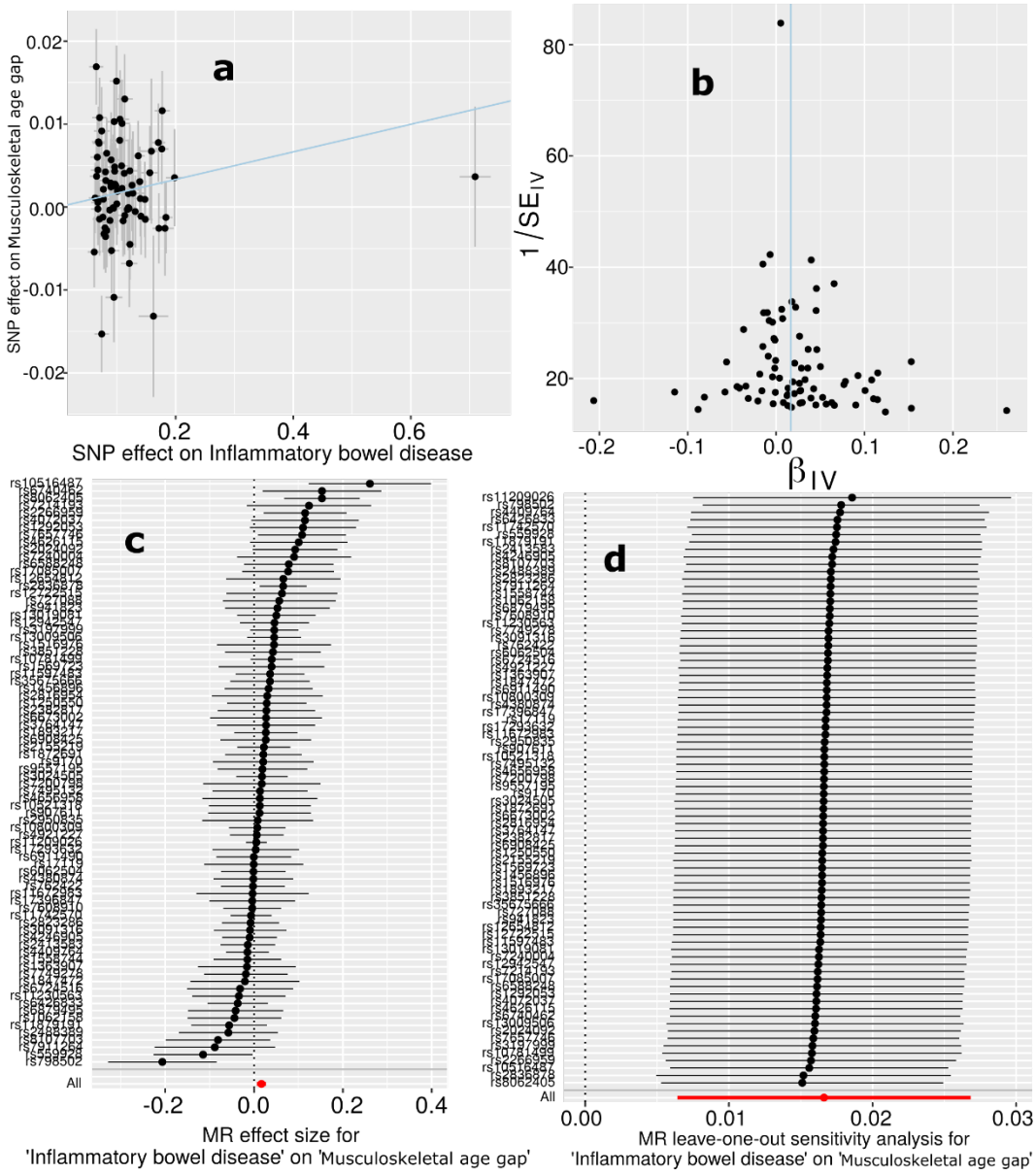

a) Scatter plot for the MR effect sizes of the exposure variable (IBD, *x*-axis, SD units) and the outcome variable (musculoskeletal BAG, *y*-axis, log OR) with standard error bars. The slopes of the regression line correspond to the causal effect sizes estimated by the IVW estimator. **b**) Funnel plot for the relationship between the causal effect of the exposure variable on the outcome variable. Each dot represents MR effect sizes estimated using each SNP as a separate instrument against the inverse of the standard error of the causal estimate. The vertical red line shows the MR estimates using all SNPs. **c**) Forest plot for the single-SNP MR results. Each line represents the MR effect (log OR) for the exposure variable on the outcome variable using only one SNP; the red line shows the MR effect using all SNPs together. **d**) Leave-one-out analysis of the exposure variable on the outcome variable. Each row represents the MR effect (log OR) and

the 95% CI by excluding that SNP from the analysis. The red line depicts the IVW estimator using all SNPs. The sample size of the BAGs is indicated in the GWAS summary statistics publicly shared on the MEDICINE portal. The measure of the center for the error bars represents the inferred statistics.

Supplementary Figure 24: Mendelian randomization sensitivity check for PBC on the musculoskeletal BAG

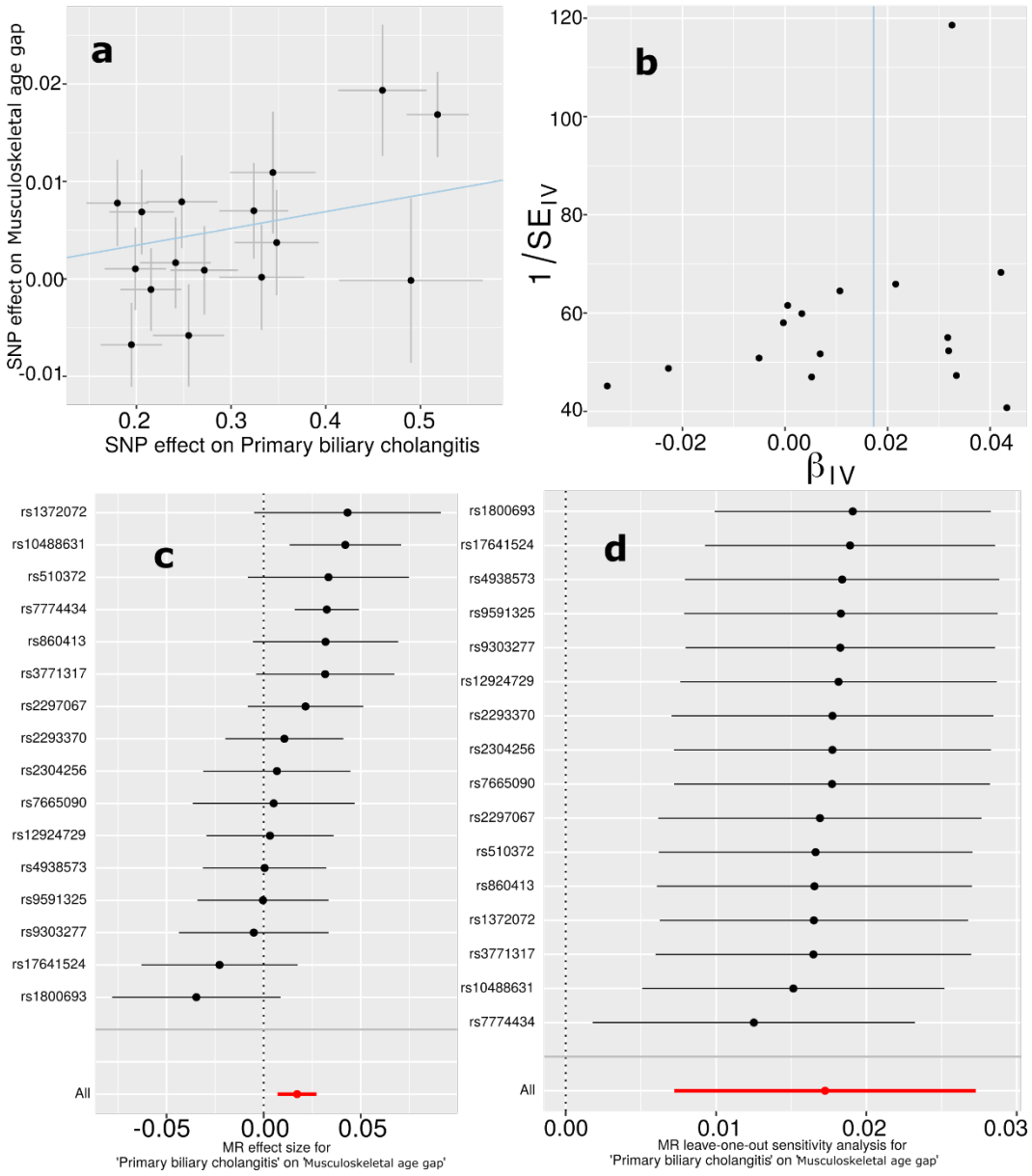

a) Scatter plot for the MR effect sizes of the exposure variable (PBC, *x*-axis, SD units) and the outcome variable (musculoskeletal BAG, *y*-axis, log OR) with standard error bars. The slopes of the regression line correspond to the causal effect sizes estimated by the IVW estimator. **b**) Funnel plot for the relationship between the causal effect of the exposure variable on the outcome variable. Each dot represents MR effect sizes estimated using each SNP as a separate instrument against the inverse of the standard error of the causal estimate. The vertical red line shows the MR estimates using all SNPs. **c**) Forest plot for the single-SNP MR results. Each line represents the MR effect (log OR) for the exposure variable on the outcome variable using only one SNP; the red line shows the MR effect using all SNPs together. **d**) Leave-one-out analysis of the exposure variable on the outcome variable. Each row represents the MR effect (log OR) and

719 the 95% CI by excluding that SNP from the analysis. The red line depicts the IVW estimator
720 using all SNPs. The sample size of the BAGs is indicated in the GWAS summary statistics
721 publicly shared on the MEDICINE portal. The measure of the center for the error bars represents
722 the inferred statistics.
723

Supplementary Figure 25: Mendelian randomization sensitivity check for weight on the musculoskeletal BAG

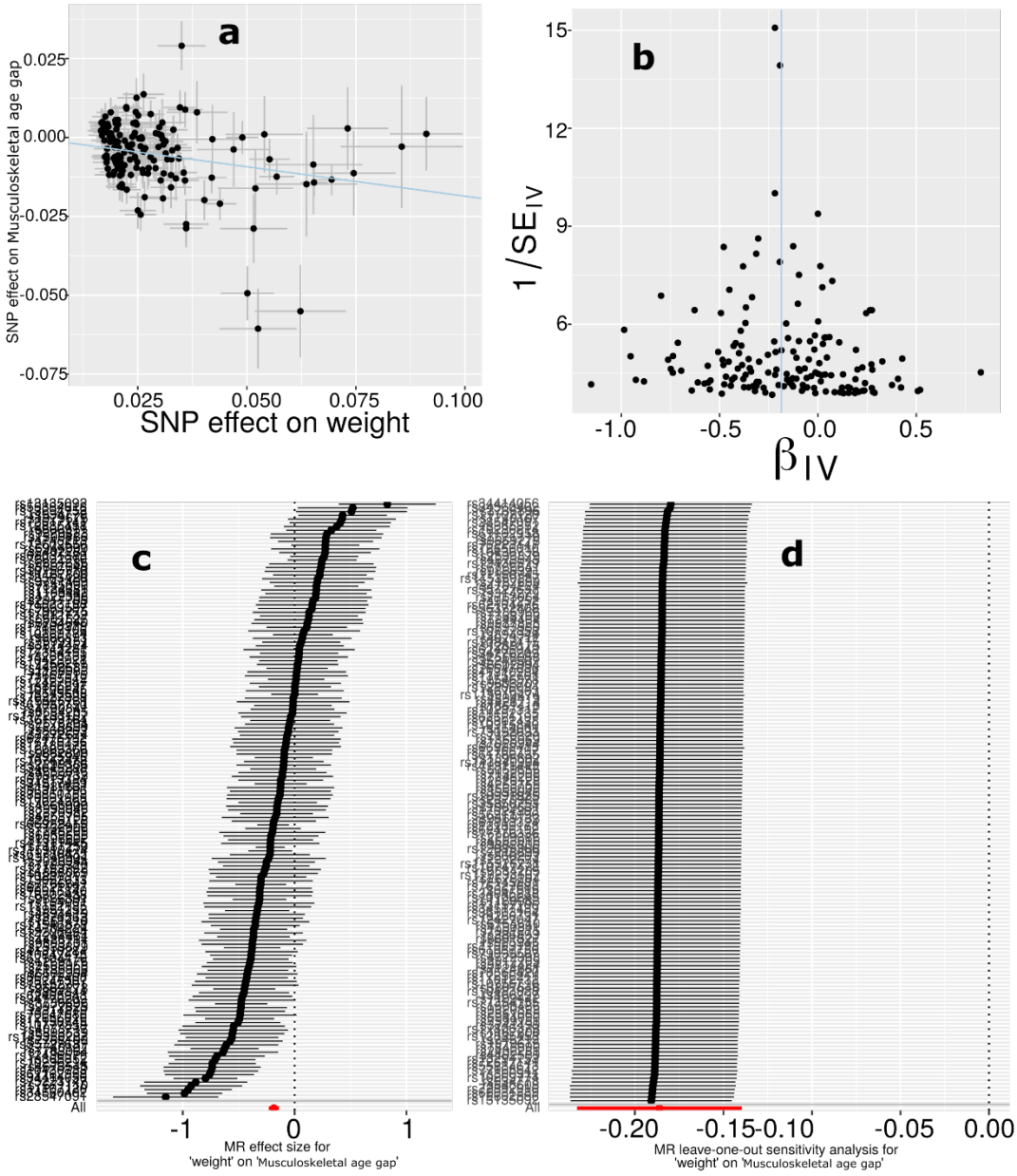

a) Scatter plot for the MR effect sizes of the exposure variable (body weight, *x*-axis, SD units) and the outcome variable (musculoskeletal BAG, *y*-axis, log OR) with standard error bars. The slopes of the regression line correspond to the causal effect sizes estimated by the IVW estimator. **b**) Funnel plot for the relationship between the causal effect of the exposure variable on the outcome variable. Each dot represents MR effect sizes estimated using each SNP as a separate instrument against the inverse of the standard error of the causal estimate. The vertical red line shows the MR estimates using all SNPs. **c**) Forest plot for the single-SNP MR results. Each line represents the MR effect (log OR) for the exposure variable on the outcome variable using only one SNP; the red line shows the MR effect using all SNPs together. **d**) Leave-one-out analysis of the exposure variable on the outcome variable. Each row represents the MR effect

737 (log OR) and the 95% CI by excluding that SNP from the analysis. The red line depicts the IVW
738 estimator using all SNPs. The sample size of the BAGs is indicated in the GWAS summary
739 statistics publicly shared on the MEDICINE portal. The measure of the center for the error bars
740 represents the inferred statistics.
741

Supplementary Figure 26: Mendelian randomization sensitivity check for weight on the pulmonary BAG

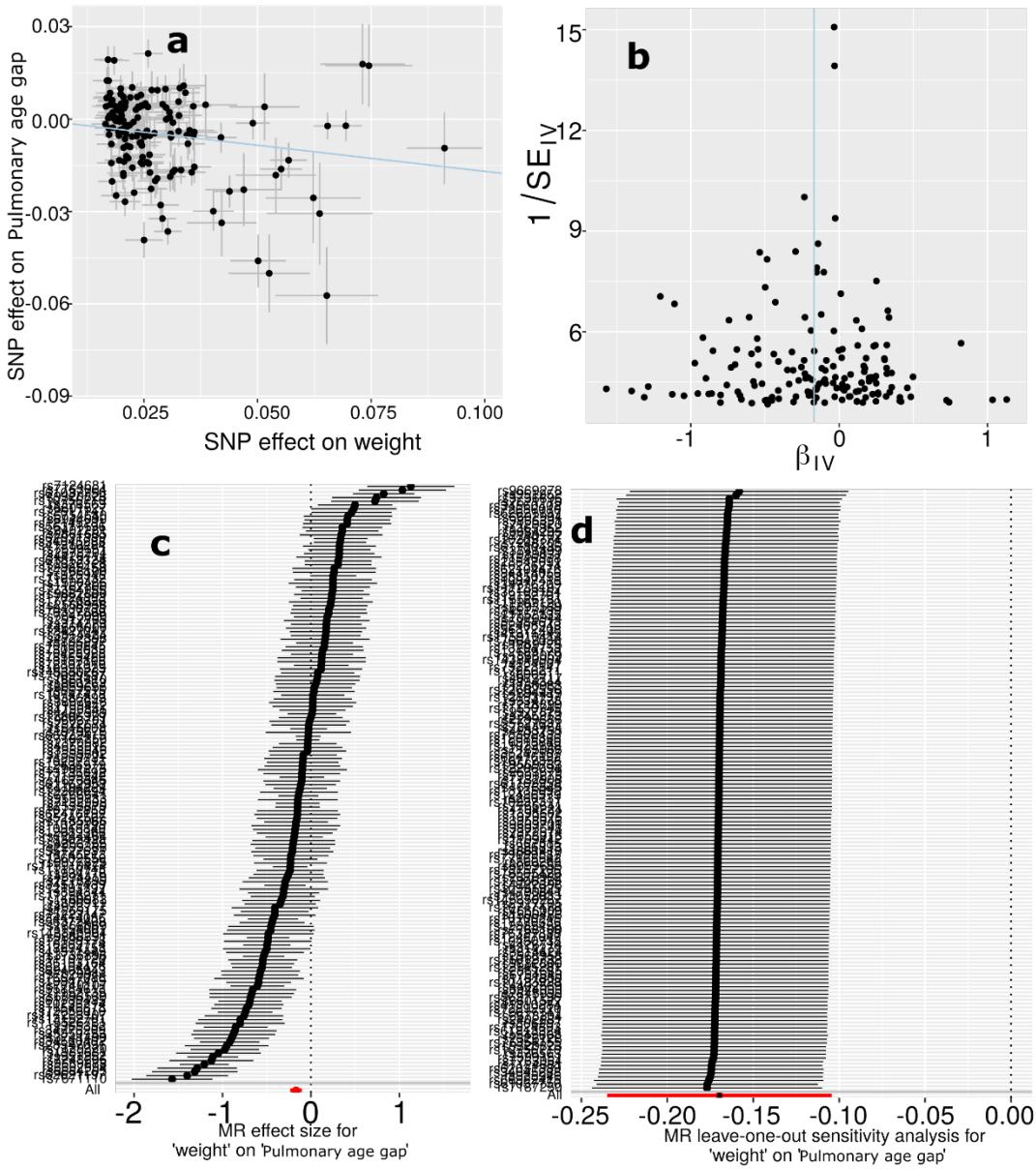

a) Scatter plot for the MR effect sizes of the exposure variable (body weight, *x*-axis, SD units) and the outcome variable (pulmonary BAG, *y*-axis, log OR) with standard error bars. The slopes of the regression line correspond to the causal effect sizes estimated by the IVW estimator. **b**) Funnel plot for the relationship between the causal effect of the exposure variable on the outcome variable. Each dot represents MR effect sizes estimated using each SNP as a separate instrument against the inverse of the standard error of the causal estimate. The vertical red line shows the MR estimates using all SNPs. **c**) Forest plot for the single-SNP MR results. Each line represents the MR effect (log OR) for the exposure variable on the outcome variable using only one SNP; the red line shows the MR effect using all SNPs together. **d**) Leave-one-out analysis of the exposure variable on the outcome variable. Each row represents the MR effect (log OR) and

the 95% CI by excluding that SNP from the analysis. The red line depicts the IVW estimator using all SNPs. The sample size of the BAGs is indicated in the GWAS summary statistics publicly shared on the MEDICINE portal. The measure of the center for the error bars represents the inferred statistics.

Supplementary Figure 27: Mendelian randomization sensitivity check for AD on the renal BAG

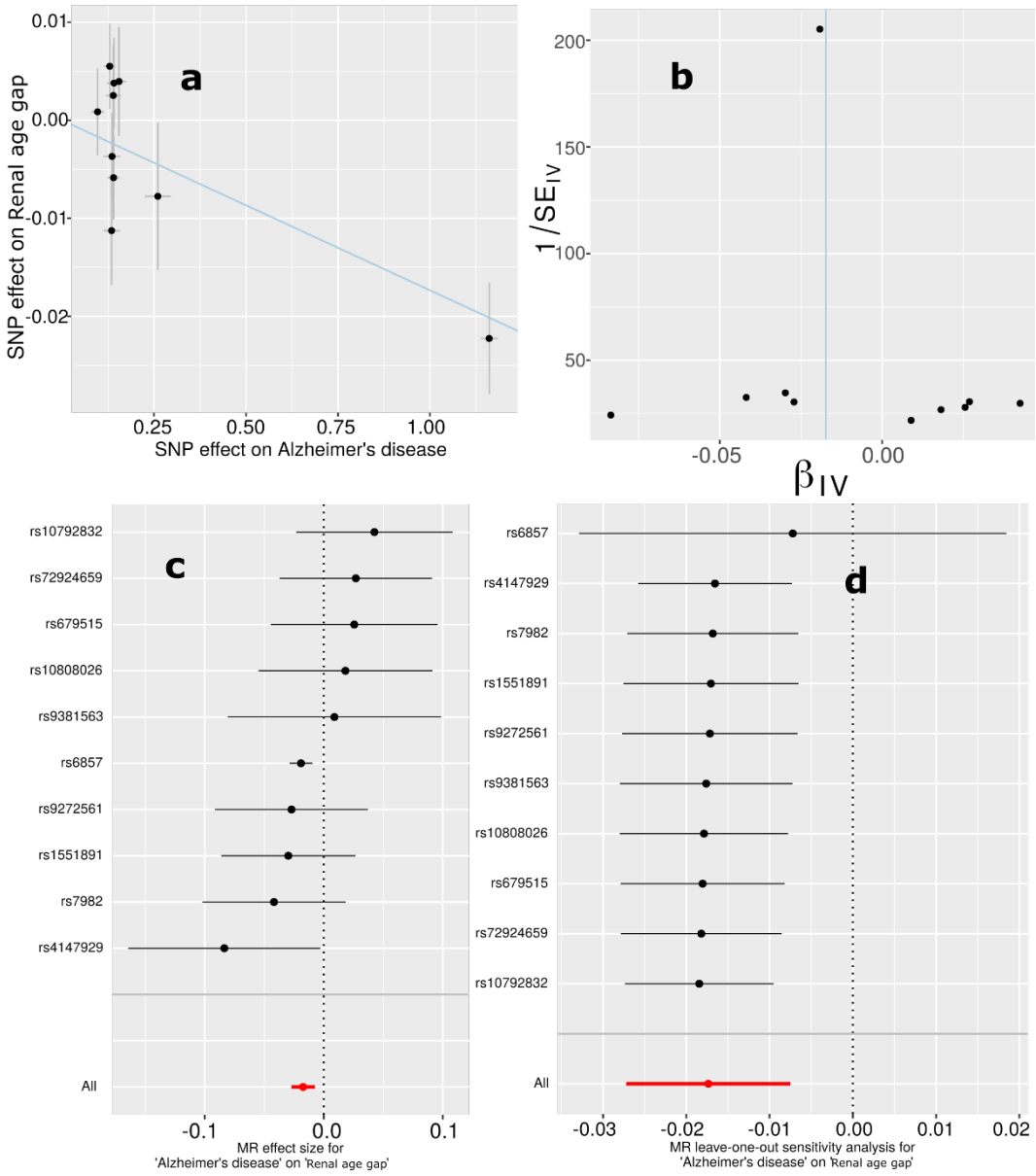

a) Scatter plot for the MR effect sizes of the exposure variable (AD, *x*-axis, SD units) and the outcome variable (renal BAG, *y*-axis, log OR) with standard error bars. The slopes of the regression line correspond to the causal effect sizes estimated by the IVW estimator. **b**) Funnel plot for the relationship between the causal effect of the exposure variable on the outcome variable. Each dot represents MR effect sizes estimated using each SNP as a separate instrument against the inverse of the standard error of the causal estimate. The vertical red line shows the MR estimates using all SNPs. **c**) Forest plot for the single-SNP MR results. Each line represents the MR effect (log OR) for the exposure variable on the outcome variable using only one SNP; the red line shows the MR effect using all SNPs together. **d**) Leave-one-out analysis of the exposure variable on the outcome variable. Each row represents the MR effect (log OR) and the

95% CI by excluding that SNP from the analysis. The red line depicts the IVW estimator using all SNPs. The sample size of the BAGs is indicated in the GWAS summary statistics publicly shared on the MEDICINE portal. The measure of the center for the error bars represents the inferred statistics.

Supplementary Figure 28: Mendelian randomization sensitivity check for weight on the renal BAG

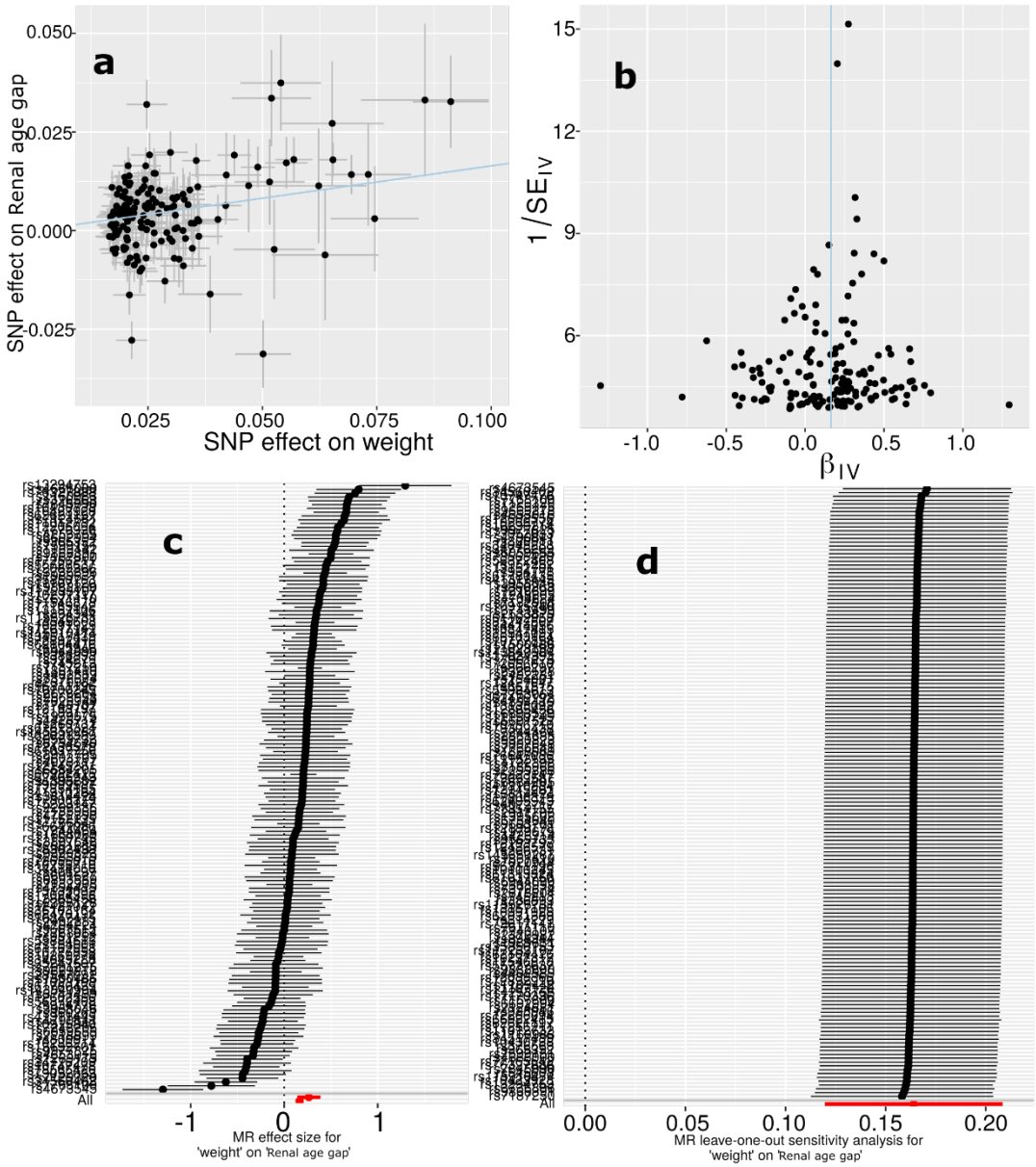

a) Scatter plot for the MR effect sizes of the exposure variable (body weight, *x*-axis, SD units) and the outcome variable (renal BAG, *y*-axis, log OR) with standard error bars. The slopes of the regression line correspond to the causal effect sizes estimated by the IVW estimator. **b**) Funnel plot for the relationship between the causal effect of the exposure variable on the outcome variable. Each dot represents MR effect sizes estimated using each SNP as a separate instrument against the inverse of the standard error of the causal estimate. The vertical red line shows the MR estimates using all SNPs. **c**) Forest plot for the single-SNP MR results. Each line represents the MR effect (log OR) for the exposure variable on the outcome variable using only one SNP; the red line shows the MR effect using all SNPs together. **d**) Leave-one-out analysis of the exposure variable on the outcome variable. Each row represents the MR effect (log OR) and the 95% CI by excluding that SNP from the analysis. The red line depicts the IVW estimator using

all SNPs. The sample size of the BAGs is indicated in the GWAS summary statistics publicly shared on the MEDICINE portal. The measure of the center for the error bars represents the inferred statistics.

Supplementary Figure 29: Mendelian randomization sensitivity check for the brain BAG on sleep duration

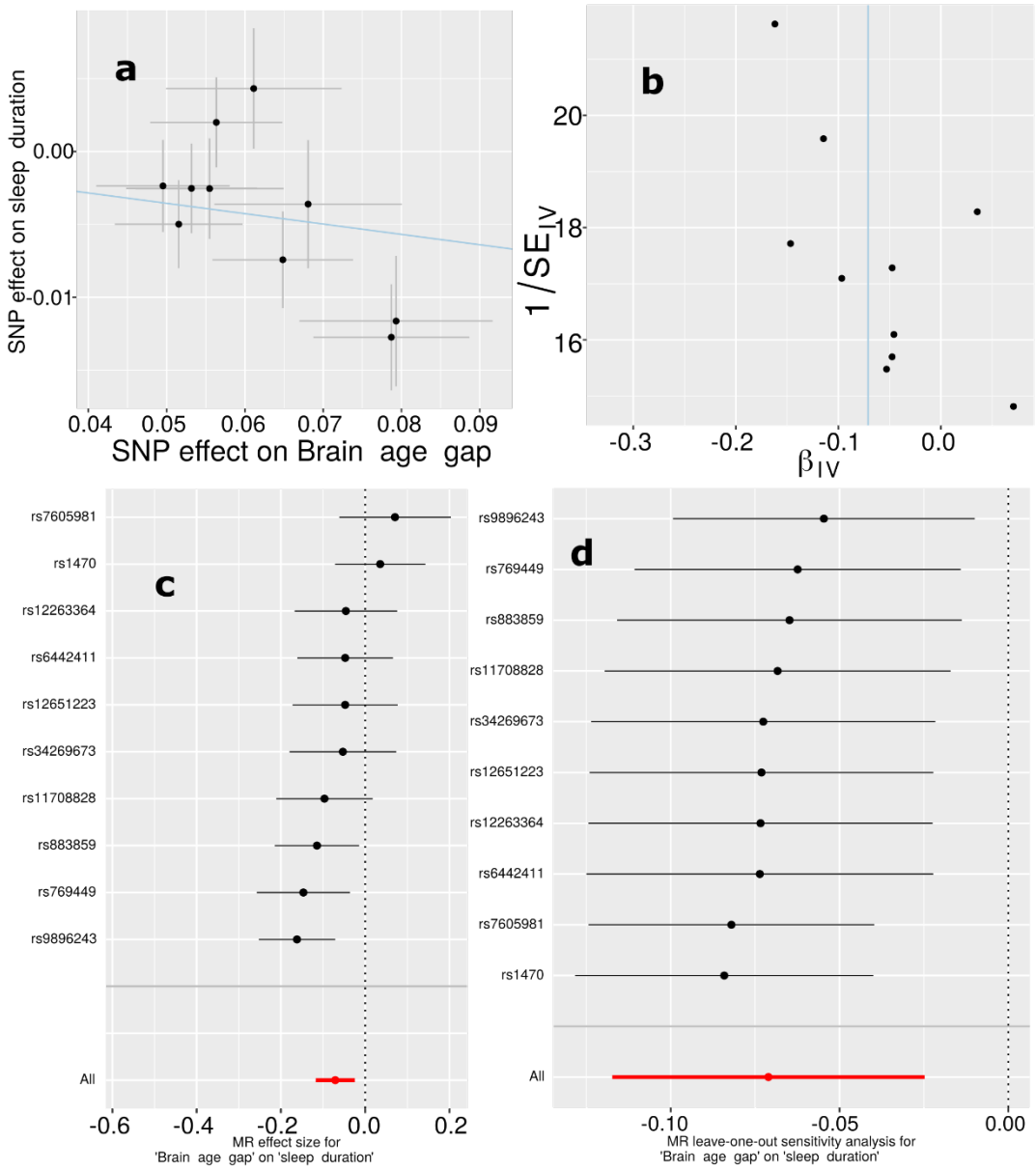

a) Scatter plot for the MR effect sizes of the exposure variable (brain BAG, *x*-axis, SD units) and the outcome variable (sleep duration, *y*-axis, log OR) with standard error bars. The slopes of the regression line correspond to the causal effect sizes estimated by the IVW estimator. **b**) Funnel plot for the relationship between the causal effect of the exposure variable on the outcome variable. Each dot represents MR effect sizes estimated using each SNP as a separate instrument against the inverse of the standard error of the causal estimate. The vertical red line shows the MR estimates using all SNPs. **c**) Forest plot for the single-SNP MR results. Each line represents the MR effect (log OR) for the exposure variable on the outcome variable using only one SNP; the red line shows the MR effect using all SNPs together. **d**) Leave-one-out analysis of the exposure variable on the outcome variable. Each row represents the MR effect (log OR) and the

95% CI by excluding that SNP from the analysis. The red line depicts the IVW estimator using all SNPs. The sample size of the BAGs is indicated in the GWAS summary statistics publicly shared on the MEDICINE portal. The measure of the center for the error bars represents the inferred statistics.

Supplementary Figure 30: Mendelian randomization sensitivity check for the cardiovascular BAG on triglycerides to lipids ratio in very large VLDL

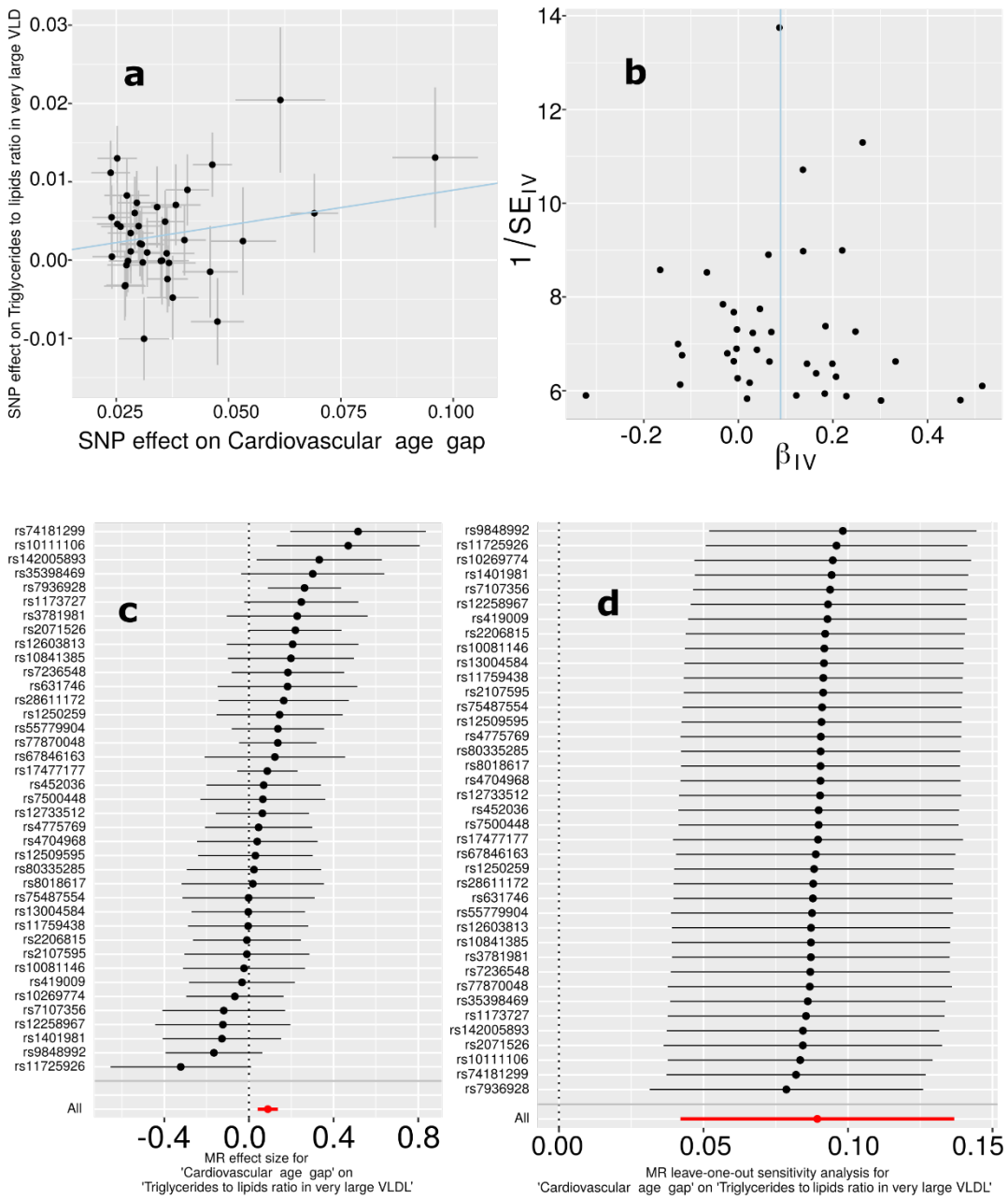

a) Scatter plot for the MR effect sizes of the exposure variable (cardiovascular BAG, *x*-axis, SD units) and the outcome variable (triglycerides to lipids ratio in very large VLDL, *y*-axis, log OR) with standard error bars. The slopes of the regression line correspond to the causal effect sizes estimated by the IVW estimator. **b**) Funnel plot for the relationship between the causal effect of the exposure variable on the outcome variable. Each dot represents MR effect sizes estimated using each SNP as a separate instrument against the inverse of the standard error of the causal estimate. The vertical red line shows the MR estimates using all SNPs. **c**) Forest plot for the single-SNP MR results. Each line represents the MR effect (log OR) for the exposure variable on the outcome variable using only one SNP; the red line shows the MR effect using all SNPs

together. **d**) Leave-one-out analysis of the exposure variable on the outcome variable. Each row represents the MR effect (log OR) and the 95% CI by excluding that SNP from the analysis. The red line depicts the IVW estimator using all SNPs. The sample size of the BAGs is indicated in the GWAS summary statistics publicly shared on the MEDICINE portal. The measure of the center for the error bars represents the inferred statistics.

Supplementary Figure 31: Mendelian randomization sensitivity check for the metabolic BAG on weight

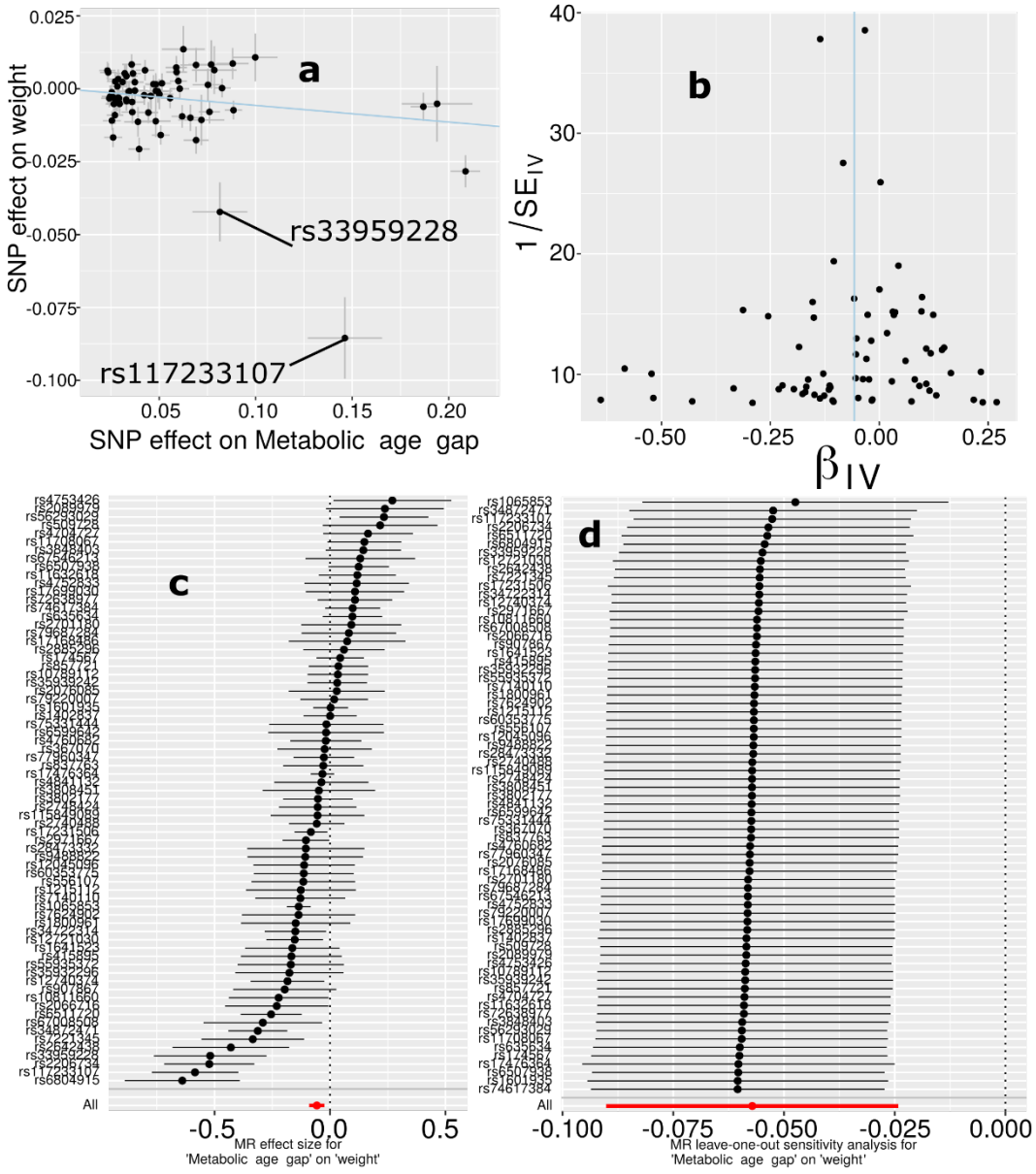

a) Scatter plot for the MR effect sizes of the exposure variable (metabolic BAG, *x*-axis, SD units) and the outcome variable (body weight, *y*-axis, log OR) with standard error bars. The slopes of the regression line correspond to the causal effect sizes estimated by the IVW estimator. **b**) Funnel plot for the relationship between the causal effect of the exposure variable on the outcome variable. Each dot represents MR effect sizes estimated using each SNP as a separate instrument against the inverse of the standard error of the causal estimate. The vertical red line shows the MR estimates using all SNPs. **c**) Forest plot for the single-SNP MR results. Each line represents the MR effect (log OR) for the exposure variable on the outcome variable using only one SNP; the red line shows the MR effect using all SNPs together. **d**) Leave-one-out analysis of the exposure variable on the outcome variable. Each row represents the MR effect

(log OR) and the 95% CI by excluding that SNP from the analysis. The red line depicts the IVW estimator using all SNPs. The sample size of the BAGs is indicated in the GWAS summary statistics publicly shared on the MEDICINE portal. The measure of the center for the error bars represents the inferred statistics.

Supplementary Figure 32: Mendelian randomization sensitivity check for the pulmonary BAG on weight

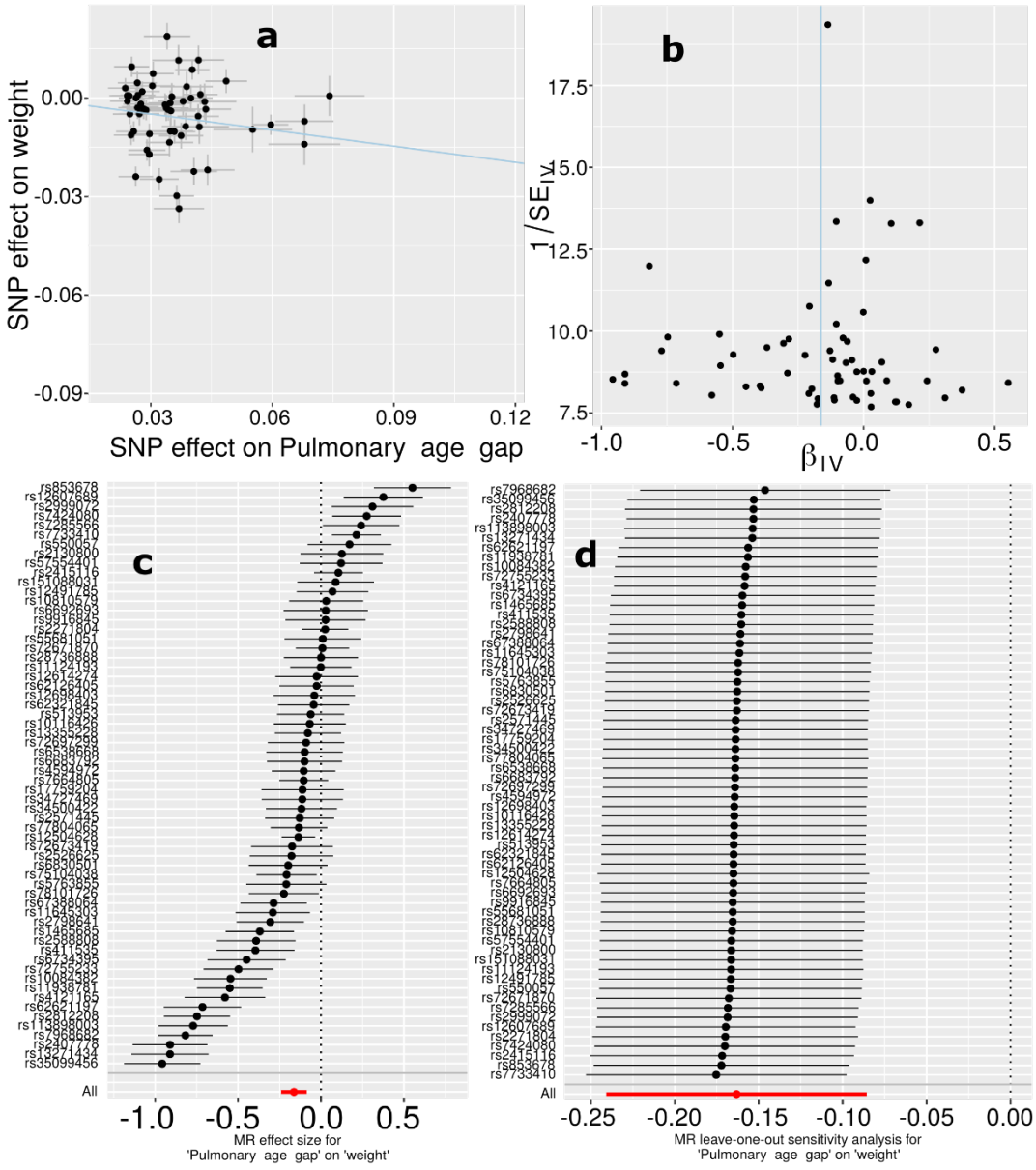

a) Scatter plot for the MR effect sizes of the exposure variable (pulmonary BAG, *x*-axis, SD units) and the outcome variable (body weight, *y*-axis, log OR) with standard error bars. The slopes of the regression line correspond to the causal effect sizes estimated by the IVW estimator. **b**) Funnel plot for the relationship between the causal effect of the exposure variable on the outcome variable. Each dot represents MR effect sizes estimated using each SNP as a separate instrument against the inverse of the standard error of the causal estimate. The vertical red line shows the MR estimates using all SNPs. **c**) Forest plot for the single-SNP MR results. Each line represents the MR effect (log OR) for the exposure variable on the outcome variable using only one SNP; the red line shows the MR effect using all SNPs together. **d**) Leave-one-out analysis of the exposure variable on the outcome variable. Each row represents the MR effect

(log OR) and the 95% CI by excluding that SNP from the analysis. The red line depicts the IVW estimator using all SNPs. The sample size of the BAGs is indicated in the GWAS summary statistics publicly shared on the MEDICINE portal. The measure of the center for the error bars represents the inferred statistics.

Supplementary Table 1: Heritability estimates using the GCTA software

The P-values obtained from the GCTA software were exceptionally small (i.e., significant) in our analyses, even smaller than the lower bound set in the software, resulting in a precision issue and yielding a result of 0.0000e+00. Hence, we report all P-values as $P < 1x10^{-100}$.

A) Original sample sizes. Original sample sizes were used to estimate the heritability for the nine organ systems.

BAG	h^2	h^2 SE	P-value	*N*
Brain	0.47	0.02	$<1x10^{-100}$	30,108
Cardiovascular	0.27	0.006	$<1x10^{-100}$	111,543
Eye	0.38	0.02	$<1x10^{-100}$	36,004
Hepatic	0.23	0.006	$<1x10^{-100}$	111,543
Immune	0.20	0.004	$<1x10^{-100}$	111,543
Metabolic	0.29	0.006	$<1x10^{-100}$	111,543
Musculoskeletal	0.24	0.004	$<1x10^{-100}$	111,543
Pulmonary	0.36	0.006	$<1x10^{-100}$	111,543
Renal	0.30	0.006	$<1x10^{-100}$	111,543

B) Down-sampled sample sizes. For the eight BAGs except for the brain BAG, we randomly down-sampled the original sample sizes to that of the brain BAG.

BAG	h^2	h^2 SE	P-value	*N*
Brain	0.47	0.02	$<1x10^{-100}$	30,108
Cardiovascular	0.35	0.07	$<1x10^{-100}$	30,108
Eye	0.42	0.02	$<1x10^{-100}$	30,108
Hepatic	0.18	0.07	$<1x10^{-100}$	30,108
Immune	0.19	0.07	$<1x10^{-100}$	30,108
Metabolic	0.16	0.07	$<1x10^{-100}$	30,108
Musculoskeletal	0.21	0.07	$<1x10^{-100}$	30,108
Pulmonary	0.39	0.07	$<1x10^{-100}$	30,108
Renal	0.28	0.07	$<1x10^{-100}$	30,108

C) Brain imaging-derived phenotypes vs. 4 pulmonary features. For the brain imaging phenotypes, we used four sets of features from our previous studies: *i*) 32 pattern of structural coavairance (PSCs) from the data-driven MuSIC atlas using T1-weighted MRI and orthogonal-projective non-negative matrix factorization[18]; *ii*) 101 GM ROIs using the ANTs (https://stnava.github.io/ANTs/) software[9]; *iii*) the 21 WM tracts for fractional anisotropy (FA) mean values[8]; and *iv*) 21 funtional node (FN) measures from resting-state functional MRI[7]. The 4 pulmonary features included forced vital capacity, forced expiratory volume, peak expiratory flow, and the ratio of forced expiratory volume to forced vital capacity. For comparison purposes, we also show the h^2estimates for the brain and pulmonary BAGs. The detailed results for all estimates are presented in **Supplementary Source Data 22**. The distribution of each phenotype group is shown in the figure below.

Organ	Phenotype group	Phenotype (mean or individual)	h^2	h^2 SE	P-value

Brain	Brain feature	MuSIC[18]	0.45	0.16	$<1x10^{-100}$
		GM-IDP[9]	0.39	0.16	$<1x10^{-100}$
		WM-IDP[8]	0.53	0.08	$<1x10^{-100}$
		FN-IDP[7]	0.29	0.06	$<1x10^{-100}$
	Brain BAG	Brain BAG	0.47	0.02	$<1x10^{-100}$
Pulmonary	Pulmonary feature	FVC	0.34	0.007	$<1x10^{-100}$
		FEV/FVC	0.41	0.007	$<1x10^{-100}$
		PEF	0.28	0.007	$<1x10^{-100}$
		FEV	0.35	0.007	$<1x10^{-100}$
	Pulmonary BAG	Pulmonary BAG	0.36	0.006	$<1x10^{-100}$

886

887 **Supplementary Table 2: The beta coefficient and its SE estimate from the full sample vs.**
888 **the down-sampled brain BAG comparable sample**
889 N_ISS: number of independent significant SNPs

BAG	Mean_beta_downsample	Mean_beta_fullsample	SE_beta_downsample	SE_beta_fullsample	t_beta	p_beta	t_se	p_se	N_ISS
Cardiovascular	0.034802	0.035822	0.010533	0.005457	-0.51317	0.608293	14.0846	1.95E-33	124
Eye	0.06527	0.064561	0.009967	0.009128	0.136138	0.891913	1.828485	0.069668	69
Hepatic	0.058408	0.057479	0.014495	0.007525	0.293471	0.769268	13.28265	2.59E-35	289
Immune	0.043347	0.041526	0.011454	0.005948	0.682463	0.495312	12.78407	5.79E-32	217
Metabolic	0.053834	0.052587	0.013227	0.006842	0.490113	0.624182	15.99737	1.7E-50	422
Musculoskeletal	0.04263	0.041015	0.011109	0.005817	0.520949	0.602797	11.23119	1.44E-24	147
Pulmonary	0.035423	0.036056	0.010959	0.005678	-0.53629	0.591975	20.08143	1.81E-67	272
Renal	0.067828	0.068927	0.014536	0.007595	-0.2335	0.815446	12.87744	5.18E-34	331

890

Supplementary Table 3: Genetic correlation analyses between the pulmonary BAG and the four features used to derive the BAG.

The P-values obtained from the LDSC software were exceptionally small (i.e., significant) in our analyses, even smaller than the lower bound set in the software, resulting in a precision issue and yielding a result of 0.0000e+00. Hence, we report all P-values as $P < 1x10^{-300}$.

BAG	Pulmonary feature	g_c mean	g_c std	P-value
Pulmonary_age_gap	forced_vital_capacity_fvc_zscore	0.6409	0.0195	$6.1x10^{-237}$
	fev1_fvc_ratio_zscore	0.5371	0.0316	$6.47x10^{-65}$
	peak_expiratory_flow_pef	-0.7903	0.0175	$<1x10^{-300}$
	forced_expiratory_volume_in_1second_fev1_zscore	0.8259	0.0111	$<1x10^{-300}$

Supplementary Table 4: Selected 41 clinical traits for genetic correlation analyses. We selected the candidate studies from the GWAS Catalog for 41 clinical traits, including chronic diseases affecting multiple organ systems, education, and intelligence. To ensure the suitability of the GWAS summary statistics, we first checked that the selected study's population was European ancestry; we then guaranteed a moderate SNP-based heritability h^2 estimate and excluded the studies with spurious low h^2 (<0.05). Abbreviations are detailed in the main text.

Primary organ system	Trait	PubMed ID	Sample size
Brain	AD	30820047	63,926
	Smile-GAN-AD1	NA	33,540
	SmileGAN-AD2	NA	33,540
	SmileGAN-AD3	NA	33,540
	SmileGAN-AD4	NA	33,540
	SurrealGAN-AD1	NA	33,540
	SurrealGAN-AD2	NA	33,540
	ADHD	30478444	53,293
	ALS	27455348	36052
	ASD	30804558	46,350
	HYDRA-ASD1	37017948	14,786
	HYDRA-ASD2	37017948	14,786
	HYDRA-ASD3	37017948	14,786
	BIP	31043756	51,710
	MDD	22472876	18,759
	HYDRA-MDD1	NA	33,540
	HYDRA-MDD2	NA	33,540
	SCZ	23974872	11,244
	HYDRA-SCZ1	32103250	14,786
	HYDRA-SCZ2	32103250	14,786
	OCD	28761083	9,725
Cardiovascular	WMH	31551276	11,226
	AF	30061737	1030,836
	Stroke	29531354	446,696
Eye	Glaucoma	33627673	330,905
Hepatic	Liver fat	34128465	32,858
	PBC	34033851	24,510
Immune	SLE	26502338	14,267
	HIV	34737426	208,808
Metabolic	DB	30054458	655,666
	Hyperlipidemia	34906840	349,222
Musculoskeletal	RA	36333501	92,044
Pulmonary	Lung carcinoma	28604730	85,716
Renal	CKD	31152163	625,219
Digestive	CD	26192919	20,883
	IBD	26192919	34652
Breast	Breast cancer	29059683	139,274

Cognition	Education	23722424	126,559
	Reaction time	29844566	330,069
	Intelligence	28530673	78,308
Lifestyle	Computer use	32317632	408,815

907 **Supplementary Table 5: Genetic correlations analyses between the nine BAGs and longevity,**
908 **household income, and telomere length**. We downloaded the GWAS summary statistics from
909 Deelen et al.[19], which performed two GWASs on longevity based on the 90th survival percentile.
910 For the household income GWAS, we downloaded from Hill et al.[20]. For the telomere length, we
911 used GWAS summary statistics from Codd et al. .
912

BAG	Trait	g_c mean	g_c std	P	PubMed ID	Sample size
Brain_age_gap	Longevity	gc_mean	gc_std	0.0931	31413236	36,745
Cardiovascular_age_gap		-0.1588	0.0946	0.0049		
Eye_age_gap		-0.2038	0.0725	0.0719		
Hepatic_age_gap		-0.1657	0.0921	0.6182		
Immune_age_gap		0.0495	0.0993	0.9299		
Metabolic_age_gap		0.0086	0.0979	0.7605		
Musculoskeletal_age_gap		0.0328	0.1074	0.1128		
Pulmonary_age_gap		-0.1193	0.0752	0.0057		
Renal_age_gap		-0.197	0.0713	0.0323		
Brain_age_gap	Household income	-0.2089	0.0403	$2.2E^{-07}$	31874048	286,301
Cardiovascular_age_gap		-0.0679	0.0356	0.0563		
Eye_age_gap		-0.066	0.0404	0.1024		
Hepatic_age_gap		-0.1026	0.0417	0.0138		
Immune_age_gap		0.0028	0.0414	0.9464		
Metabolic_age_gap		-0.0671	0.0389	0.0841		
Musculoskeletal_age_gap		-0.2867	0.0308	$1.4E^{-20}$		
Pulmonary_age_gap		-0.1567	0.0286	$4.4E^{-08}$		
Renal_age_gap		-0.0989	0.0321	0.002		
Brain_age_gap	Telomere length	0.0273	0.0506	0.5897	34611362	472,174
Cardiovascular_age_gap		-0.0005	0.0038	0.9897		
Eye_age_gap		-0.0124	0.0439	0.7769		
Hepatic_age_gap		-0.0042	0.0306	0.9089		
Immune_age_gap		-0.1338	0.0377	0.0004		
Metabolic_age_gap		-0.0514	0.0393	0.1905		
Musculoskeletal_age_gap		0.0045	0.0333	0.8932		
Pulmonary_age_gap		-0.0993	0.0331	0.0027		
Renal_age_gap		-0.029	0.0293	0.3222		

913

Supplementary Table 6: Additional sensitivity checks for the causal relationships

A) GWAS without and with body weight as a covariate for the causal relationship from the hepatic BAG to the musculoskeletal BAG.

Weight	Outcome (split2)	Exposure (split1)	Method	nSNP	BETA	SE	P	OR	CI_low	CI_high
N	Musculoskeletal	Hepatic	MR Egger	19	0.51783336	0.14070786	0.00185593	1.67838725	1.27385274	2.21138886
	Musculoskeletal	Hepatic	Weighted median	19	0.35295633	0.06606437	9.16E-08	1.42326899	1.25040832	1.62002649
	Musculoskeletal	Hepatic	Inverse variance weighted	19	0.38344296	0.07834137	9.85E-07	1.46732785	1.25846644	1.71085295
	Musculoskeletal	Hepatic	Simple mode	19	0.15733154	0.10700058	0.15872332	1.17038357	0.94895908	1.44347395
	Musculoskeletal	Hepatic	Weighted mode	19	0.46614953	0.08121762	1.93E-05	1.59384531	1.35929067	1.86887391
Y	Musculoskeletal	Hepatic	MR Egger	18	0.51517011	0.14245065	0.00231711	1.67392323	1.26613232	2.21305384
	Musculoskeletal	Hepatic	Weighted median	18	0.35613857	0.06002398	2.97E-09	1.42780539	1.26933301	1.60606258
	Musculoskeletal	Hepatic	Inverse variance weighted	18	0.38926537	0.0792834	9.12E-07	1.47589615	1.2634801	1.72402356
	Musculoskeletal	Hepatic	Simple mode	18	0.24697399	0.11293776	0.04302518	1.28014581	1.02594689	1.59732761
	Musculoskeletal	Hepatic	Weighted mode	18	0.47542746	0.06925444	2.74E-06	1.60870171	1.40451037	1.84257891

B) GWAS without and with body weight as a covariate for the causal relationship from the musculoskeletal BAG to the hepatic BAG.

Weight	Outcome (split2)	Exposure (split1)	Method	nSNP	BETA	SE	P	OR	CI_low	CI_high
N	Hepatic	Musculoskeletal	MR Egger	9	1.82825 01	0.24293965	0.00013439	6.22298749	3.8654897	10.018283 9
	Hepatic	Musculoskeletal	Weighted median	9	0.92114305	0.13768954	2.23E-11	2.51216028	1.9179781	3.2904178
	Hepatic	Musculoskeletal	Inverse variance weighted	9	1.02402966	0.18103365	1.54E-08	2.78439235	1.9526818	3.9703554 1
	Hepatic	Musculoskeletal	Simple mode	9	1.20577311	0.18620161	0.000193	3.33933976	2.31826245	4.8101499 5
	Hepatic	Musculoskeletal	Weighted mode	9	1.25833413	0.13034769	1.10E-05	3.51955347	2.7260472	4.5440360 1
Y	Hepatic	Musculoskeletal	MR Egger	9	1.69092352	0.35916855	0.00218827	5.42448802	2.68304718	10.967034 2
	Hepatic	Musculoskeletal	Weighted median	9	0.85408009	0.13197703	9.71E-11	2.34921232	1.81376558	3.0427297 8
	Hepatic	Musculoskeletal	Inverse variance weighted	9	0.99179962	0.19767923	5.24E-07	2.69608204	1.83005923	3.9719252 1
	Hepatic	Musculoskeletal	Simple mode	9	1.23665687	0.15851732	5.23E-05	3.44408019	2.52429777	4.6990052
	Hepatic	Musculoskeletal	Weighted mode	9	1.27628794	0.1538585	3.36E-05	3.58331353	2.65043899	4.8445317 4

C) GWAS without and with rs429358 as an IV for the causal relationship from the hepatic BAG to the musculoskeletal BAG.

rs429358	Outcome (split2)	Exposure (split1)	Method	nSNP	BETA	SE	P	OR	CI_low	CI_high
N	Musculoskeletal	Hepatic	MR Egger	18	0.51522659	0.12736616	0.00093844	1.67401778	1.30419881	2.14870271
	Musculoskeletal	Hepatic	Weighted median	18	0.36478773	0.06339608	8.71E-09	1.44020827	1.27192489	1.63075657
	Musculoskeletal	Hepatic	Inverse variance weighted	18	0.41660503	0.07146014	5.55E-09	1.5168033	1.31856385	1.74484706
	Musculoskeletal	Hepatic	Simple mode	18	0.15924454	0.09710274	0.11938508	1.17262466	0.96940109	1.41845167
	Musculoskeletal	Hepatic	Weighted mode	18	0.45942325	0.07899932	2.07E-05	1.58316063	1.35606155	1.84829191
Y	Musculoskeletal	Hepatic	MR Egger	19	0.51783336	0.14070786	0.00185593	1.67838725	1.27385274	2.21138886
	Musculoskeletal	Hepatic	Weighted median	19	0.35295633	0.06606437	9.16E-08	1.42326899	1.25040832	1.62002649
	Musculoskeletal	Hepatic	Inverse variance weighted	19	0.38344296	0.07834137	9.85E-07	1.46732785	1.25846644	1.71085295
	Musculoskeletal	Hepatic	Simple mode	19	0.15733154	0.10700058	0.15872332	1.17038357	0.94895908	1.44347395
	Musculoskeletal	Hepatic	Weighted mode	19	0.46614953	0.08121762	1.93E-05	1.59384531	1.35929067	1.86887391

D) **Causal analysis using the LCV method**. We performed causal analysis using the LCV method for the bi-directional causality between hepatic and musculoskeletal BAGs, the 9 BAGs and longevity, and the 9 BAGs and telomere length. GCP: genetic causality proportion.

Trait1	Trait2	GCP	GCP_se	P	PubMed ID	Sample size
Musculoskeletal_age_gap	Hepatic_age_gap	-0.75144	0.143475	9.37E-12	NA	111,543
Brain_age_gap	Longevity (99th percentile)	-0.45597	0.208644	**0.047488**	31874048	286,301
Cardiovascular_age_gap		-0.21694	0.395088	0.547241		
Eye_age_gap		-0.07761	0.565366	0.639544		
Hepatic_age_gap		-0.53253	0.321599	0.089042		
Immune_age_gap		-0.15001	0.356513	0.868225		
Musculoskeletal_age_gap		-0.26633	0.440294	0.827824		
Metabolic _age_gap		-0.3153	0.391594	0.866896		
Pulmonary_age_gap		-0.18056	0.375253	0.210053		
Renal_age_gap		-0.33425	0.403767	0.573389		
Brain_age_gap	Telomere length	-0.05796	0.55584	0.713688	34611362	472,174
Cardiovascular_age_gap		-0.32007	0.294362	0.421771		
Eye_age_gap		-0.11877	0.49709	0.926991		
Hepatic_age_gap		-0.00755	0.332263	0.792948		
Immune_age_gap		-0.3321	0.126005	**0.002502**		
Metabolic_age_gap		-0.07943	0.45872	0.705827		
Musculoskeletal_age_gap		-0.15992	0.478106	0.821179		
Pulmonary_age_gap		-0.67193	0.198345	**3.57E-16**		
Renal_age_gap		-0.17496	0.500093	0.6767		

Supplementary Table 7: Selected 17 clinical traits for Mendelian randomization analyses. We unbiasedly and systematically selected 17 clinical traits, including chronic diseases affecting multiple organ systems, cognition, and lifestyle factors. The selection procedure is detailed in the main text (**Method 2J**).

Primary organ system	Trait	PubMed ID	IEU-ID (If applicable)	Number of IVs (forward MR)
Brain	AD	24162737	ebi-a-GCST002245	10
	BIP	31043756	ieu-a-1126	12
Metabolic	Type 2 diabetes	22885922	ieu-a-26	10
	Triglyceride-to-lipid ratio	32114887	met-d-XL_VLDL_TG_pct	41
Eye	Glaucoma	NA	finn-b-H7_GLAUCOMA	9
Musculoskeletal	RA	23143596	ebi-a-GCST005569	11
Hepatic	PBC	26394269	ebi-a-GCST003129	16
Digestive	CD	26192919	ieu-a-12	77
	IBD	23128233	ieu-a-292	81
Breast	Breast cancer	29059683	ieu-a-1126	86
Cognition	Reaction time	NA	Local-UKBB	18
Lifestyle	Coffee intake	NA	Local-UKBB	11
	Fresh fruit	NA	Local-UKBB	15
	Tea intake	NA	Local-UKBB	12
	Sleep duration	NA	Local-UKBB	8
	Summer outdoor activity hour	NA	Local-UKBB	14
	Body weight	NA	Local-UKBB	161

Supplementary References

1. Elliott, L. T. *et al.* Genome-wide association studies of brain imaging phenotypes in UK Biobank. *Nature* **562**, 210–216 (2018).
2. Kurki, M. I. *et al.* FinnGen provides genetic insights from a well-phenotyped isolated population. *Nature* **613**, 508–518 (2023).
3. Giambartolomei, C. *et al.* Bayesian Test for Colocalisation between Pairs of Genetic Association Studies Using Summary Statistics. *PLOS Genetics* **10**, e1004383 (2014).
4. Mummery, C. J. *et al.* Tau-targeting antisense oligonucleotide MAPTRx in mild Alzheimer's disease: a phase 1b, randomized, placebo-controlled trial. *Nat Med* 1–11 (2023) doi:10.1038/s41591-023-02326-3.
5. Wen, J. *et al.* The genetic architecture of multimodal human brain age. *Nat Commun* **15**, 2604 (2024).
6. Wen, J. *et al.* Genomic loci influence patterns of structural covariance in the human brain. *Proceedings of the National Academy of Sciences* **120**, e2300842120 (2023).
7. Zhao, B. *et al.* Common variants contribute to intrinsic human brain functional networks. *Nat Genet* **54**, 508–517 (2022).
8. Zhao, B. *et al.* Common genetic variation influencing human white matter microstructure. *Science* **372**, (2021).
9. Zhao, B. *et al.* Genome-wide association analysis of 19,629 individuals identifies variants influencing regional brain volumes and refines their genetic co-architecture with cognitive and mental health traits. *Nat Genet* **51**, 1637–1644 (2019).
10. Bowden, J. *et al.* A framework for the investigation of pleiotropy in two-sample summary data Mendelian randomization. *Stat Med* **36**, 1783–1802 (2017).

961 11. Burgess, S. & Thompson, S. G. Interpreting findings from Mendelian randomization
962 using the MR-Egger method. *Eur J Epidemiol* **32**, 377–389 (2017).
963 12. Chang, C.-C. & Lin, C.-J. LIBSVM: A library for support vector machines. *ACM Trans.*
964 *Intell. Syst. Technol.* **2**, 1–27 (2011).
965 13. Tian, Y. E. *et al.* Heterogeneous aging across multiple organ systems and prediction of
966 chronic disease and mortality. *Nat Med* 1–11 (2023) doi:10.1038/s41591-023-02296-6.
967 14. Cole, J. H., Marioni, R. E., Harris, S. E. & Deary, I. J. Brain age and other bodily 'ages':
968 implications for neuropsychiatry. *Mol Psychiatry* **24**, 266–281 (2019).
969 15. Jones, D. T., Lee, J. & Topol, E. J. Digitising brain age. *The Lancet* **400**, 988 (2022).
970 16. Peng, H., Gong, W., Beckmann, C. F., Vedaldi, A. & Smith, S. M. Accurate brain age
971 prediction with lightweight deep neural networks. *Medical Image Analysis* **68**, 101871 (2021).
972 17. Bashyam, V. M. *et al.* MRI signatures of brain age and disease over the lifespan based on
973 a deep brain network and 14 468 individuals worldwide. *Brain* **143**, 2312–2324 (2020).
974 18. Wen, J. *et al.* Novel genomic loci and pathways influence patterns of structural
975 covariance in the human brain. 2022.07.20.22277727 Preprint at
976 https://doi.org/10.1101/2022.07.20.22277727 (2022).
977 19. Deelen, J. *et al.* A meta-analysis of genome-wide association studies identifies multiple
978 longevity genes. *Nat Commun* **10**, 3669 (2019).
979 20. Hill, W. D. *et al.* Genome-wide analysis identifies molecular systems and 149 genetic
980 loci associated with income. *Nat Commun* **10**, 5741 (2019).
981 21. Codd, V. *et al.* Polygenic basis and biomedical consequences of telomere length
982 variation. *Nat Genet* **53**, 1425–1433 (2021).
983